NATIONAL AERONAUTICS AND SPACE ADMINISTRATION

TECHNICAL MEMORANDUM X-580

MEASURED AND ESTIMATED AERODYNAMIC CHARACTERISTICS

FOR A MODEL OF A ROCKET BOOSTER AT MACH NUMBERS

FROM 0.6 TO 4 AND AT ANGLES OF

ATTACK FROM 0° TO 180°*

By Leland H. Jorgensen and Stuart L. Treon

SUMMARY

Aerodynamic characteristics of normal force, axial force, and pitching moment have been measured for a model of a rocket-powered booster at Mach numbers from 0.60 to 4.06. The model had external fittings and engine fairings such as might be used on a large liquid-fuel booster. The model was tested throughout the angle-of-attack range of 0° to 180° at bank angles of 0° and 90°. In addition to tests of this model, selected tests were made of the model with the external fittings removed and the model with the external fittings and engine fairings removed. For all tests the Reynolds number ranged from 0.22×10^6 to 0.93×10^6, based on model diameter.

Large changes in the aerodynamic characteristics resulted from changes in Mach number, changes in angle of bank, and removal of the booster engine fairings. The external fittings (other than the engine fairings) had relatively small influence on the forces and moments.

An analytical method for estimating the aerodynamic characteristics of boosters has been assessed by comparing computed with experimental results. The comparisons show that the normal-force variation with angle of attack can be predicted reasonably well at supersonic Mach numbers. However, at subsonic Mach numbers the method loses accuracy primarily because of failure to fully account for a significant amount of normal force from the engine fairings. With the engine fairings removed the method predicts the experimental normal forces fairly well at subsonic as well as at supersonic Mach numbers. At all Mach numbers there is still much to be desired in the prediction of pitching moments, and the computed centers of pressure at some angles of attack can be in error by as much as half a body diameter.

INTRODUCTION

Following ejection of a manned space capsule from a booster because of an abort during launch, it is imperative that the booster fly a trajectory in which it cannot collide with the capsule. In order to compute the trajectories for the booster and capsule, aerodynamic force and moment coefficients for these vehicles at various speeds are required. Because of the lack of experimental force and moment characteristics for boosters over wide ranges of Mach numbers and angles of attack, a wind-tunnel investigation of a model of a typical rocket-powered booster has been conducted. Aerodynamic data for this model both with and without simulated external fittings and engine fairings have been obtained. The model was tested over the Mach number range of 0.6 to 4 at bank angles of 0° and 90° and at angles of attack ranging from 0° to 180°. Force and moment characteristics also have been computed for the model at these test conditions, and comparisons of computed with measured results have been made. The purpose of this report then is twofold: first, to present the experimental results and, second, to show the comparisons of the computed with the experimental results.

NOTATION

A cross-sectional area of cylindrical portion of body

A_b area over which base pressure, p_b, is considered acting

A_p plan-form area

C_A axial-force coefficient, $\dfrac{\text{axial force}}{q_\infty A}$

C_{d_c} crossflow drag coefficient of circular cylinder based on cylinder diameter, $\dfrac{\text{cross force}}{q_N l_{cy} d_{cy}}$

C_m pitching-moment coefficient about reference center shown in figure 1(a), $\dfrac{\text{pitching moment}}{q_\infty A d_{cy}}$

C_N normal-force coefficient, $\dfrac{\text{normal force}}{q_\infty A}$

C_p pressure coefficient, $\dfrac{p - p_\infty}{q_\infty}$

d   diameter of specified body section

l length of specified body section

M_N component of Mach number normal to body axis, $M_\infty \sin \alpha$

M_∞ free-stream Mach number

p   pressure

p_∞ free-stream static pressure

Q   body volume

q_∞ free-stream dynamic pressure

x_c distance from nose face to centroid of body plan-form area

x_{cp} center of pressure measured from nose face

x_m distance from nose face to pitching-moment reference center

α angle of attack

φ angle of bank about body longitudinal axis (see fig. 1(a))

Subscripts

a   nose adapter

b   base

cone   cone

cy   cylinder

f   cone frustum

SF   skin friction

stag   stagnation

T   total

EXPERIMENTAL CONSIDERATIONS

Wind Tunnels

The experimental investigation was conducted in the Ames 2- by 2-foot transonic wind tunnel and the 1- by 3-foot supersonic wind tunnel No. 1. The 2- by 2-foot transonic tunnel is of the closed-circuit, variable-pressure type. It has a flexible-plate nozzle followed by a perforated test section which permits continuous choke-free operation at Mach numbers up to 1.4. The 1- by 3-foot supersonic tunnel is also a closed-circuit, variable-pressure type with a flexible-plate nozzle that provides a variation of Mach number from about 1.4 to 6. In both tunnels the Reynolds number is changed by varying the total pressure within the approximate limits of 1/5 of an atmosphere to 4 atmospheres.

The water content of the air in the tunnels is maintained at less than 0.0003 pound of water per pound of dry air. Consequently, any effect of humidity on the flow is negligible.

Models and Supports

Sketches of the models tested are shown in figure 1. The model in figure 1(a) had external fittings and engine fairings such as might be expected on a large liquid-fuel booster. In addition, the model had a flat-faced adapter section for attachment of a payload. The model in figure 1(b) was the same as that in figure 1(a) except that the external fittings were removed. For the model in figure 1(c) the external fittings and the booster engine fairings were removed, leaving a clean cylindrical body. The model bodies were constructed of aluminum and the fittings and fairings of brass. Photographs of the complete model mounted in the test sections of the 1- by 3-foot and 2- by 2-foot wind tunnels are presented in figure 2. The support mountings shown in the photographs are explained in the next paragraph.

In order to test the models throughout the desired angle-of-attack range of about 0° to 180°, four support mountings were employed - mountings A, B, C, and D oriented as indicated in figure 3. The angle-of-attack ranges obtained with these mountings were approximately as follows: -4° to 40° with A, 155° to 184° with B, 35° to 100° with C, and 95° to 160° with D. For the base and front mountings (A and B) a strain-gage balance was positioned inside the model. For the side mountings (C and D) the balance was positioned just external to the model and shielded with a shroud. For the model mountings sketched in figure 3 the model is shown at zero bank angle ($\varphi = 0^\circ$). Provision was made to mount the models also at 90° bank angle.

Tests

Balance measurements of normal force, axial force, and pitching moment were obtained for the complete booster model (fig. 1(a)) at free-stream Mach numbers of 0.60, 0.80, 0.90, 1.00, 1.10, 1.30, 1.39, 1.98, 2.94, and 4.06. The other two models (figs. 1(b) and (c)) were tested only at Mach numbers of 0.60, 1.00, 1.98, and 4.06. The Reynolds number, based on model diameter, ranged from 0.22×10^6 to 0.93×10^6 for the tests. Except for Mach numbers 1.10, 1.30, and 1.39, where the angle-of-attack range was limited because of tunnel blockage and support vibrations, the models were tested at angles of attack from about $-4°$ to $184°$. The complete booster model was tested at bank angles (φ) of $0°$ and $90°$. The other models were tested at $\varphi = 90°$ (see fig. 1(a) for φ orientation).

For all tests the shadowgraph technique was employed to observe model flow fields. Shadowgraph pictures were taken, some of which are presented later. Selected tests at both subsonic and supersonic Mach numbers also were made with the models painted with a subliming solution. The sublimation technique was used in conjunction with the shadowgraph to ascertain the state of the boundary-layer flow. For the sublimation technique the models were sprayed with an 8-percent solution of biphenyl in petroleum ether. This solution dries on contact with the model surface and presents a white appearance. As the wind tunnel is operated, sublimation takes place with laminar regions remaining white and turbulent regions showing the basic model surface.

Reduction and Precision of Data

All the force and moment data have been reduced to coefficient form and are referred to the body axes system. Pitching-moment coefficients are taken about the model reference center shown in figure 1(a). All coefficients are based on the maximum cross-sectional area A of the cylindrical portion of the body with no fittings included. The diameter d of the cylindrical portion is taken as the reference length in the moment coefficients.

Axial-force coefficients presented in this report were obtained from the expression

$$C_A = C_{A_T} - C_{A_b} \cos \delta$$

where C_{A_T} is the total axial-force coefficient measured along the balance axis; δ is the angle between the longitudinal axes of the model and balance for the various model mountings (fig. 3); and

$$C_{A_b} = - \frac{p_b - p_\infty}{q_\infty} \left(\frac{A_b}{A} \right)$$

In this relation for C_{A_b}, p_b is the balance pressure measured at the balance-model connection, and A_b is the area over which p_b is considered acting. For the models mounted from the base (mounting A), A_b is taken as the area of the cylindrical body and $A_b/A = 1$. For the models mounted from the front (mounting B), A_b is taken as the frontal area of the nose adapter, and $A_b/A = 0.399$. For the side mountings (C and D), A_b is assumed to be zero.

The precision of the final data is affected by uncertainties in the measurement of the forces and moments, and in the determination of the stream static and dynamic pressures used in reducing the forces and moments to coefficient form. These individual uncertainties led to estimated uncertainties which are listed as follows:

C_N	± 0.08	α	$\pm 0.1^\circ$
C_A	± 0.08	M_∞	± 0.01
	C_m	± 0.15	

Any effects of possible sting-support interference on the model have been neglected in estimating the precision.

ANALYTICAL CONSIDERATIONS

Estimation of Aerodynamic Characteristics
of Booster at Angle of Attack

Most analytical procedures for computing the aerodynamic characteristics of bodies and missile-type configurations have been based on potential theory and are limited in usefulness to low angles of attack. Allen in references 1 and 2 proposed a method for predicting the forces and moments for bodies inclined to angles of attack considerably higher than those for which theories based only on potential-flow concepts are known to apply. In this method a crossflow lift attributed to flow separation is added to the lift predicted by slender-body potential theory. This procedure has been used quite successfully in estimating the aerodynamic coefficients of inclined bodies, although most data available for study have been for bodies at angles of attack below about 20°. In the present investigation the method has been adapted for use in estimating the forces and moments for the models inclined at angles of attack up to 180°.
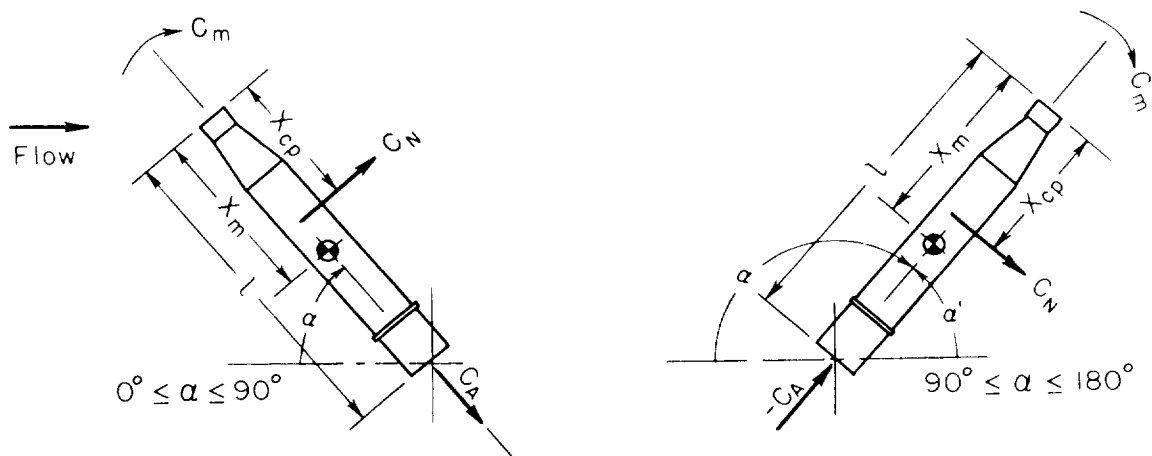
For the sign convention in the above sketch, the formulas for normal-force, axial-force, and pitching-moment coefficient are

$$C_N = \frac{A_b}{A} \sin 2\alpha' \cos \frac{\alpha'}{2} + \eta C_{d_c} \frac{A_p}{A} \sin^2\alpha'; \qquad 0^\circ \leq \alpha \leq 180^\circ \qquad (1)$$

$$C_A = C_{A_{\alpha=0^\circ}} \cos^2\alpha'; \qquad 0^\circ \leq \alpha \leq 90^\circ \qquad (2)$$

$$C_A = C_{A_{\alpha=180^\circ}} \cos^2\alpha'; \qquad 90^\circ \leq \alpha \leq 180^\circ \qquad (3)$$

$$C_m = \left[\frac{Q - A_b(l - x_m)}{Ad} \right] \sin 2\alpha' \cos \frac{\alpha'}{2}$$

$$+ \eta C_{d_c} \frac{A_p}{A} \left(\frac{x_m - x_c}{d} \right) \sin^2\alpha'; \qquad 0^\circ \leq \alpha \leq 90^\circ \qquad (4)$$

and

$$C_m = - \left(\frac{Q - A_b x_m}{Ad} \right) \sin 2\alpha' \cos \frac{\alpha'}{2}$$

$$+ \eta C_{d_c} \frac{A_p}{A} \left(\frac{x_m - x_c}{d} \right) \sin^2\alpha'; \qquad 90^\circ \leq \alpha \leq 180^\circ \qquad (5)$$

where

$$\alpha' = \alpha \text{ for } 0^\circ \leq \alpha \leq 90^\circ \text{ and } \alpha' = 180 - \alpha \text{ for } 90^\circ \leq \alpha \leq 180^\circ$$

The center of pressure measured from the nose face is then given by

$$x_{cp} = \left(\frac{x_m}{d} - \frac{C_m}{C_N}\right) d \qquad (6)$$

In the expressions for C_N and C_m, C_{d_c} is the crossflow drag coefficient for a circular cylinder placed normal to an airstream; C_{d_c} is a function of the Mach number normal to the cylinder axis and may be approximated by the data in figure 4. The experimental curve in figure 4 was determined from data plotted in references 3 and 4. The curves by Newtonian and modified Newtonian theory (e.g., ref. 4) are merely shown for comparison.

Also in the expressions for C_N and C_m, η is the ratio of crossflow drag coefficient for a body of finite fineness ratio to that for a body of infinite fineness ratio. Unfortunately, cylinder drag coefficients from which η can be computed have been measured, to the authors' knowledge, only at very low Mach numbers (refs. 5 and 6). For subsonic free-stream Mach numbers, the value of η for the present study ($\eta=0.65$) has been taken from a plot of η versus l/d in reference 5. For supersonic free-stream Mach numbers, η has been assumed to be unity, an assumption indicated as being essentially correct from past investigations (e.g., refs. 2, 7, and 8).

It should be recognized that, in the strictest sense, the specified method for estimating the aerodynamic characteristics is only applicable for sharp-nosed slender bodies because of the potential lift term (see, e.g., first term in eq. (1)). However, except for angles of attack near $0°$ and $180°$, the potential term is fairly insignificant, most of the lift coming from the semiempirical crossflow lift term.

Estimation of Axial-Force Coefficient of Booster at Angles of Attack of $0°$ and $180°$

To predict the variation of C_A with angle of attack by equations (2) and (3), either computed or measured values of axial-force coefficient at α of $0°$ and $180°$ are required. As a first approximation in estimating $C_{A_{\alpha=0°}}$ and $C_{A_{\alpha=180°}}$, it is assumed that the booster is essentially a body of revolution consisting of a flat-faced capsule adapter, a conical frustum, and a cylindrical body section.

When base axial force is omitted,

$$C_{A_{\alpha=0°}} = C_{A_a} + C_{A_f} + C_{A_{SF}} \qquad (7)$$

where C_{A_a} represents the pressure contribution of the nose adapter, C_{A_f} the pressure contribution of the conical frustum, and $C_{A_{SF}}$ the skin-friction contribution.

For supersonic Mach numbers it is assumed that the pressure over the face of the adapter is equal to stagnation pressure; hence,

$$C_{A_a} = C_{p_{stag}} \left(\frac{d_a}{d_{cy}}\right)^2 \tag{8}$$

where $C_{p_{stag}}$ as a function of Mach number is plotted in figure 5.

For the conical frustum,

$$C_{A_f} = \left[1-\left(\frac{d_a}{d_{cy}}\right)^2\right] C_{A_{cone}} \tag{9}$$

where $C_{A_{cone}}$ is the axial-force coefficient for the cone given by "exact" cone theory. Values of $C_{A_{cone}}$ can be obtained from the plots in reference 9. For the booster in the transonic regime, no estimates of C_{A_a} and C_{A_f} are attempted.

The skin-friction contribution, $C_{A_{SF}}$, can be readily computed by the classical methods outlined in reference 10. For most boosters it is probably realistic to assume a turbulent boundary layer and compute the skin friction by the T' method (see ref. 10).

For the configuration at $\alpha = 180^\circ$, the axial-force coefficient is assumed to be given approximately by the addition of $C_{p_{stag}}$ and $C_{A_{SF}}$. In all the estimations, the axial-force contributions of the external fittings and engine fairings have been omitted.

RESULTS AND DISCUSSION

Experimental values of C_N, C_A, and C_m as functions of angle of attack are plotted in figures 6 through 9. In addition, shadowgraph pictures of the models at supersonic Mach numbers are presented without comment in figures 10 through 17. (Shadowgraph pictures of the models at the lower Mach numbers were not of sufficient quality for reproduction.)

In the following brief discussion some of the data are used to illustrate the effects on the forces and moments resulting from change in Mach number, change in angle of bank, and removal of external fittings and

engine fairings. Center-of-pressure curves have been computed from experimental C_N and C_m curves and are presented along with these curves. From shadowgraph and sublimation studies it was concluded that the measured values of C_A were for the models with essentially all-turbulent boundary layers. In the discussion, some of the experimental results are used in an assessment of the previously outlined analytical method for estimating booster force and moment characteristics.

Experimental Force and Moment Characteristics

Effect of Mach number.- As shown in figure 18 changes in Mach number had considerable effect on the booster aerodynamic characteristics. The variations in the characteristics were largest throughout the range from $M_\infty = 0.6$ to about $M_\infty = 2$ and at angles of attack from about 40° to 140°. In general, C_N increased with increase in Mach number throughout this range (fig. 18(a)). At Mach numbers above about 2 there was, in general, a gradual decline in C_N with further increase in Mach number. It is well to note that, in contrast to the results at α from about 40° to 140°. there was little effect of Mach number on C_N at α up to about 10° and higher than 170°. However, at these angles of attack the greatest variations in center of pressure with Mach number occurred (see fig. 18(d)).

Effect of angle of bank.- The effect on the aerodynamic characteristics of change in angle of bank (φ) from 0° to 90° can be seen from figure 19. Apparently because of about 13 percent greater lifting area for the booster model at $\varphi = 90^\circ$ than at $\varphi = 0^\circ$, the maximum values of C_N (fig. 19(a)) were about 10 to 13 percent higher at $\varphi = 90^\circ$. However, except for α from about 30° to 150°, there was essentially no effect of φ on C_N. As might be then expected, the effect of φ on C_A (fig. 19(b)) is only noticeable at α from about 30° to 150°.

Although at both $\varphi = 0^\circ$ and $\varphi = 90^\circ$ the booster was unstable except at very high α, the instability was less at $\varphi = 90^\circ$ because the engine fairings at the rear provided additional rearward lifting area (fig. 19(c)). With the fairings at the rear, the booster at $\varphi = 90^\circ$ trimmed at lower α than at $\varphi = 0^\circ$. It is interesting to note that with increase in Mach number the trim α decreased for $\varphi = 90^\circ$ and increased for $\varphi = 0^\circ$. At all Mach numbers the center of pressure (fig. 19(d)) moved rearward as the booster was rotated from $\varphi = 0^\circ$ to $\varphi = 90^\circ$.

Effects of external fittings and engine fairings.- In order to assess the effects of the external fittings and engine fairings on the aerodynamic characteristics, selected tests were made of a model with the external fittings removed and of a model with both the external fittings and engine fairings removed. Results from these tests are compared in figures 20 and 21. The comparisons indicate that the external fittings had small effect

on the forces and moments, whereas the engine fairings had considerable effect (see fig. 21). An appreciable amount of normal force can be attributed to the engine fairings, especially at α near maximum C_N. At both $\phi = 0°$ and $\phi = 90°$ the fairings provided a stabilizing effect by moving the center of pressure rearward. This rearward shift no doubt resulted from additional rearward lift caused by the fairings. Even with the model oriented at $\phi = 0°$ so that the fairings did not contribute to the plan area, additional lift resulted. A similar result was observed in reference 11 in a study of elliptic cones. Elliptic cones oriented with the major axes in the lift direction developed more lift than circular cones of the same lifting plan area.

Comparisons of Estimated and Experimental
Force and Moment Characteristics

Axial forces at $\alpha = 0°$ and $\alpha = 180°$.- In figure comparisons are made of computed and measured variations of axial-force coefficient, C_A, with Mach number for the model without external fittings and the fairings. The various components of C_A, which were computed by methods previously outlined, are also indicated. It is seen that throughout the supersonic speed range the computed and measured results are reasonably close, although the computed values are a little higher than the measured. (No computations were attempted for the transonic range. Measured values of C_A for the complete model (fittings and fairings included) are also plotted for comparison. Because the differences between the measured C_A for the models with and without external fittings are not large, the computed axial-force curve for the model without fittings can be used as an estimate for the complete model.

Forces and moments at angles of attack from $0°$ to $180°$.- In figures 23 and 24 comparisons are made of computed and experimental aerodynamic characteristics for the models at angle of attack. The computed curves were determined by equations (1) through (5). Except for the axial-force comparisons, the calculations have been made both for the complete model and the model without external fittings and engine fairings. In each case the appropriate plan-form area, A_p, has been used in the C_N and C_m equations. Axial-force coefficients have been estimated only for the model without external fittings and engine fairings, and a turbulent boundary layer has been assumed.

The comparisons show that the experimental variation of C_N with α is predicted best at supersonic Mach numbers (see figs. 23(a) and 24(a)). The analytical method fails at subsonic Mach numbers in predicting the rapid rise of C_N with α attributed to the addition of fittings and engine fairings to the basic body. With the engine fairings and fittings removed, however, the method predicts the experimental C_N results fairly well at subsonic as well as at supersonic Mach numbers. Unfortunately, at all Mach numbers the prediction of C_m with α (figs. 23(c) and 24(c)) leaves

something to be desired for all models. As a result, the center-of-pressure predictions at some angles of attack are in error by as much as half a body diameter (see figs. 23(d) and 24(d)).

CONCLUDING REMARKS

It has been shown that significant changes in booster force and moment
characterist s can result from changes in Mach number. It also has been
demonstrated ' typical engine fairings can contribute substantially to
the character .cs. Even with a booster banked so that the engine fair-
ings did not itribute to the lifting plan area, there was an appreciable
increase in al force over that for a model without fairings. In con-
trast to the ine fairings, the external fittings had little effect.

An an 1 method for computing the force and moment characteris-
tics for at angles of attack from $0°$ to $180°$ has been presented.
From com f computed with experimental results, it appears that
the vari ormal-force coefficient with angle of attack can be
estimate ly well at supersonic Mach numbers. However, at sub-
sonic Ma the method fails to account for the large influence
of the e ttings and engine fairings in increasing C_N. At all
Mach num. is still much to be desired in the prediction of C_m.

Ames Resear nter
    National Aeronautics and Space Administration
        Moffett Field, Calif., July 17, 1961

REFERENCES

1. Allen, H. Julian: Estimation of the Forces and Moments Acting on Inclined Bodies of Revolution of High Fineness Ratio. NACA RM A9I26, 1949.

2. Allen, H. Julian, and Perkins, Edward W.: A Study of Effects of Viscosity on Flow Over Slender Inclined Bodies of Revolution. NACA Rep. 1048, 1951.

3. Gowen, Forrest E., and Perkins, Edward W.: Drag of Circular Cylinders for a Wide Range of Reynolds Numbers and Mach Numbers. NACA TN 2960, 1953.

4. Penland, Jim A.: Aerodynamic Characteristics of a Circular Cylinder at Mach Number 6.86 and Angles of Attack Up to 90°. NACA TN 3861, 1957.

5. Goldstein, S.: Modern Developments in Fluid Dynamics. Oxford, The Clarendon Press, vol. 2, sec. 195, 1938, pp. 439-440.

6. McKinney, Linwood W.: Effects of Fineness Ratio and Reynolds Number on the Low-Speed Crosswind Drag Characteristics of Circular and Modified-Square Cylinders. NASA TN D-549, 1960.

7. Perkins, Edward W., and Kuehn, Donald M.: Comparison of the Experimental and Theoretical Distributions of Lift on a Slender Inclined Body of Revolution at $M = 2$. NACA RM A53E01, 1953.

8. Jorgensen, Leland H.: Inclined Bodies of Various Cross Sections at Supersonic Speeds. NASA MEMO 10-3-58A, 1958.

9. Ames Research Staff: Equations, Tables, and Charts for Compressible Flow. NACA Rep. 1135, 1953.

10. Shapiro, A. H.: The Dynamics and Thermodynamics of Compressible Fluid Flow. Vol. II, chs. 26 and 27, The Ronald Press Co., New York, 1953.

11. Jorgensen, Leland H.: Elliptic Cones Alone and With Wings at Supersonic Speeds. NACA Rep. 1376, 1958.

14
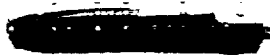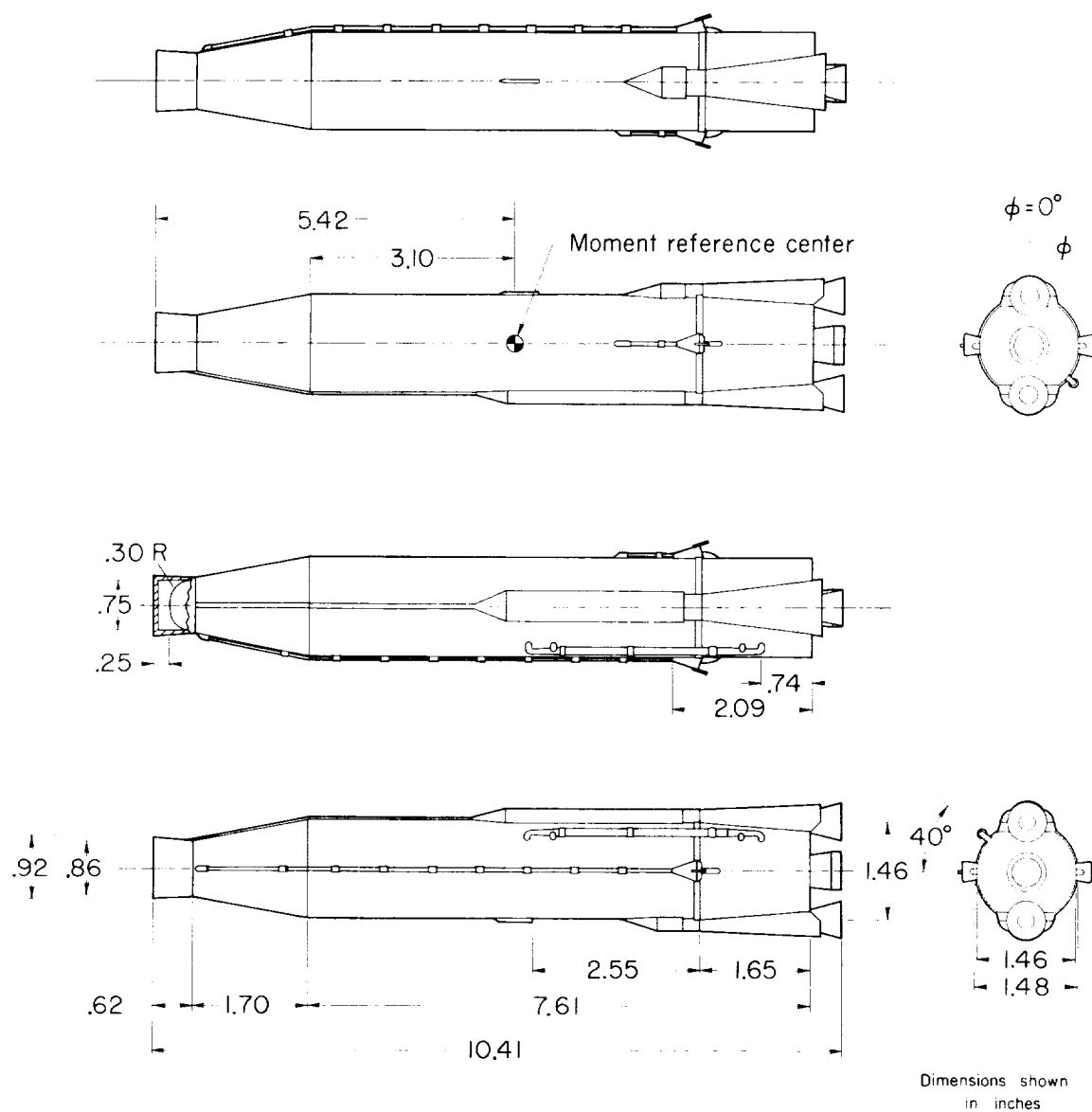
(a) Complete model.

Figure 1.- Sketches of models.

Preceding page blank

$\phi = 0°$

$\phi = 90°$
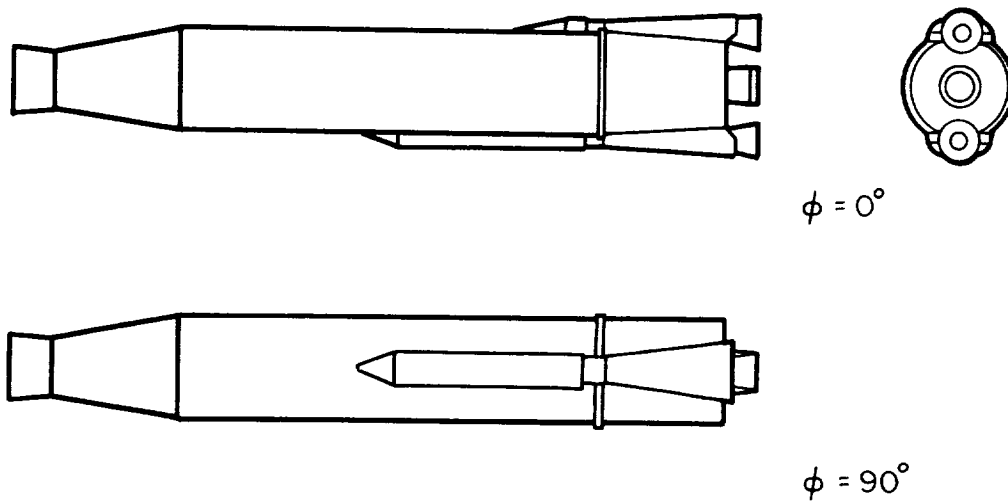
(b) Model without external fittings.

(c) Model without external fittings and engine fairings.

Figure 1.- Concluded.

NOT REPRODUCIBLE
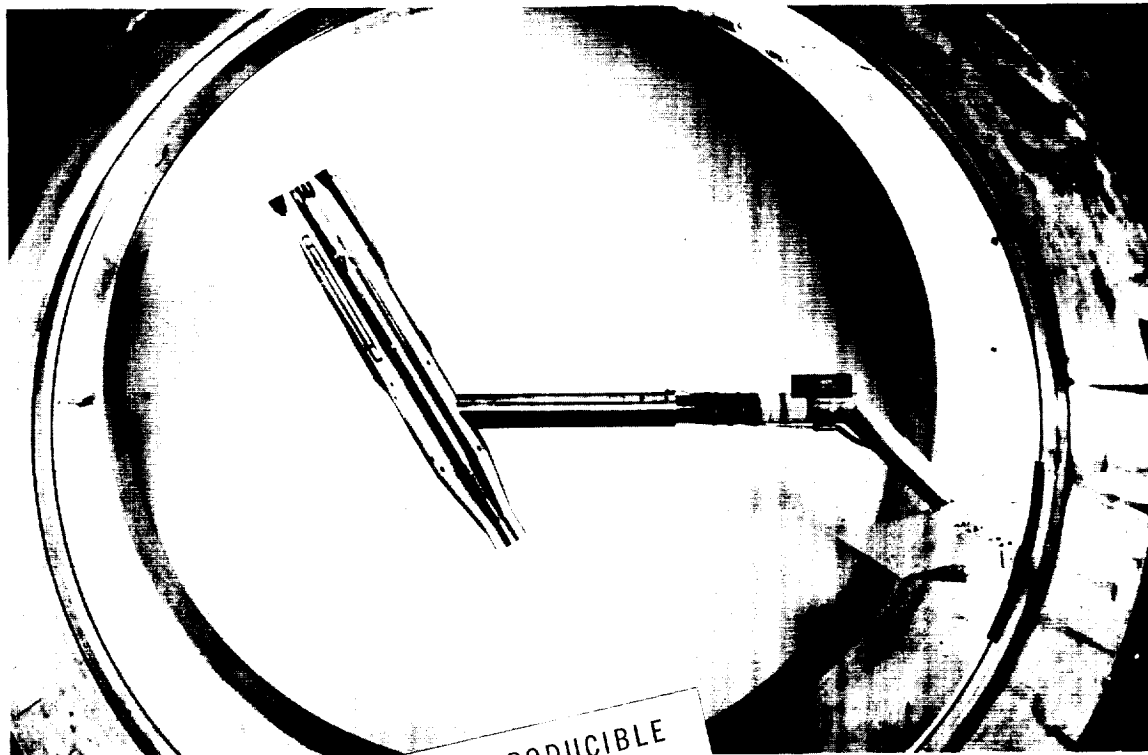
A-26684

(a) Model on mounting D in the Ames 1- by 3-foot wind tunnel.

Figure 2.- Photographs of the complete model.
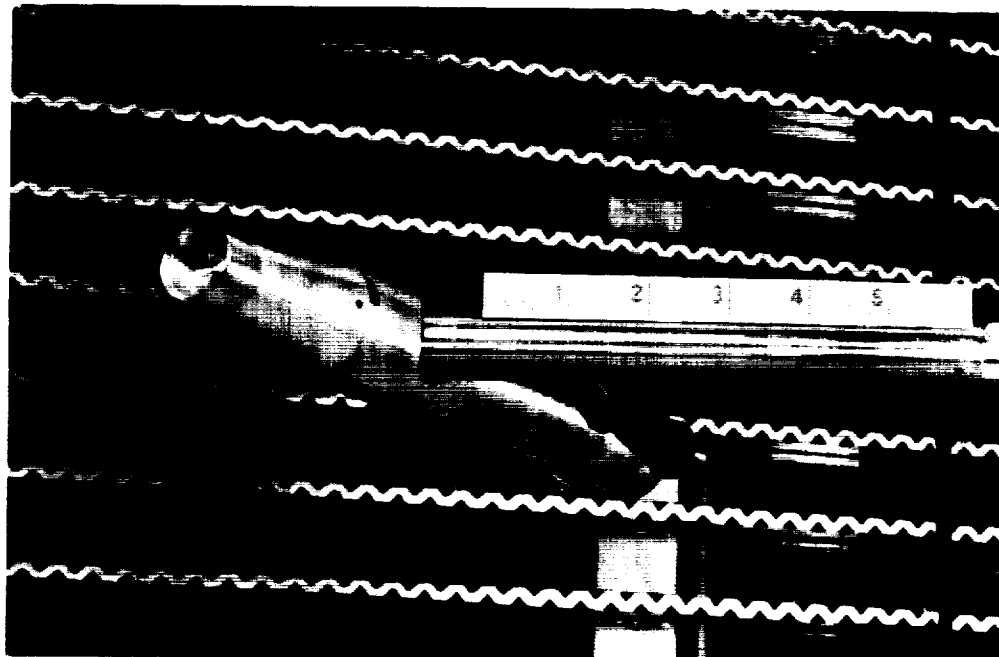
A-26580

(b) Model on mounting C in the Ames 2- by 2-foot transonic wind tunnel.
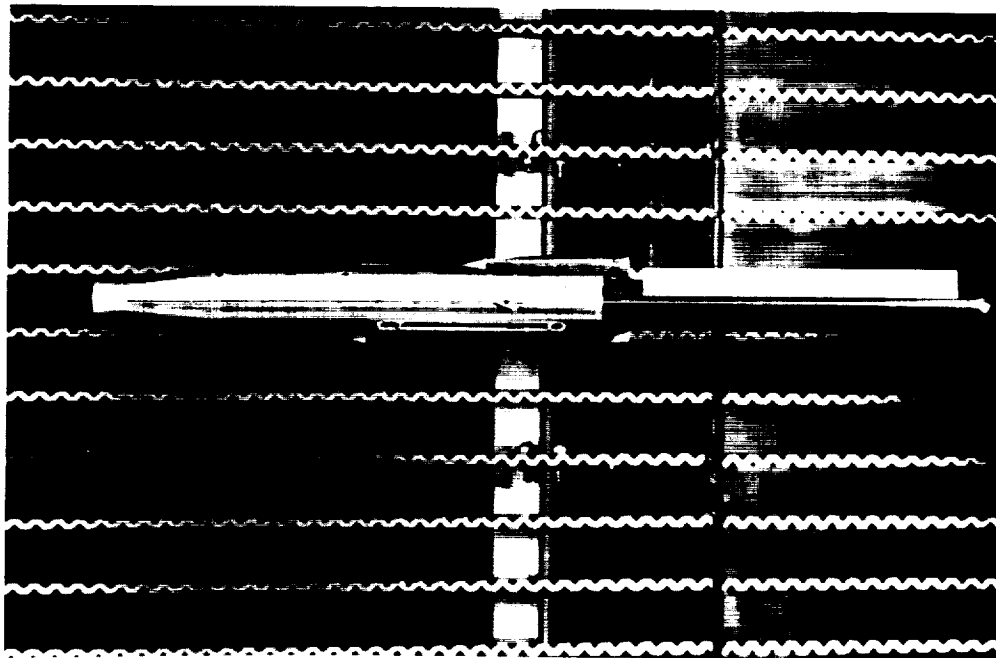
A-26581

(c) Model on mounting A in the Ames 2- by 2-foot transonic wind tunnel.

Figure 2.- Concluded.
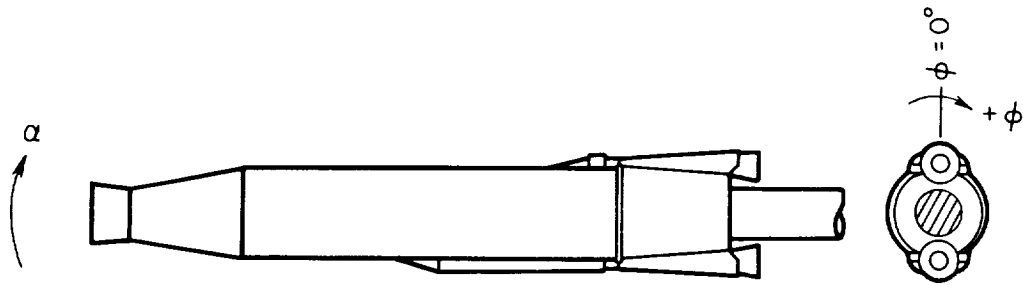
Mounting A, $\delta = 0°$
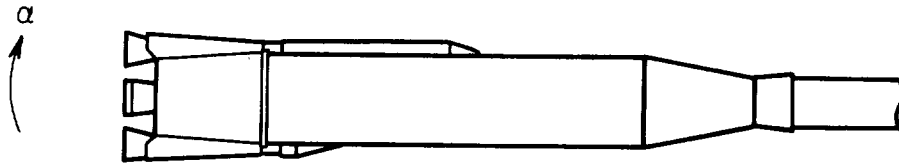
Mounting B, $\delta = 180°$

Mounting C

$\delta = 60°$

$\delta = 120°$
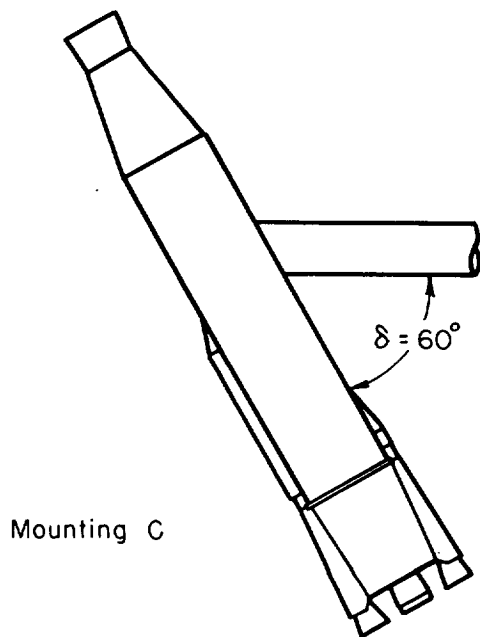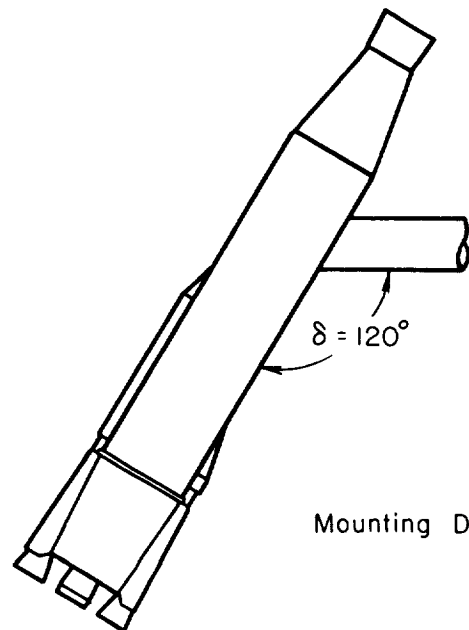
Mounting D

Figure 3.- Model mounting orientation.
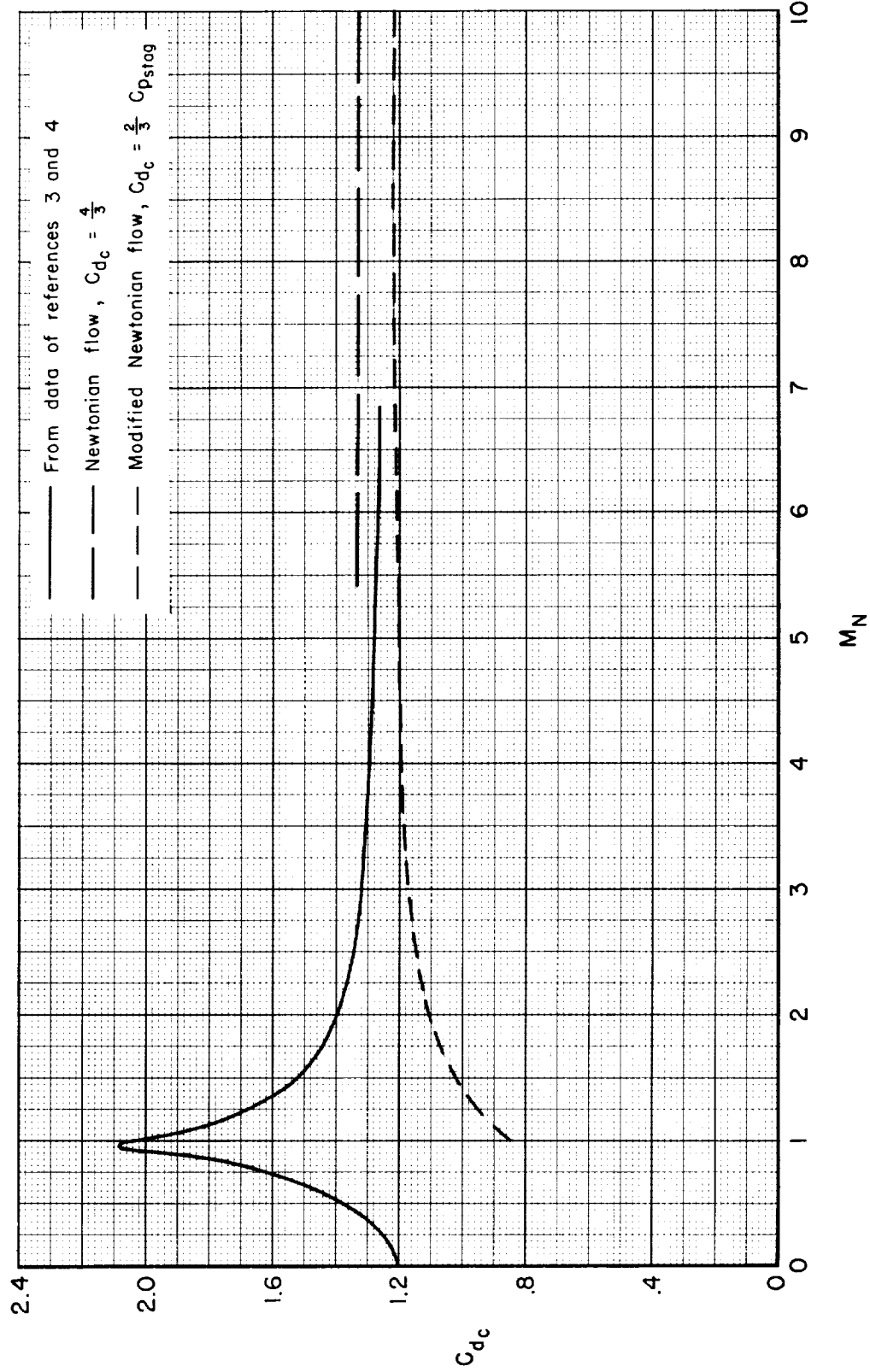
Figure 4.- Variation with normal Mach number of crossflow drag coefficient of a circular cylinder.
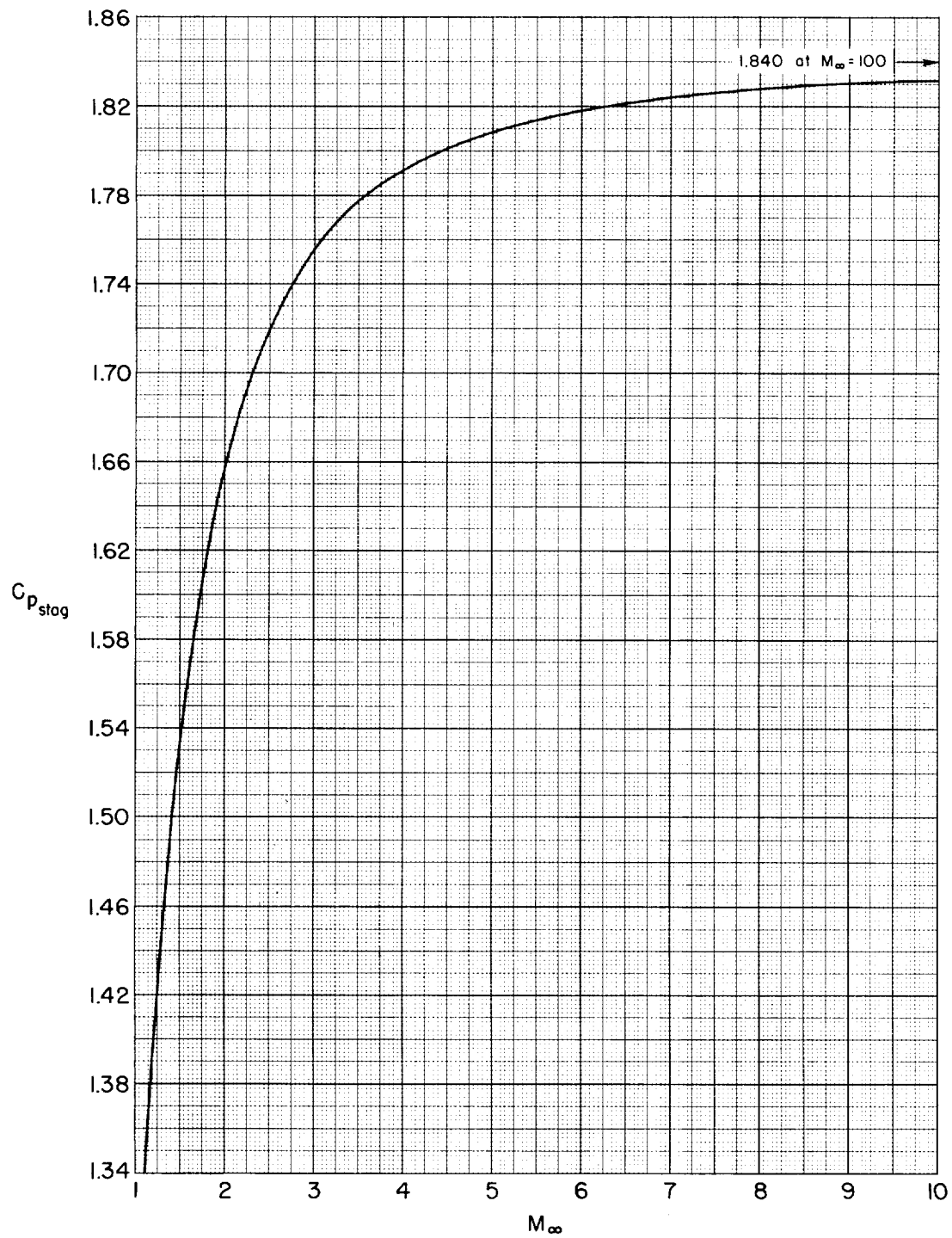
Figure 5.- Variation with Mach number of the stagnation pressure coefficient computed from perfect-gas relations.
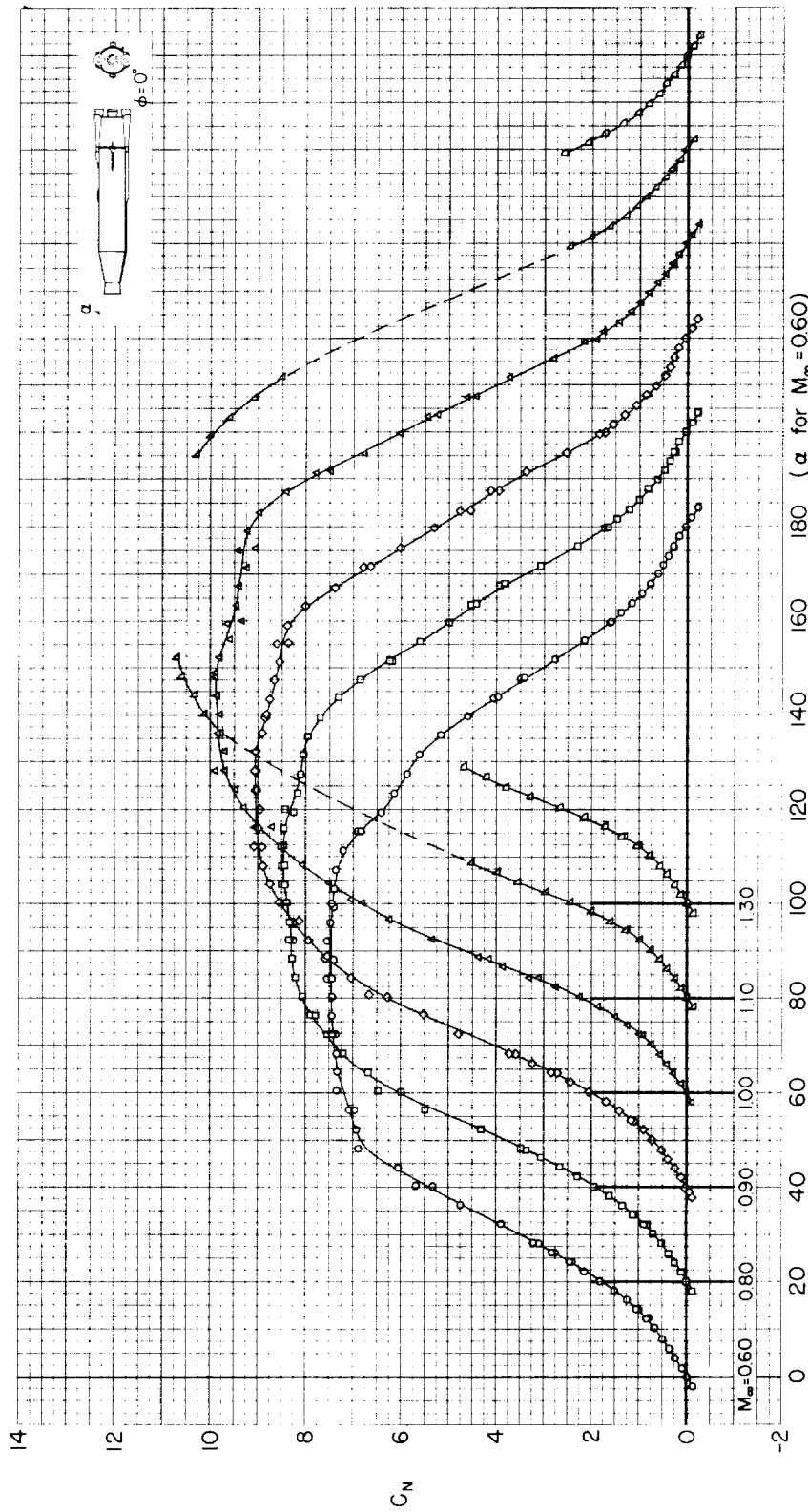
(a) C_N vs α ; $M_\infty = 0.60$ to 1.30

Figure 6.– Static aerodynamic coefficients for the complete model; $\phi = 0°$.
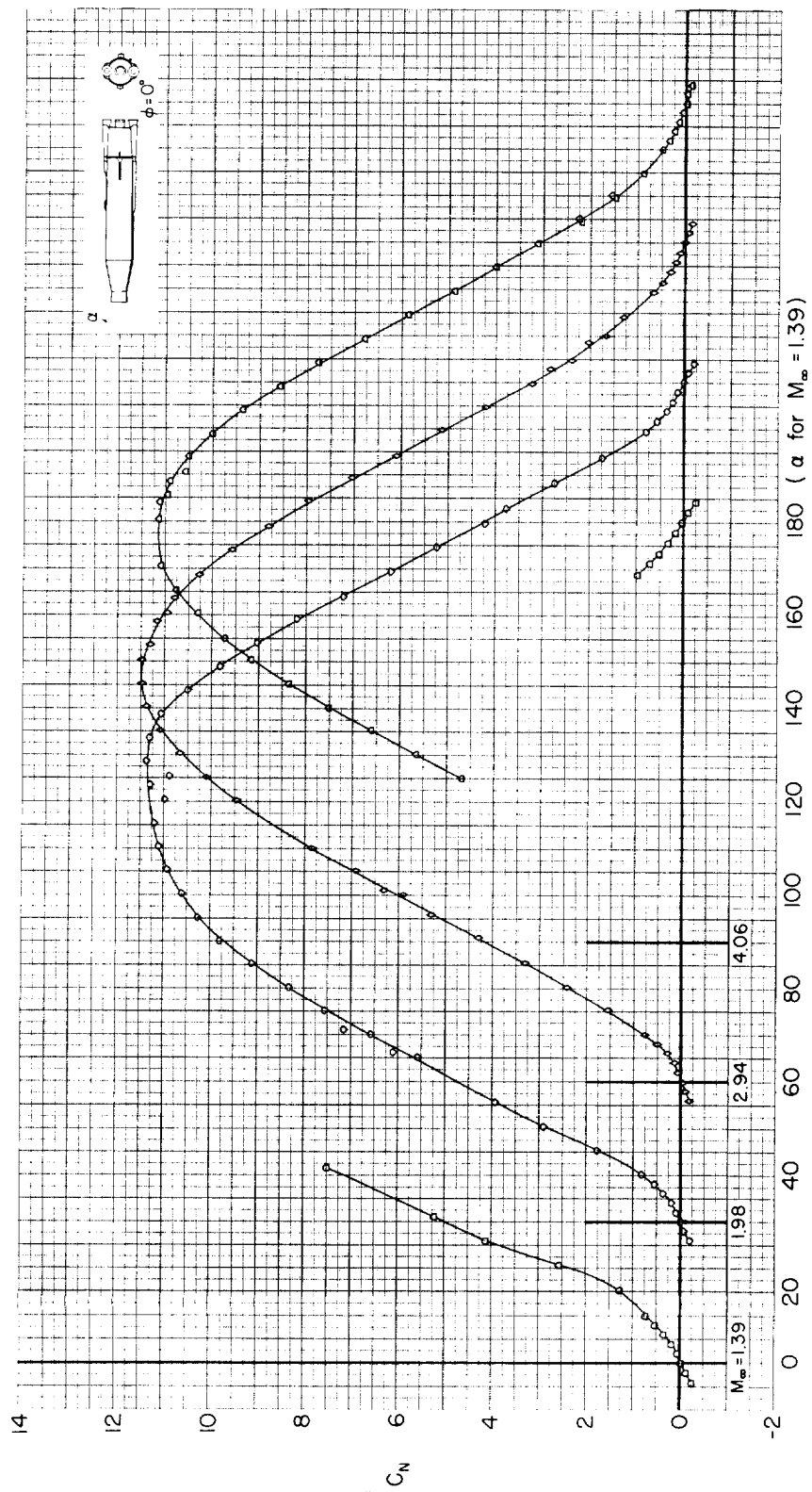
(b) C_N vs α; $M_\infty = 1.39$ to 4.06

Figure 6.- Continued.
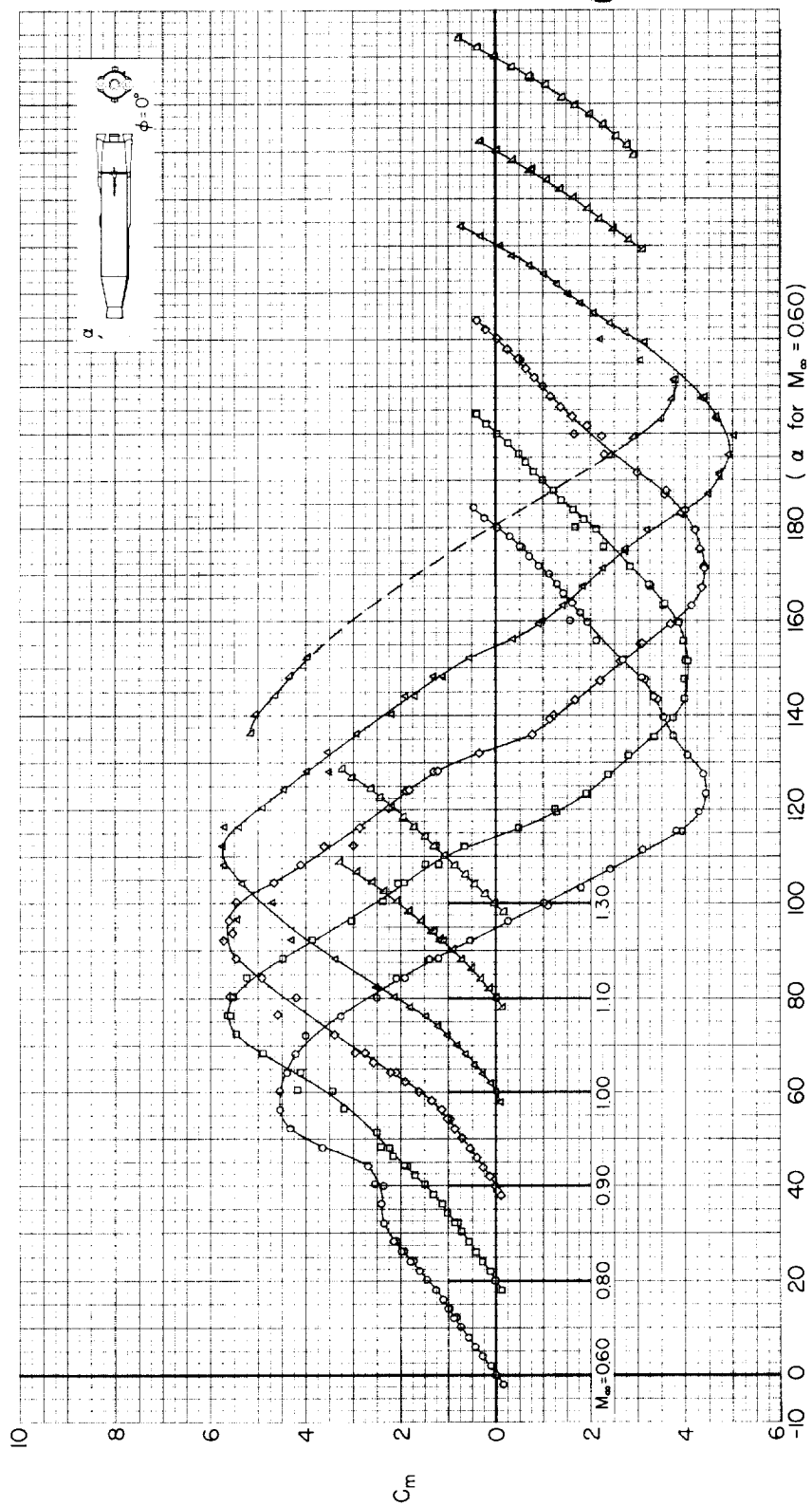
(c) C_m vs α; $M_\infty = 0.60$ to 1.30

Figure 6.- Continued.
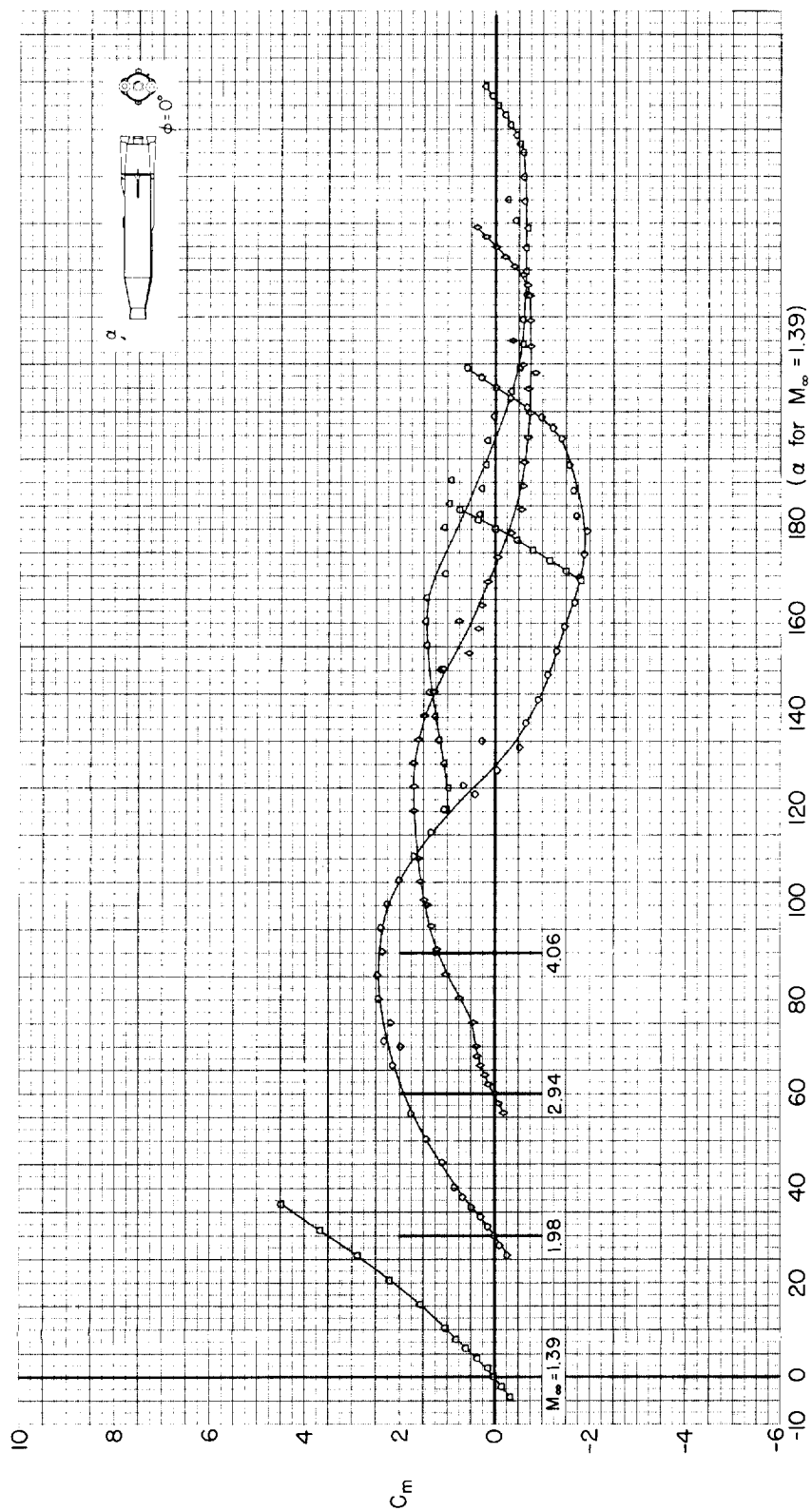
(d) C_m vs α; $M_\infty = 1.39$ to 4.06

Figure 6.- Continued.
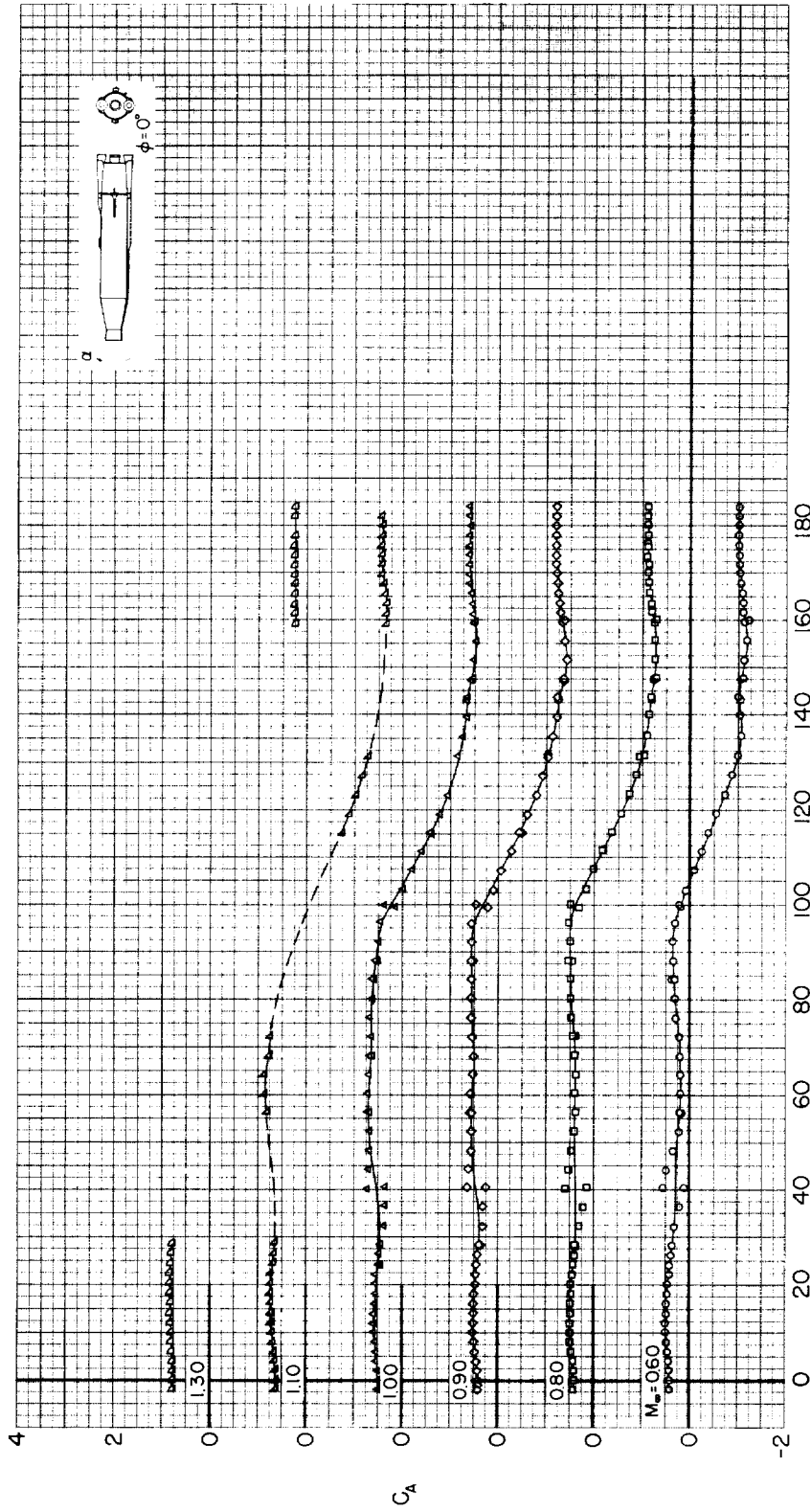
(e) C_A vs α; $M_\infty = 0.60$ to 1.30

Figure 6.- Continued.
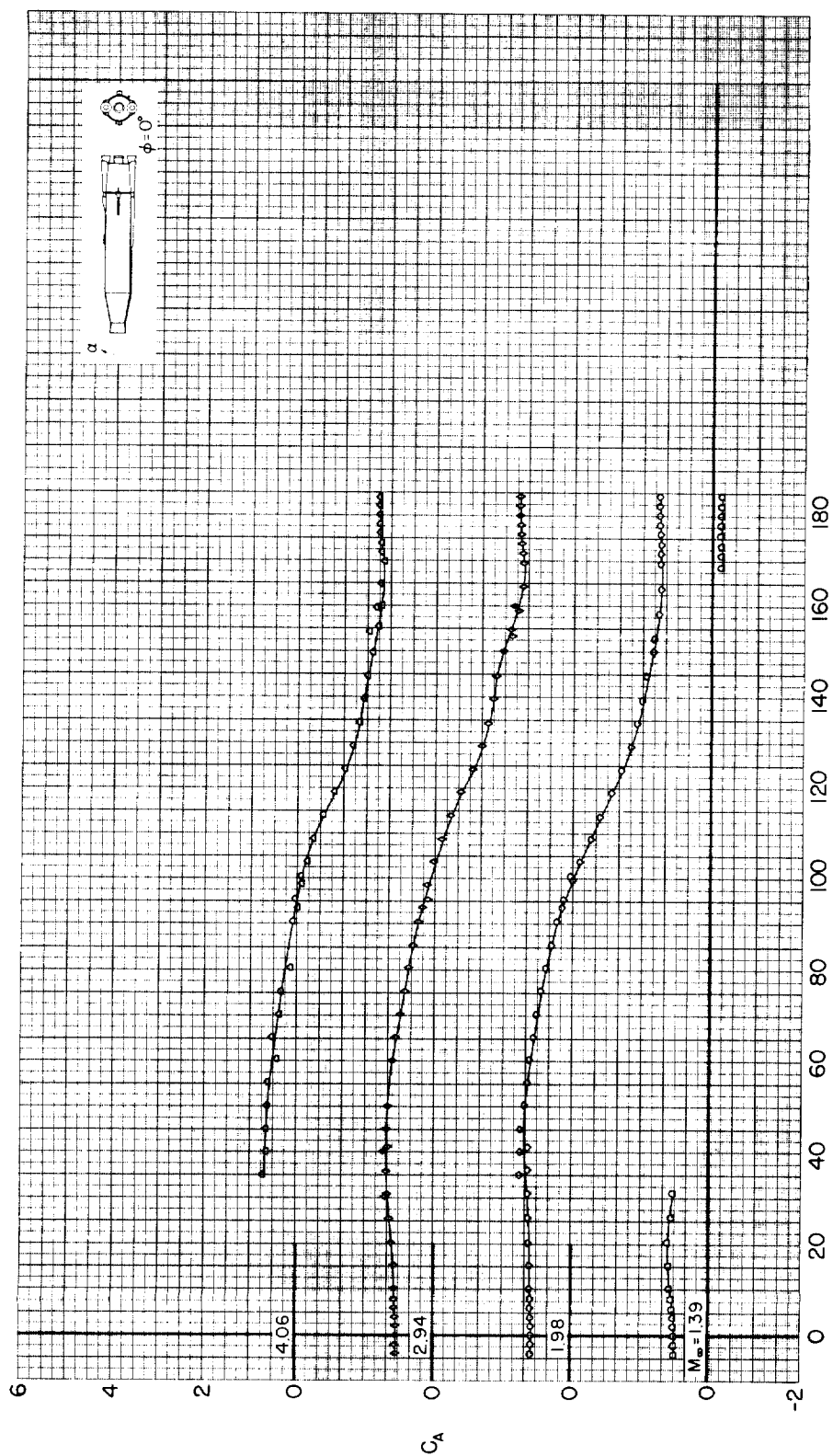
(f) C_A vs α ; M_∞ = 1.39 to 4.06

Figure 6.- Concluded.
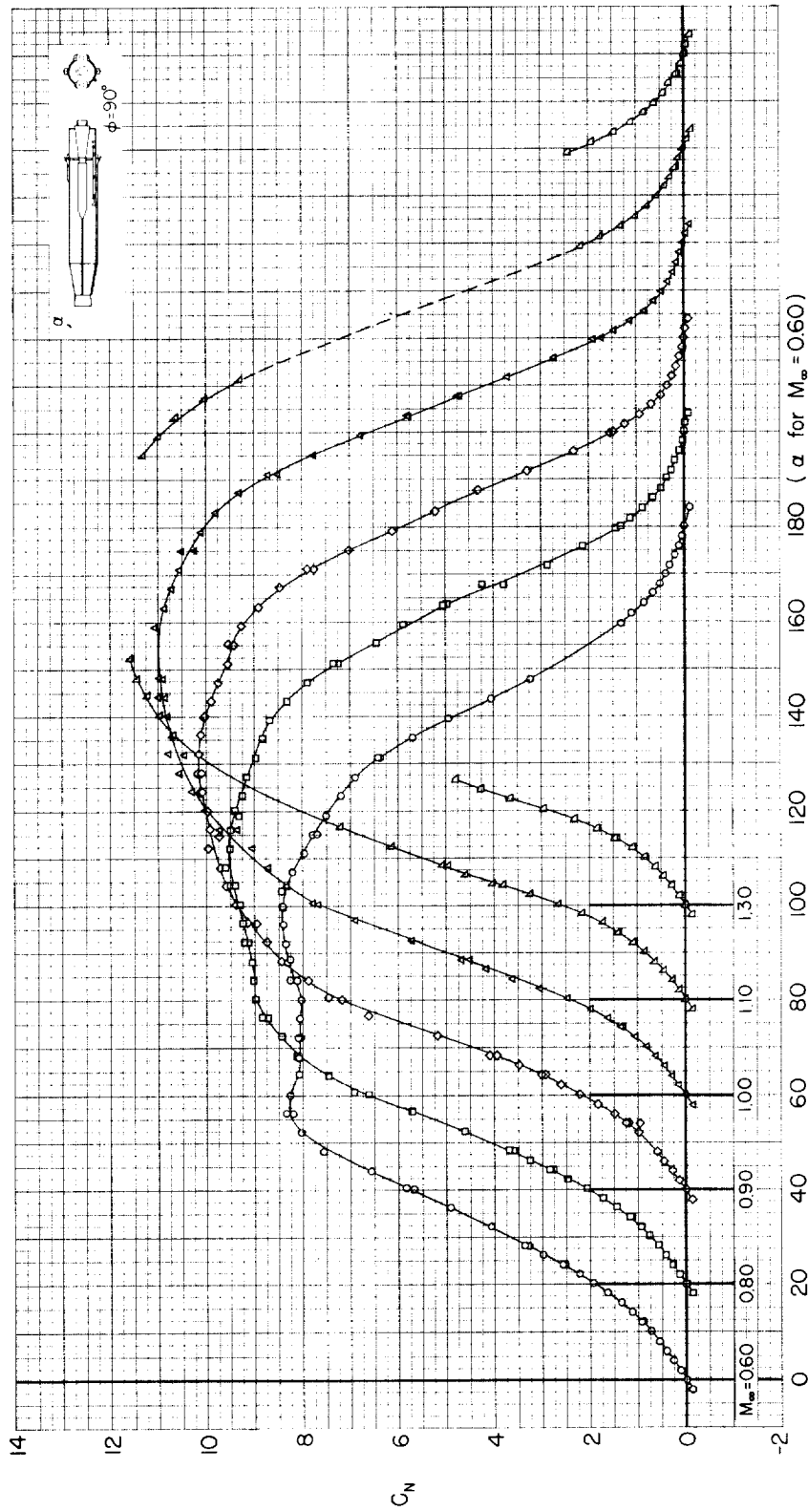
(a) C_N vs α; $M_\infty = 0.60$ to 1.30

Figure 7.- Static aerodynamic coefficients for the complete model; $\psi = 90°$.
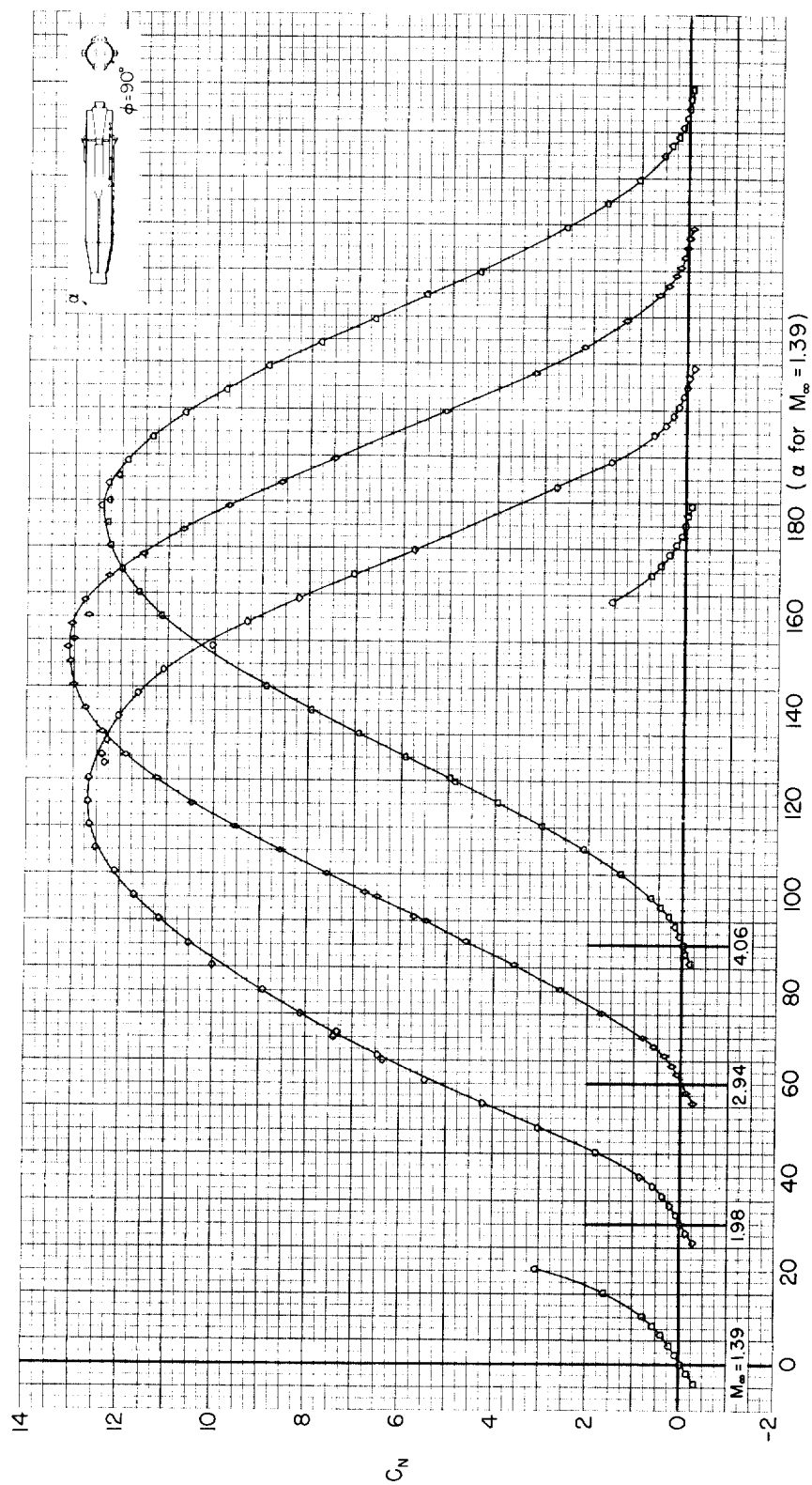
(b) C_N vs α; $M_\infty = 1.39$ to 4.06

Figure 7.- Continued.
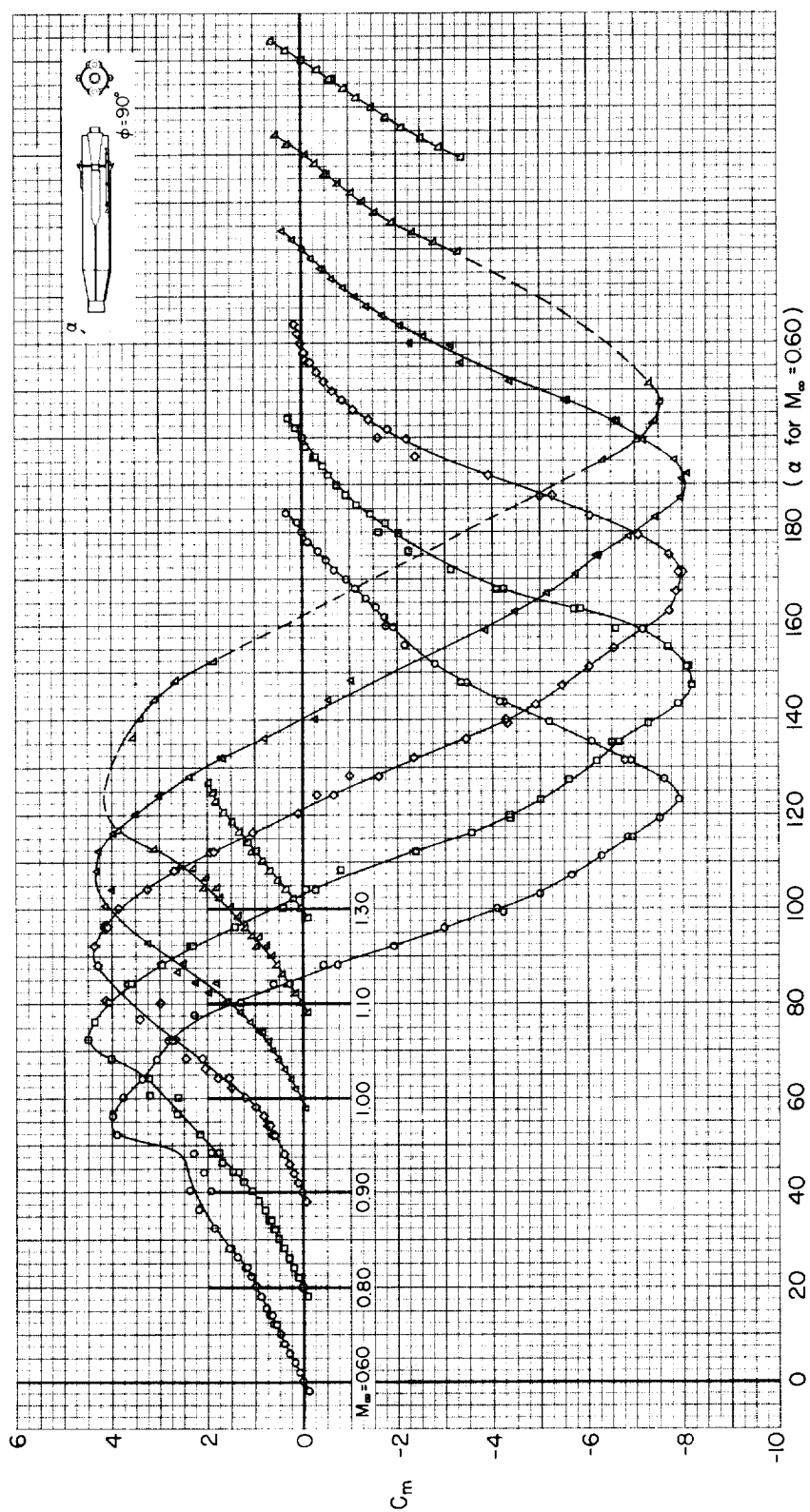
(c) C_m vs α; $M_\infty = 0.60$ to 1.30

Figure 7.- Continued.
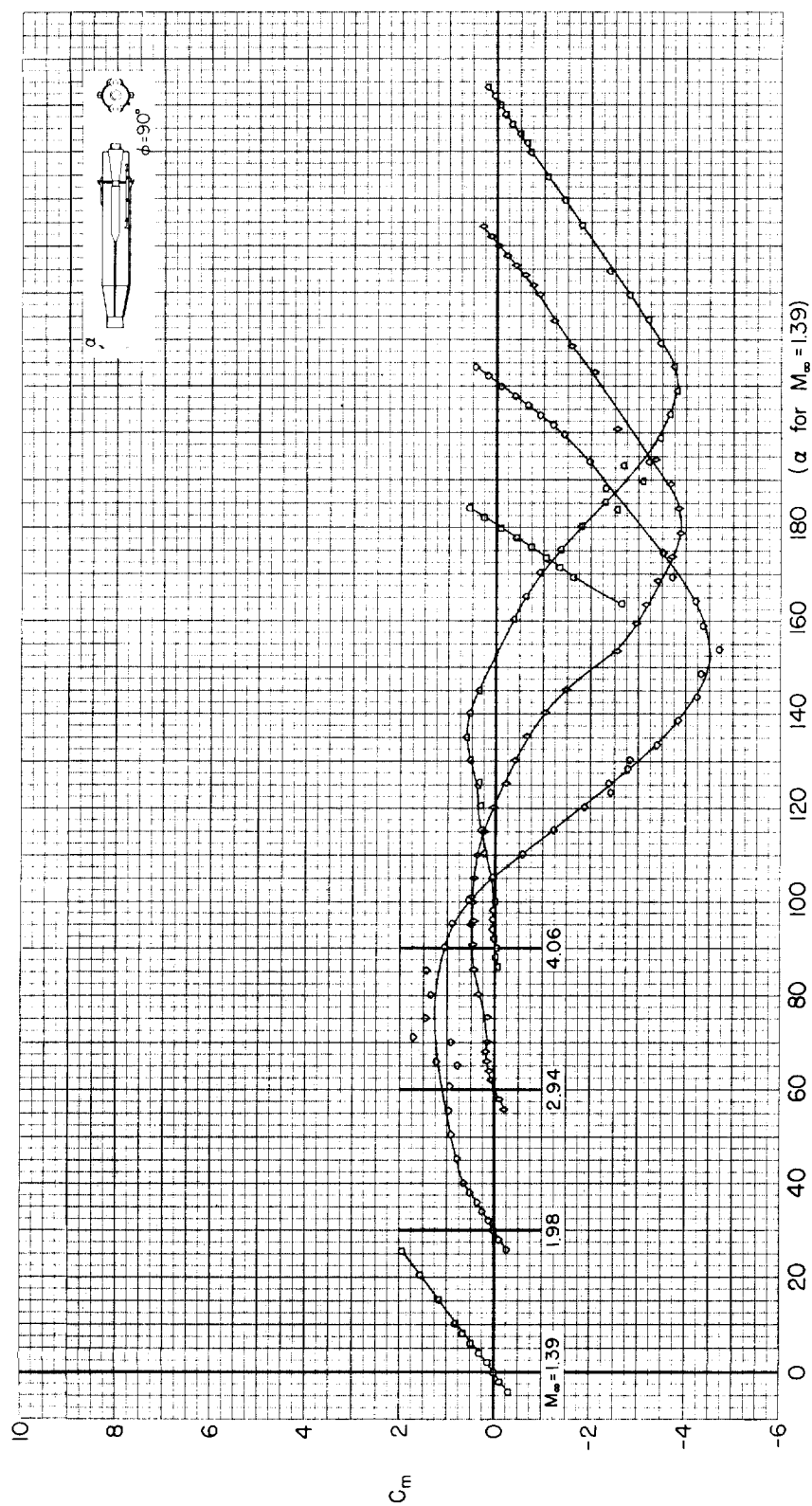
(d) C_m vs α; $M_\infty = 1.39$ to 4.06

Figure 7.- Continued.
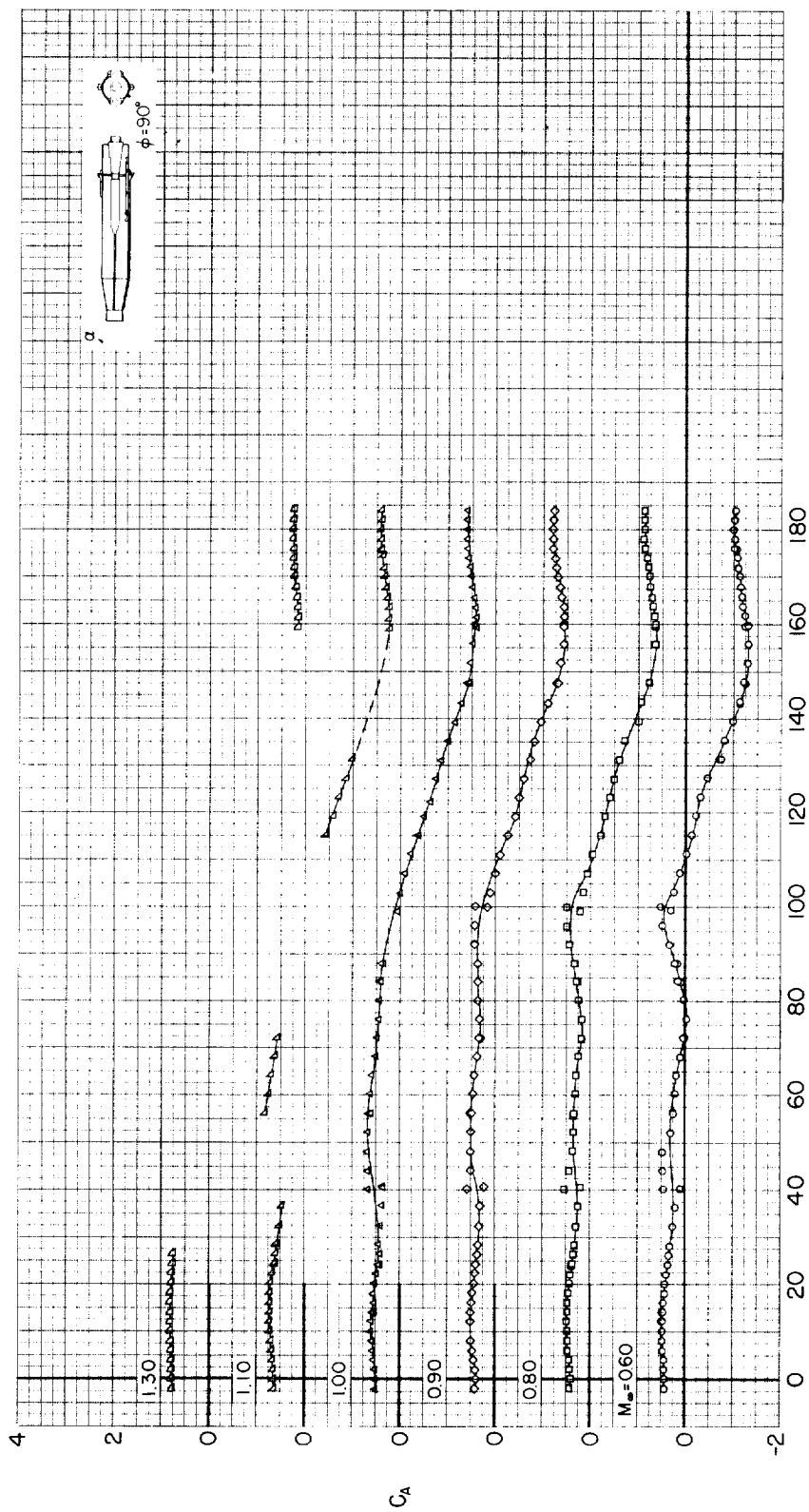
(e) C_A vs α; $M_\infty = 0.60$ to 1.30.

Figure 7.- Continued.
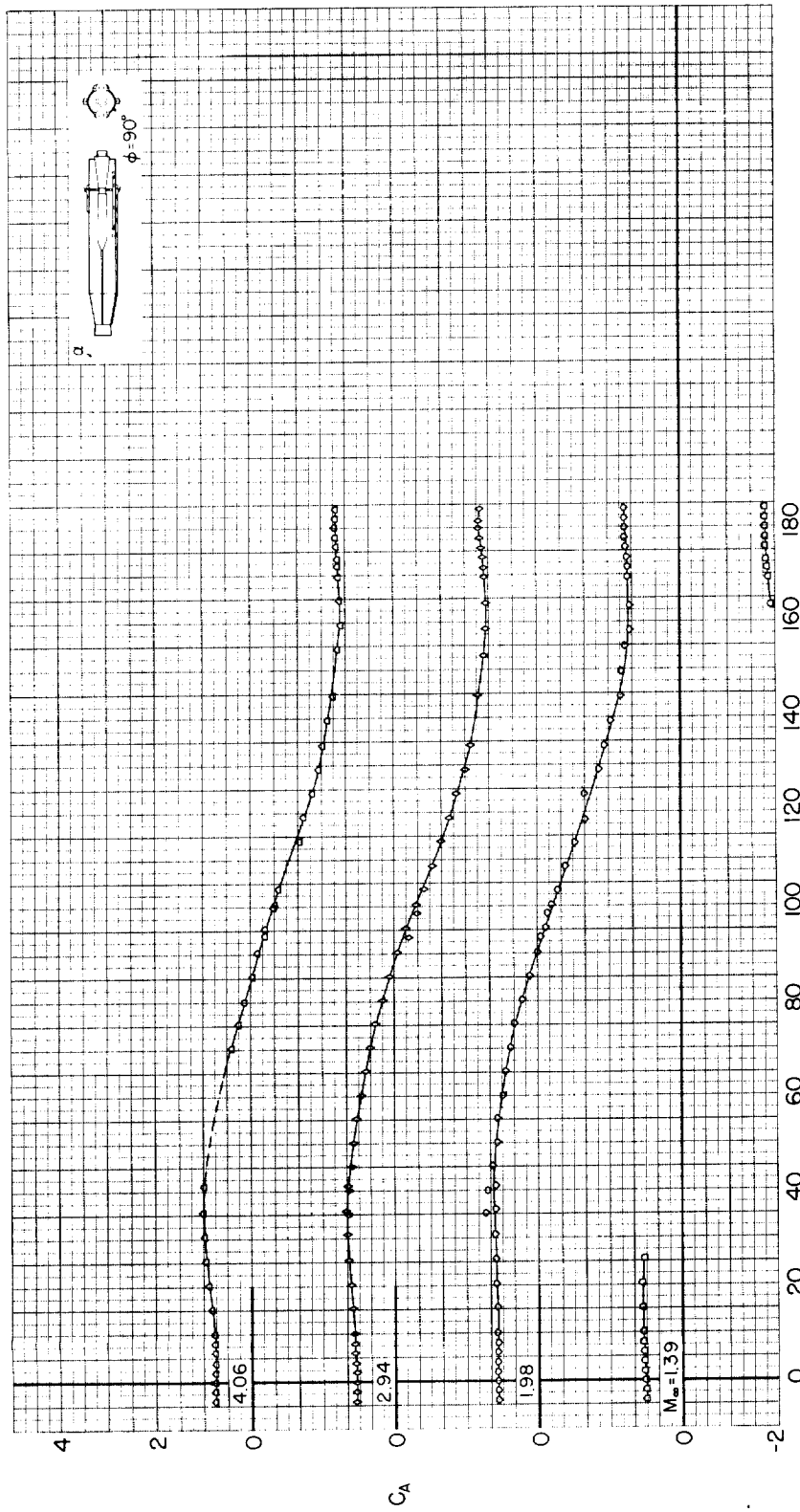
(f) C_A vs α; M_∞ = 1.39 to 4.06

Figure 7.- Concluded.
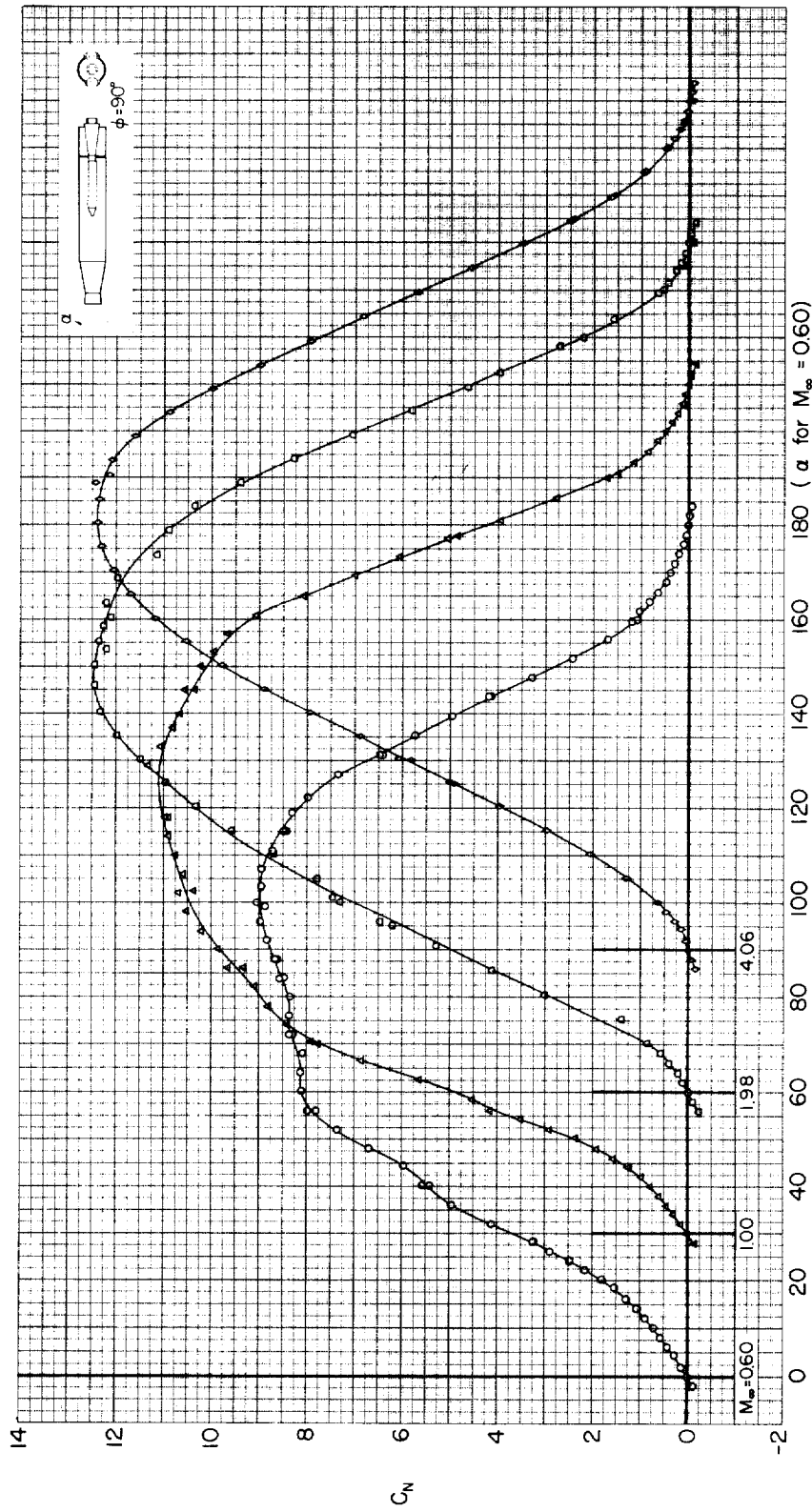
(a) C_N vs α; $M_\infty = 0.60$ to 4.06

Figure 8.- Static aerodynamic coefficients for the model without external fittings; $\varphi = 90°$.
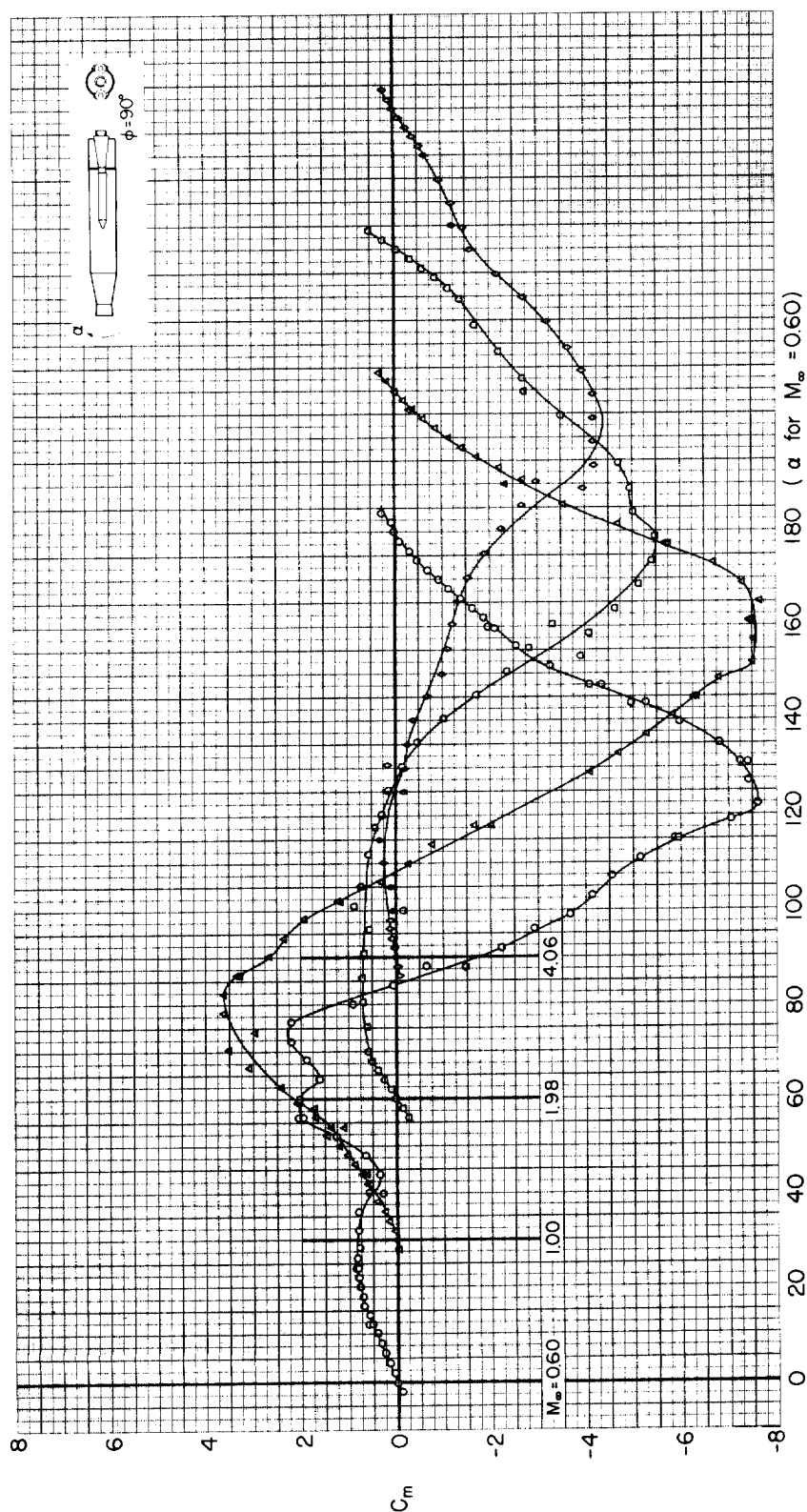
(b) C_m vs α; $M_\infty = 0.60$ to 4.06

Figure 8.- Continued.
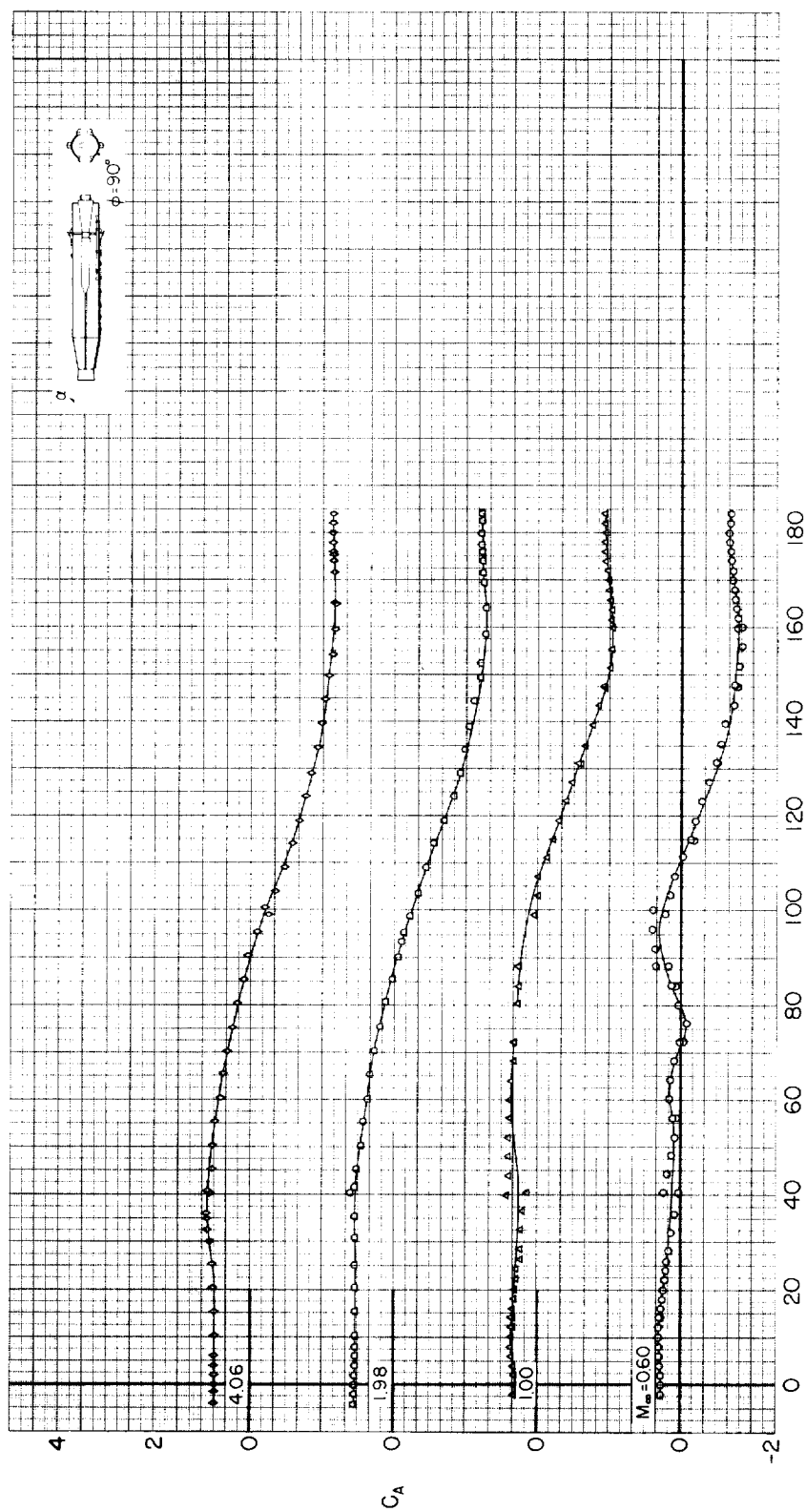
(c) C_A vs α, $M_\infty = 0.60$ to 4.06

Figure 8.- Concluded.
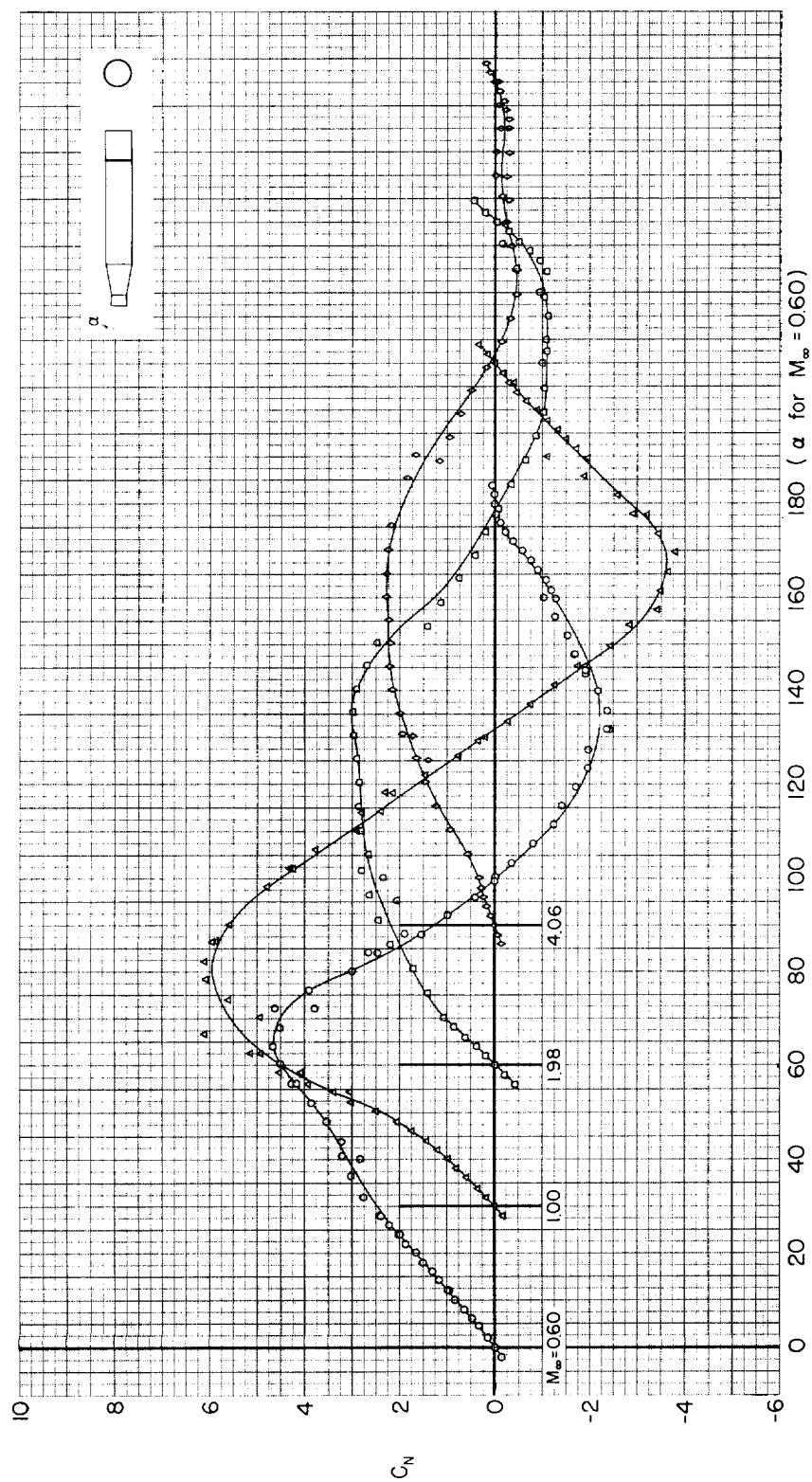
(a) C_N vs α ; $M_\infty = 0.60$ to 4.06

Figure 9.- Static aerodynamic coefficients for the model without external fittings and engine fairings.
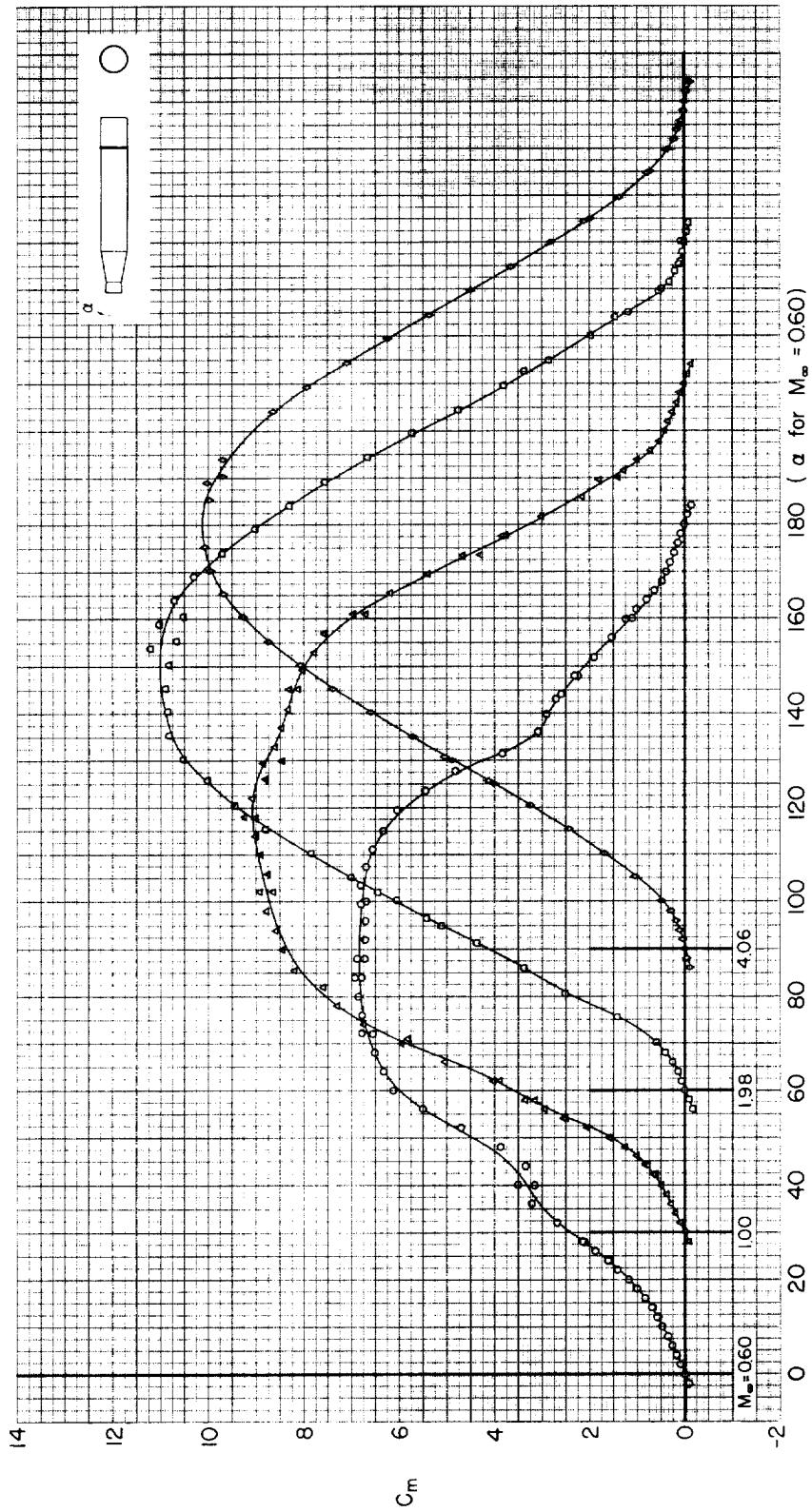
(b) C_m vs α; $M_\infty = 0.60$ to 4.06

Figure 9.- Continued.
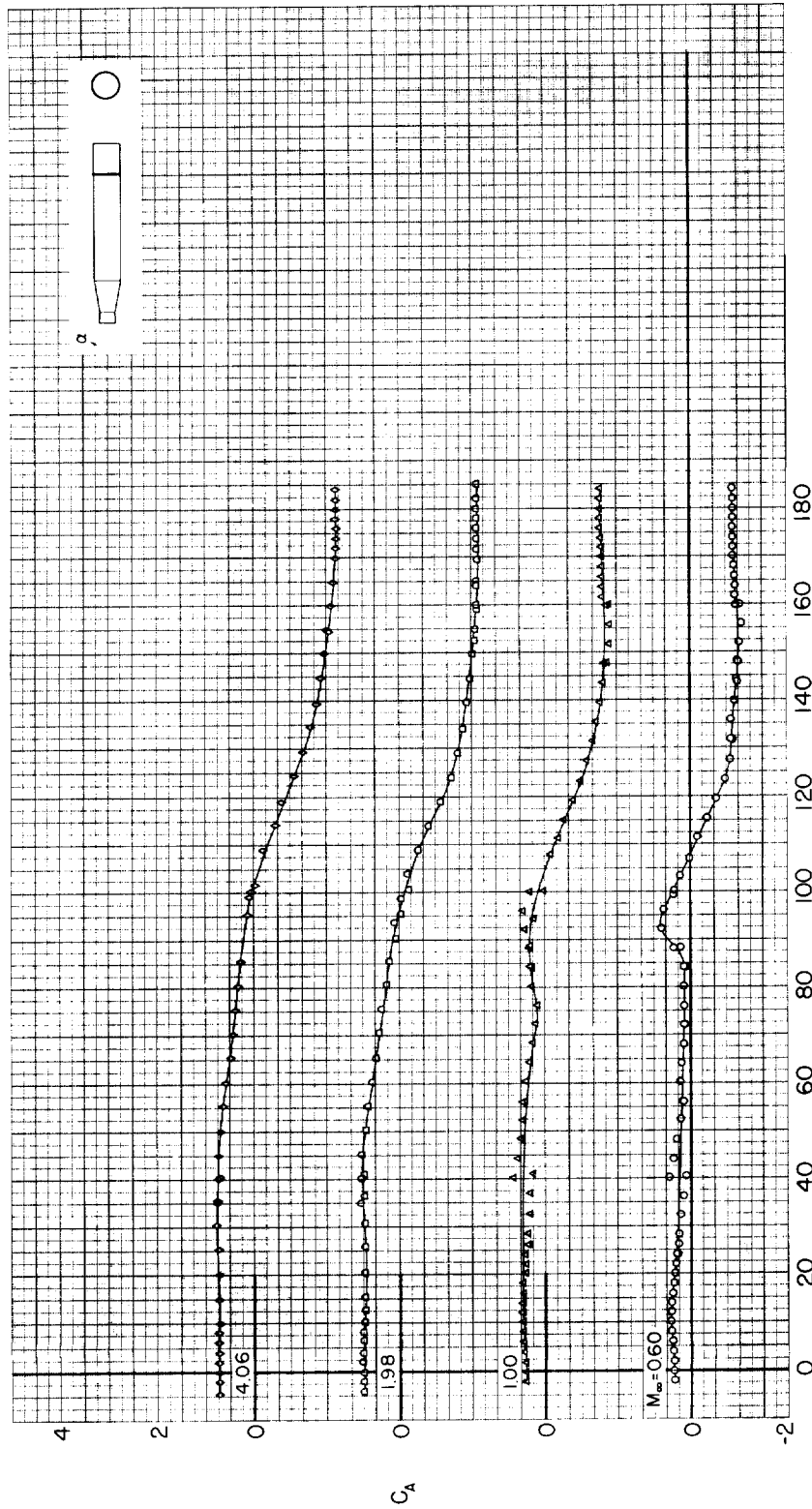
(c) C_A vs α ; $M_\infty = 0.60$ to 4.06

Figure 9.- Concluded.
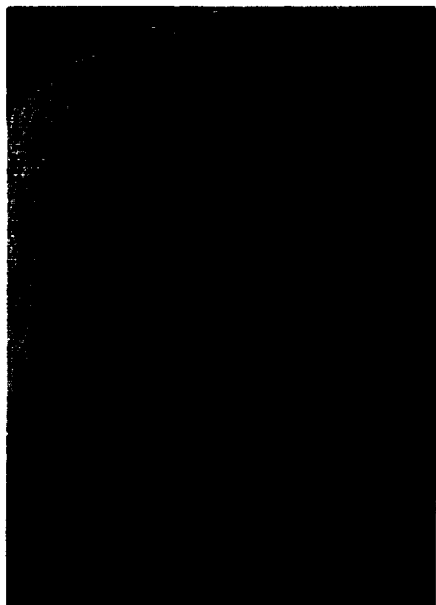
$\alpha = 40°$

$\alpha = 180°$

$\alpha = 0°$

$\alpha = 10°$

Figure 10.- Shadowgraph pictures of the complete model at $M_\infty = 1.39$, $\varphi = 0°$.

A
4
9
6

$\alpha = 40^{\circ}$

$\alpha = 180^{\circ}$

$\alpha = 0^{\circ}$

$\alpha = 10^{\circ}$

Figure 11.- Shadowgraph pictures of the complete model at $M_{\infty} = 1.39$, $\varphi = 90^{\circ}$.

$\alpha = 0^{\circ}$

$\alpha = 10^{\circ}$

$\alpha = 30^{\circ}$
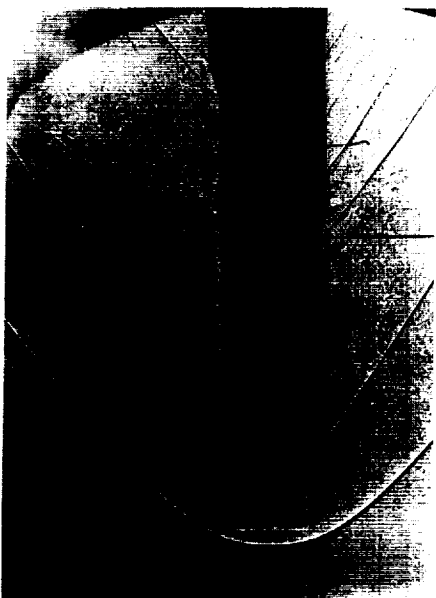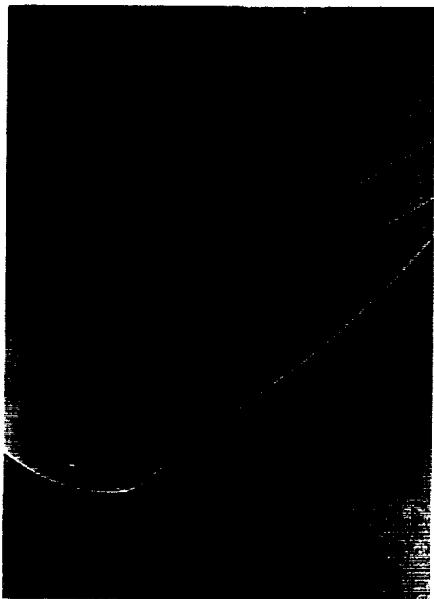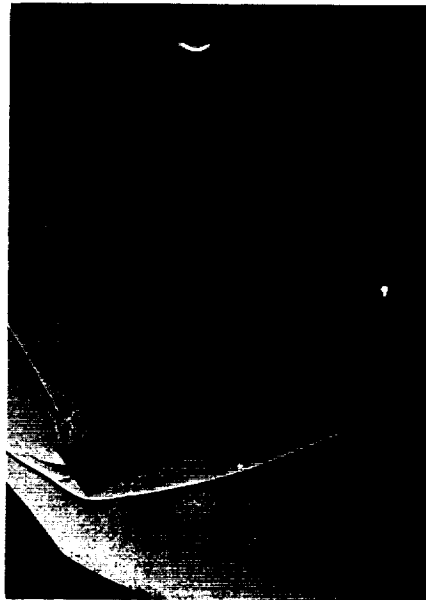
$\alpha = 60^{\circ}$

(a) $\alpha = 0^{\circ}$ to 60°

Figure 12.- Shadowgraph pictures of the complete model at $M_{\infty} = 1.98$, $\varphi = 0^{\circ}$.

A
4
9
6

A
4
9
6
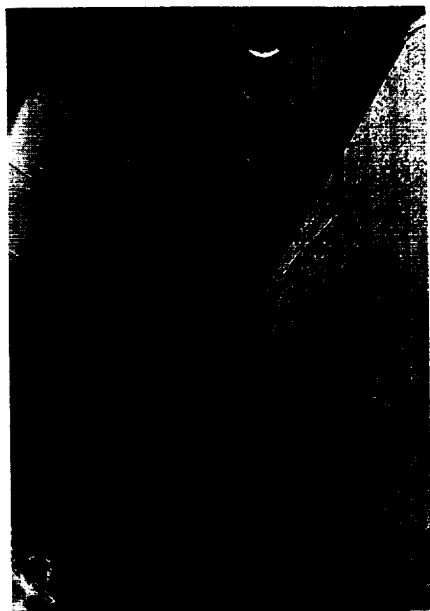
$\alpha = 150^\circ$
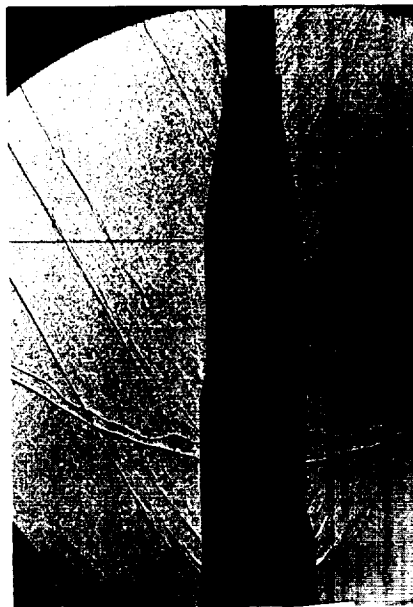
$\alpha = 180^\circ$

$\alpha = 90^\circ$

$\alpha = 120^\circ$
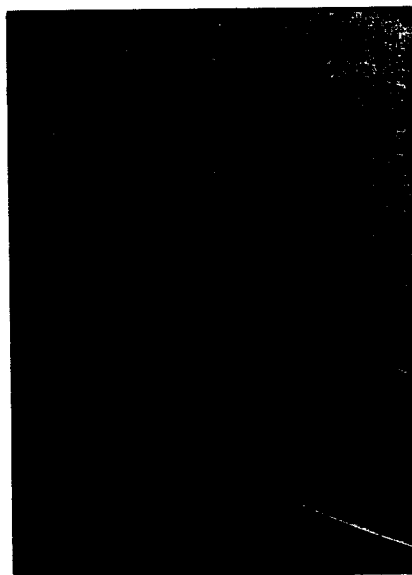
NOT REPRODUCIBLE

(b) $\alpha = 90^\circ$ to 180°

Figure 12.- Concluded.

$\alpha = 0^{o}$

$\alpha = 30^{o}$

$\alpha = 10^{o}$

$\alpha = 60^{o}$

(a) $\alpha = 0^{o}$ to 60°
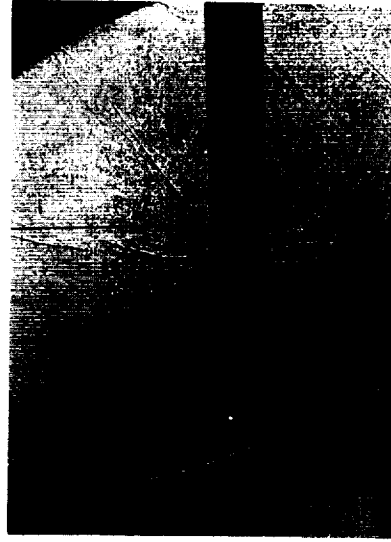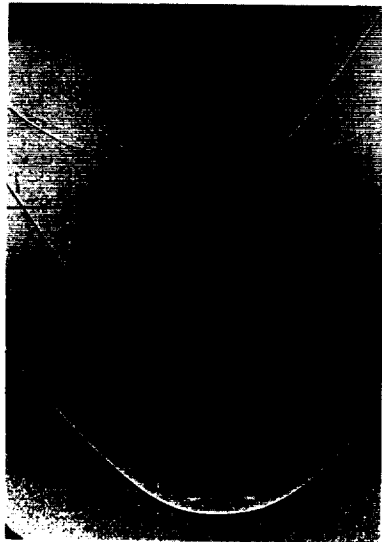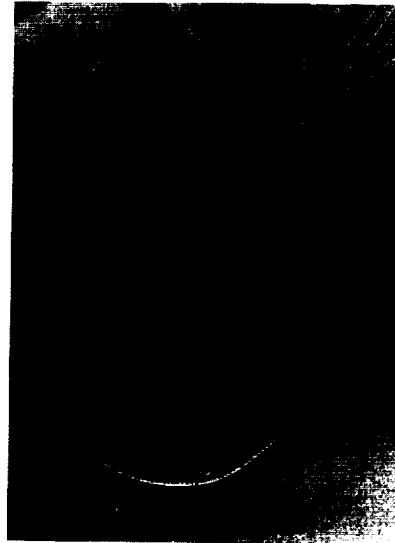
Figure 13.- Shadowgraph pictures of the complete model at $M_{\infty} = 1.98$, $\varphi = 90^{o}$.

A
4
9
6

α = 150°

α = 180°

α = 90°

α = 120°

NOT REPRODUCIBLE

(b) α = 90° to 180°

Figure 13.- Concluded.
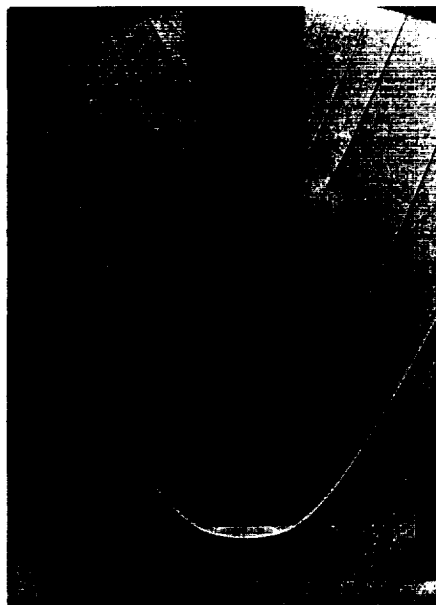
$\alpha = 0^{\circ}$

$\alpha = 120^{\circ}$
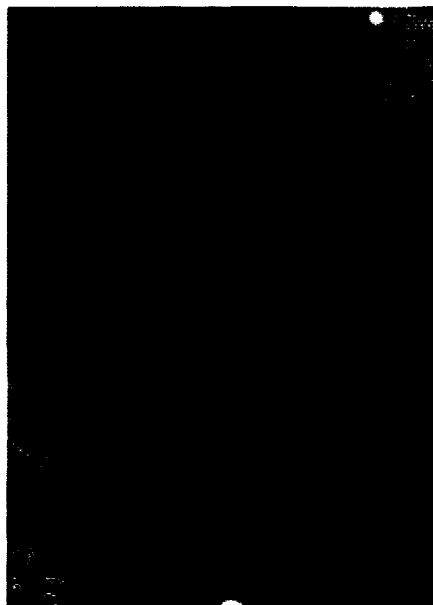
$\alpha = 60^{\circ}$
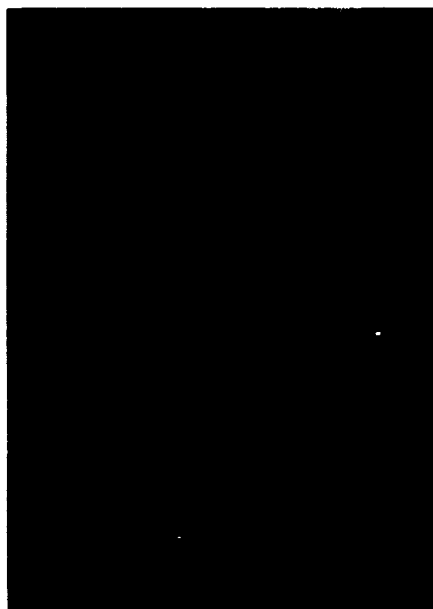
$\alpha = 180^{\circ}$

Figure 14.- Shadowgraph pictures of the complete model at $M_{\infty} = 2.94$, $\varphi = 0^{\circ}$.

α = 0°

α = 10°

α = 30°
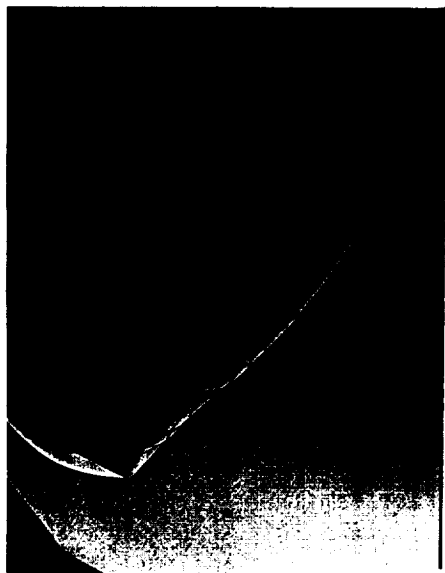
α = 60°

NOT REPRODUCIBLE
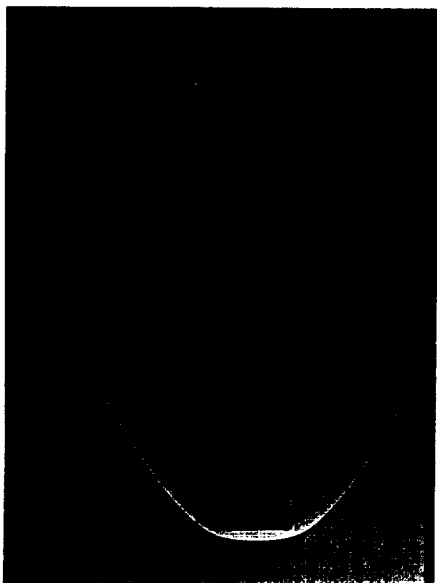
(a) α = 0° to 60°

Figure 15.- Shadowgraph pictures of the complete model at $M_\infty = 2.94$, $\varphi = 90°$.

$\alpha = 90^{\circ}$

$\alpha = 150^{\circ}$

$\alpha = 110^{\circ}$

$\alpha = 180^{\circ}$
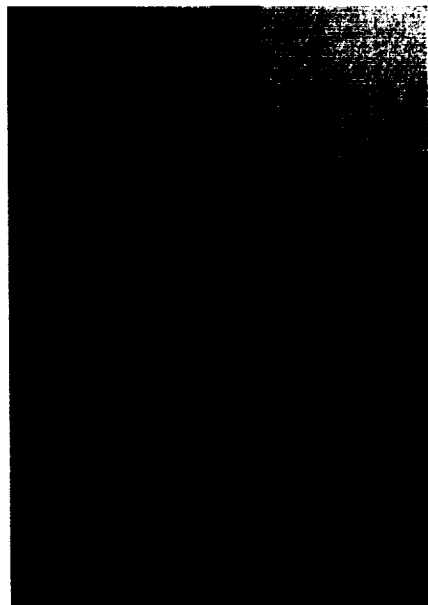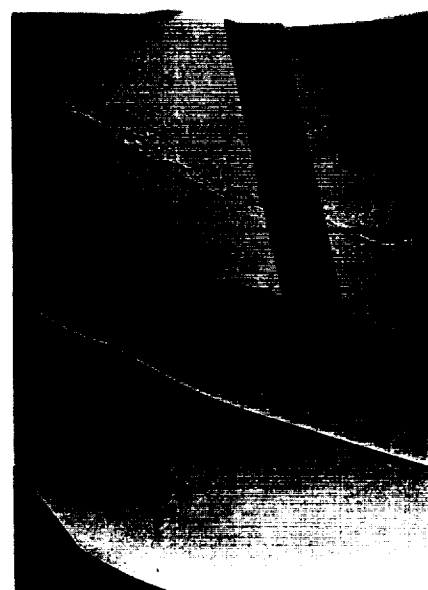
(b) $\alpha = 90^{\circ}$ to 180°

Figure 15.- Concluded.

$\alpha = 60^{\circ}$

$\alpha = 70^{\circ}$

$\alpha = 50^{\circ}$

$\alpha = 40^{\circ}$
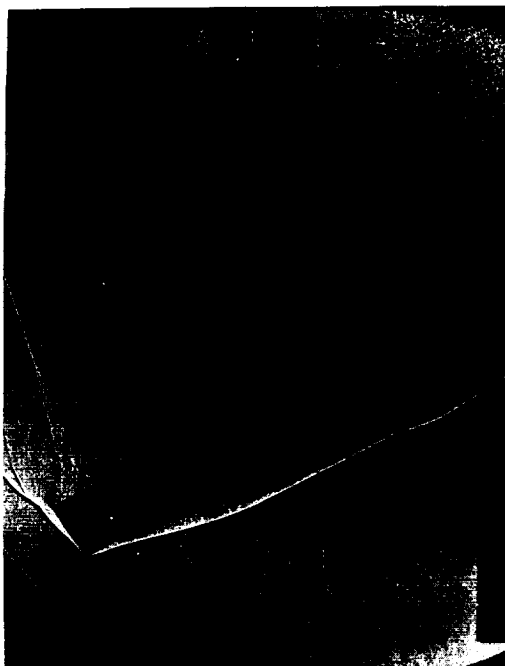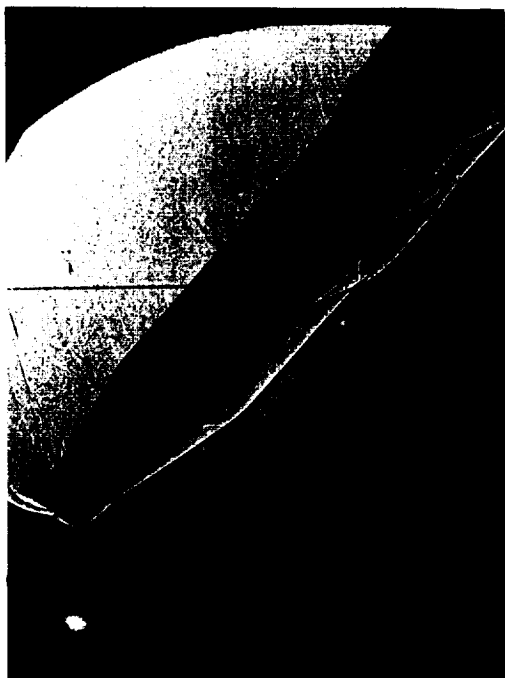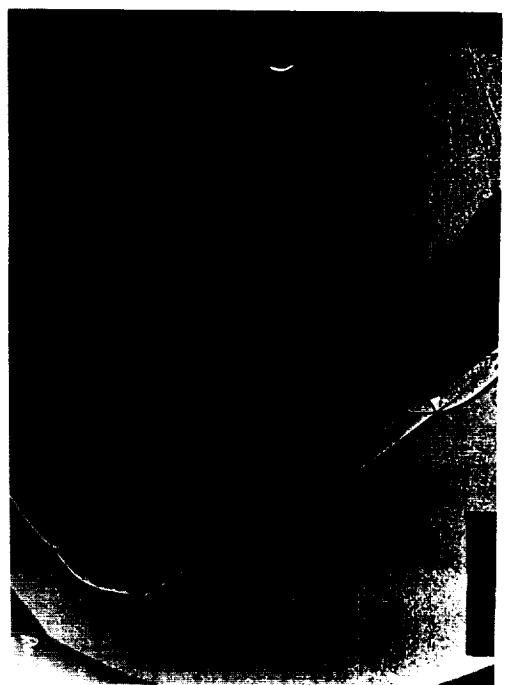
NOT REPRODUCIBLE

(a) $\alpha = 40^{\circ}$ to 70°

Figure 16.- Shadowgraph pictures of the complete model at $M_\infty = 4.06$, $\varphi = 0^{\circ}$.

$\alpha = 150^{\circ}$

$\alpha = 180^{\circ}$

$\alpha = 90^{\circ}$

$\alpha = 120^{\circ}$
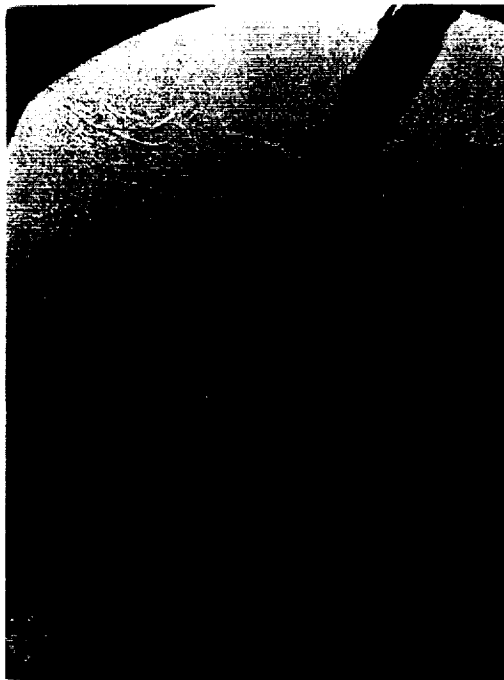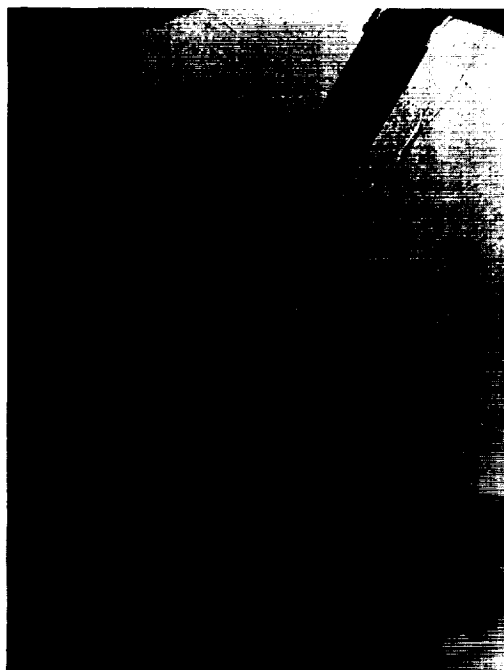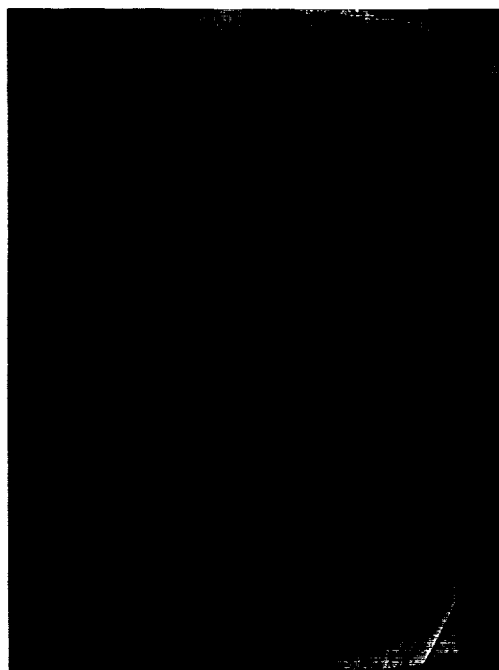
(b) $\alpha = 90^{\circ}$ to 180°

Figure 16.- Concluded.

A
4
9
6

NOT REPRODUCIBLE

$\alpha = 0^{\circ}$

$\alpha = 30^{\circ}$

$\alpha = 10^{\circ}$

$\alpha = 60^{\circ}$
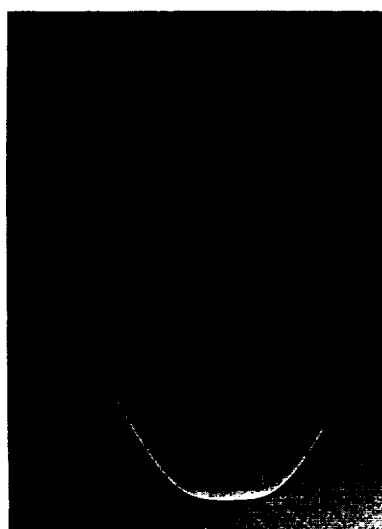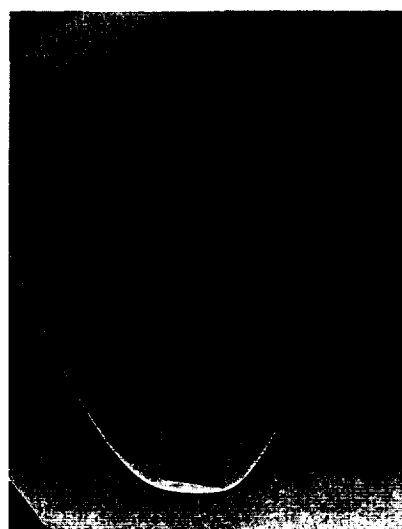
(a) $\alpha = 0^{\circ}$ to 60°

Figure 17.- Shadowgraph pictures of the complete model at $M_{\infty} = 4.06$, $\varphi = 90^{\circ}$.

$\alpha = 150^\circ$

$\alpha = 180^\circ$

$\alpha = 90^\circ$

$\alpha = 120^\circ$
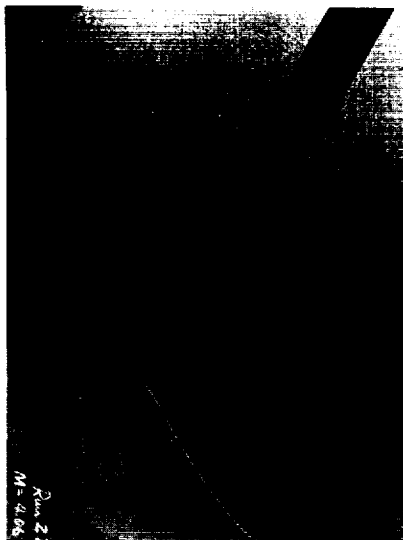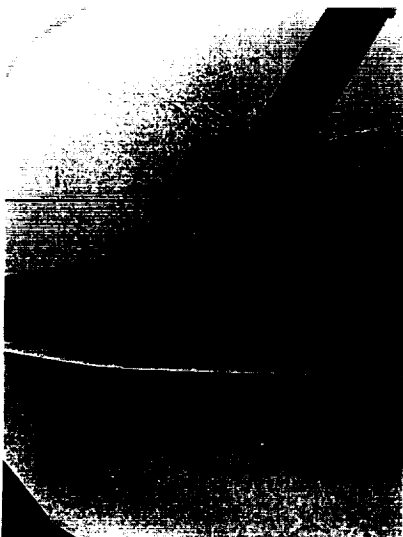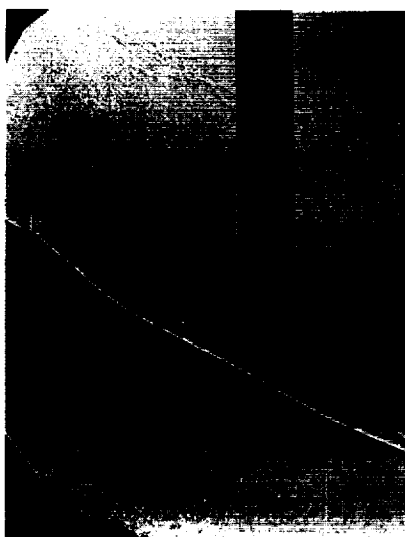
(b) $\alpha = 90^\circ$ to 180°

Figure 17.- Concluded.
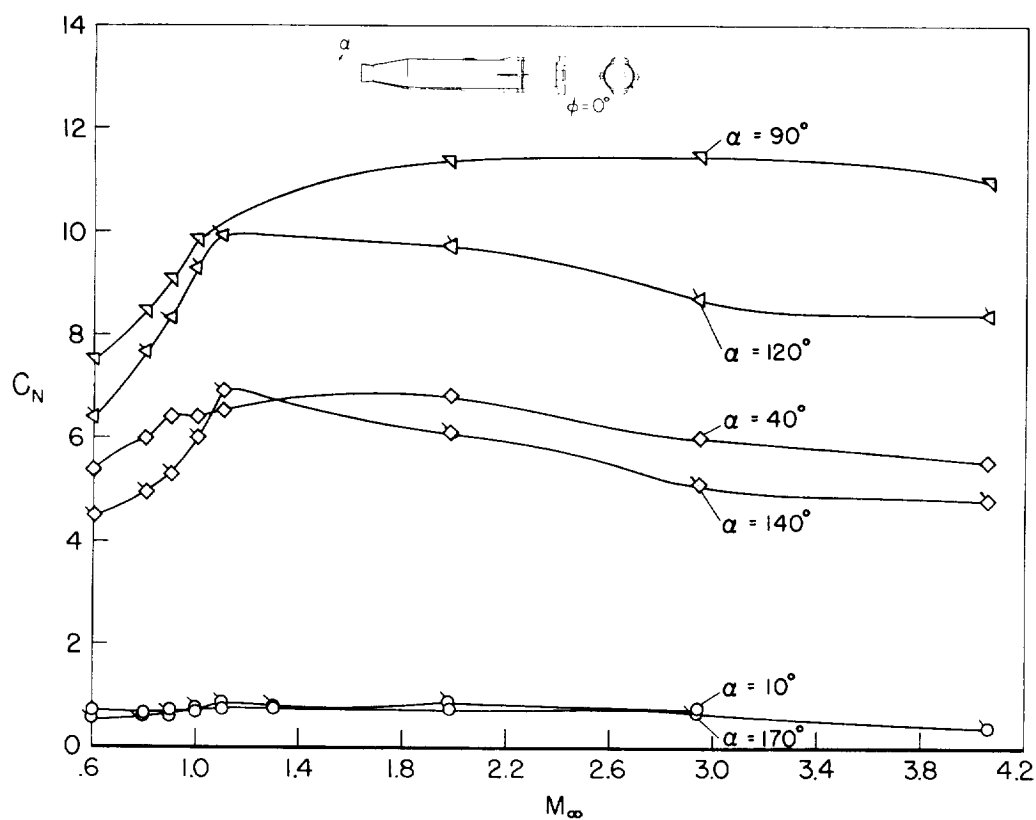
(a) Normal force.
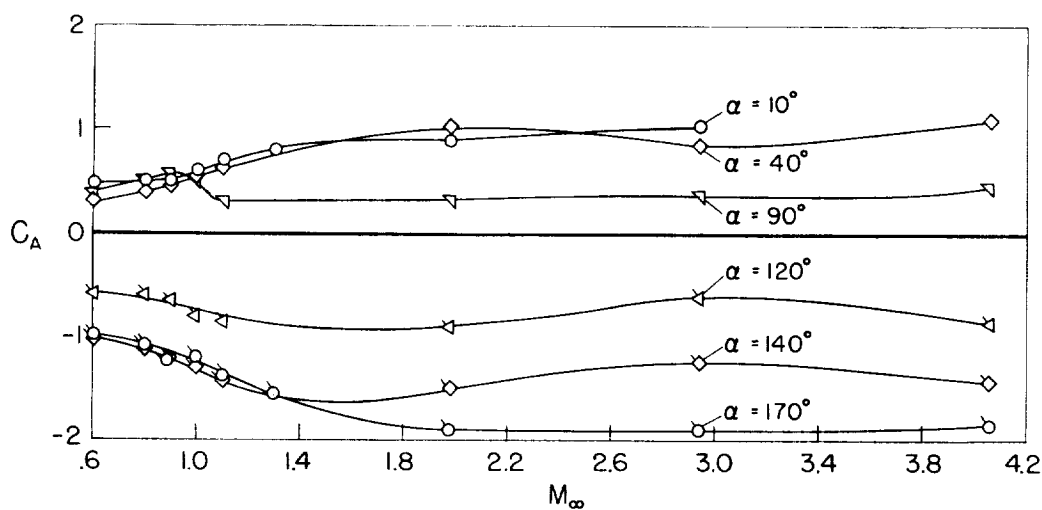
(b) Axial force.

Figure 18.- Effect of Mach number on aerodynamic characteristics of the complete model at $\phi = 0°$.

(c) Pitching moment.

(d) Center of pressure.
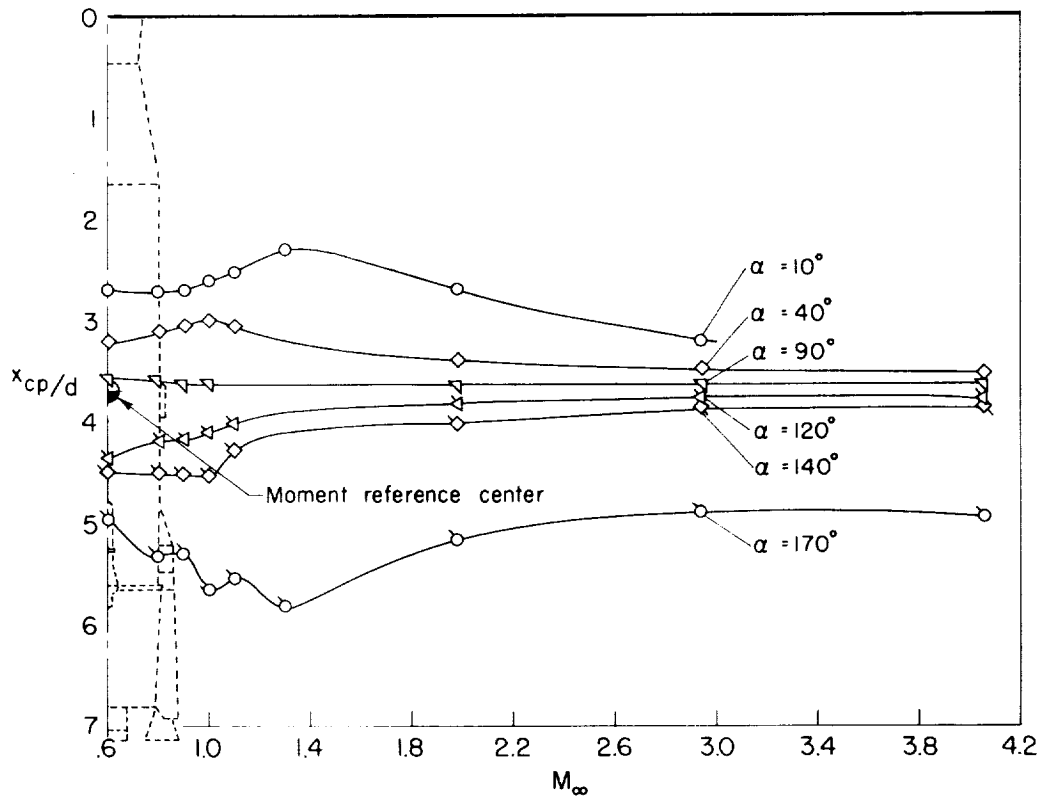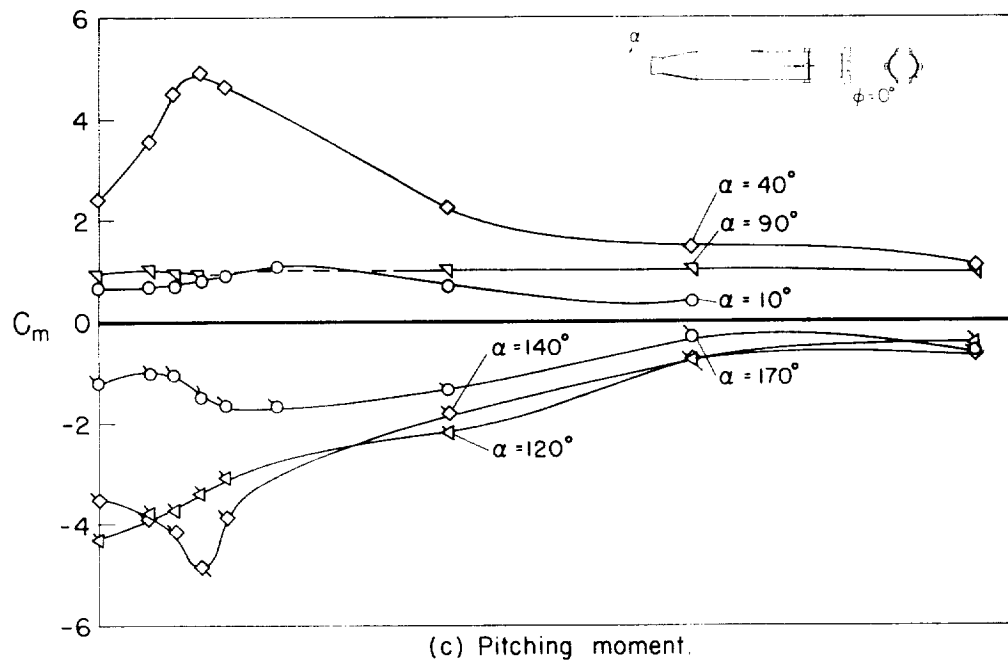
Figure 18.- Concluded.
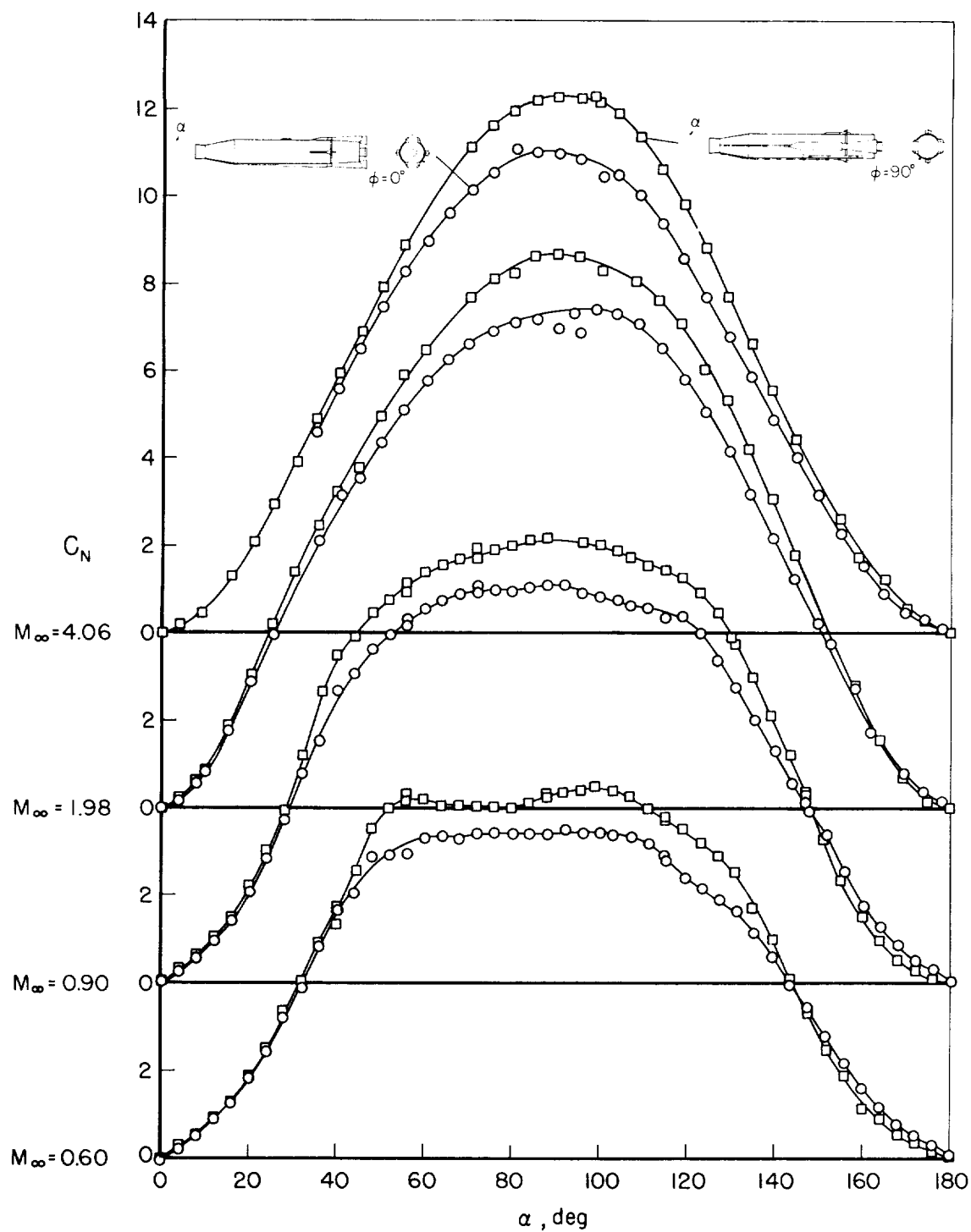
(a) Normal force.

Figure 19.- Effect of angle of bank on aerodynamic characteristics of the complete model.
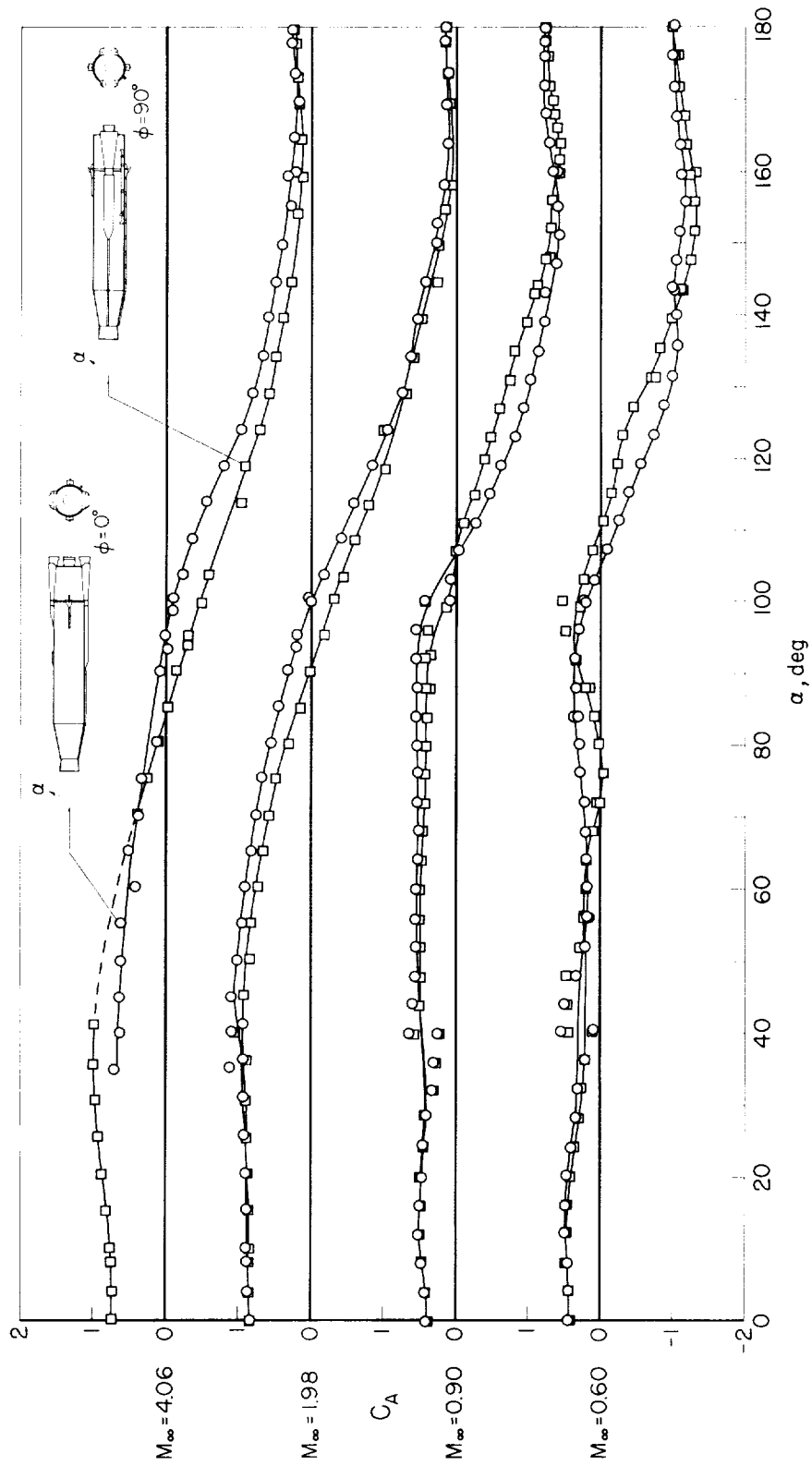
(b) Axial force

Figure 19.- Continued.
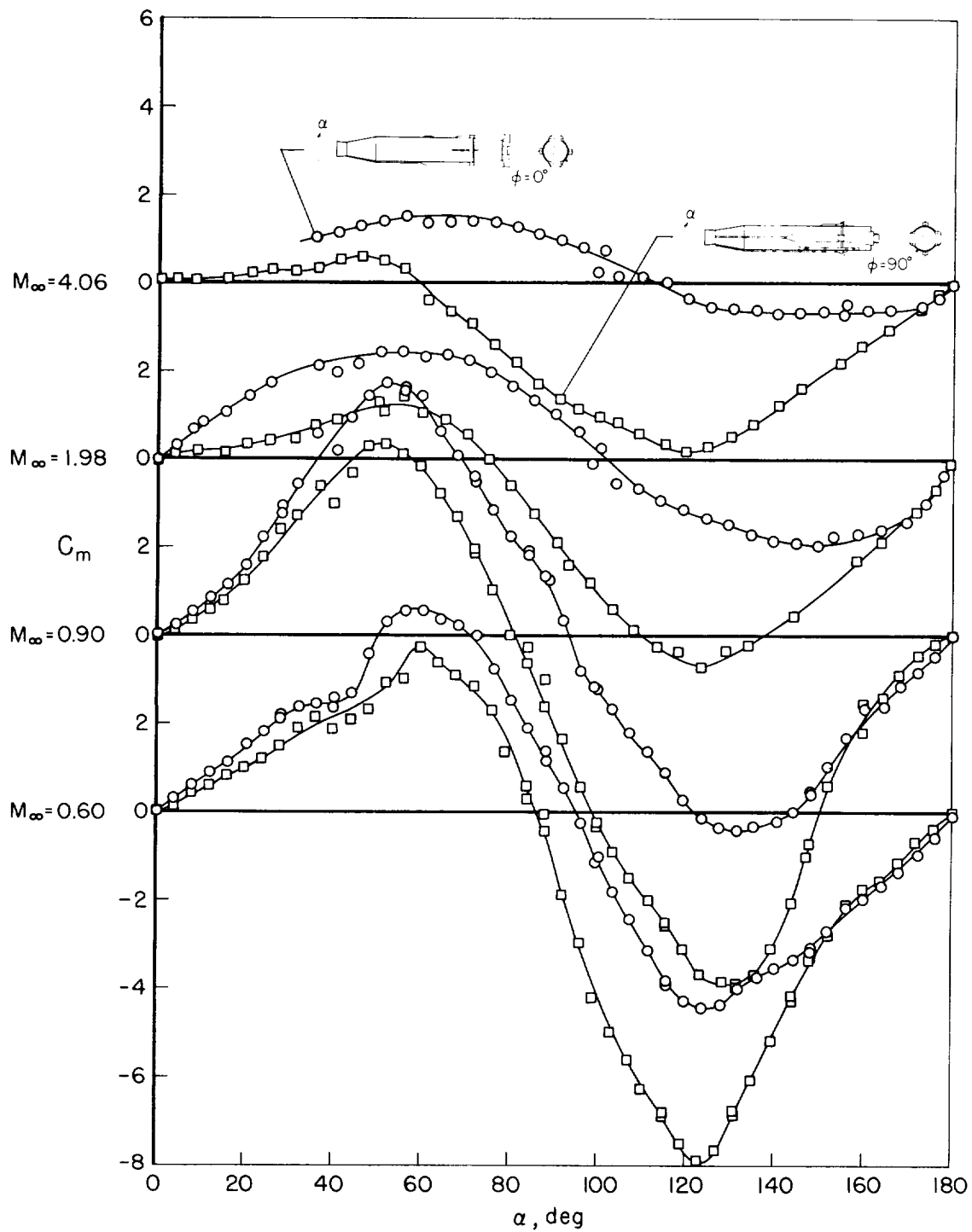
(c) Pitching moment.

Figure 19.- Continued.
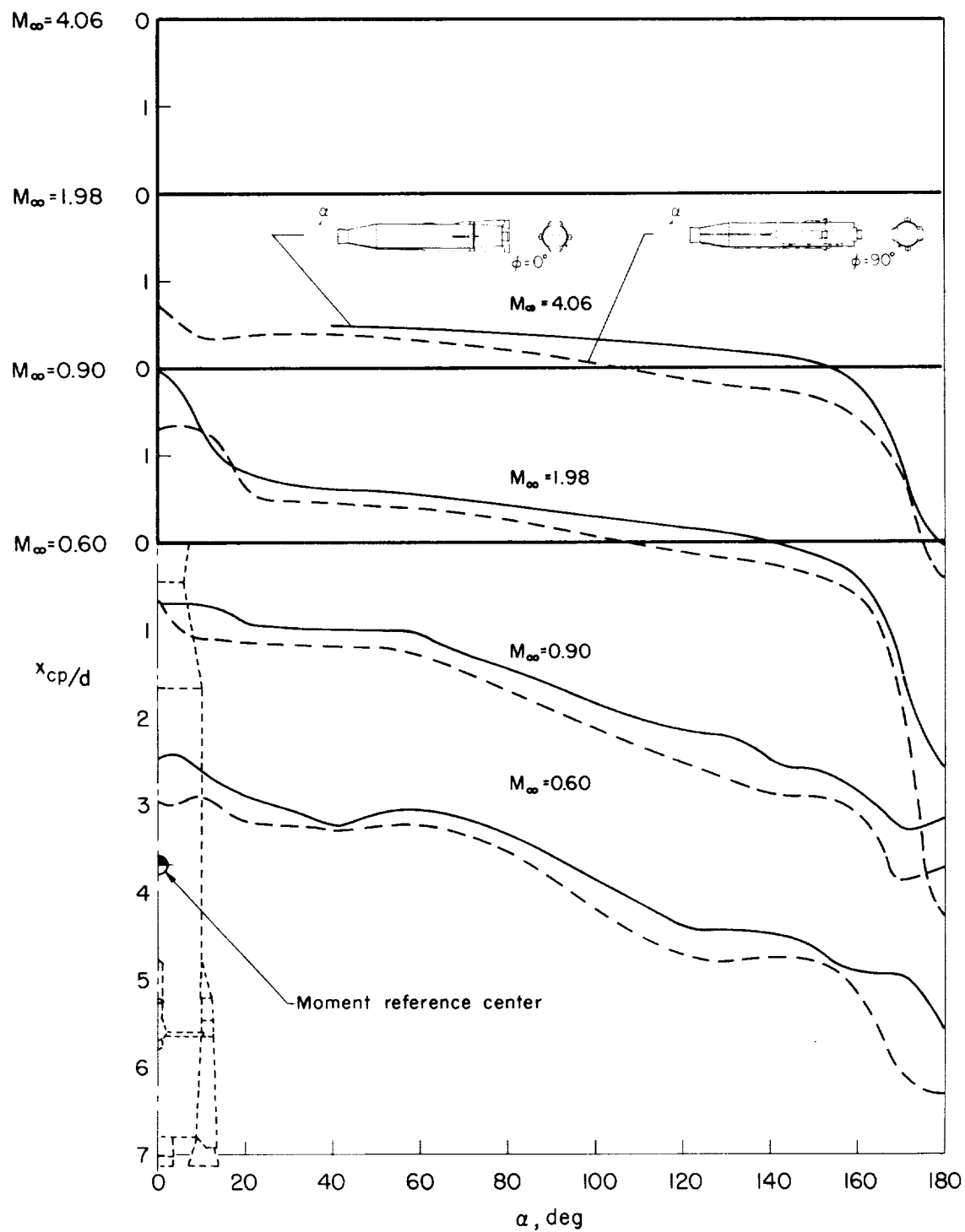
(d) Center of pressure.

Figure 19.- Concluded.

(a) Normal force.
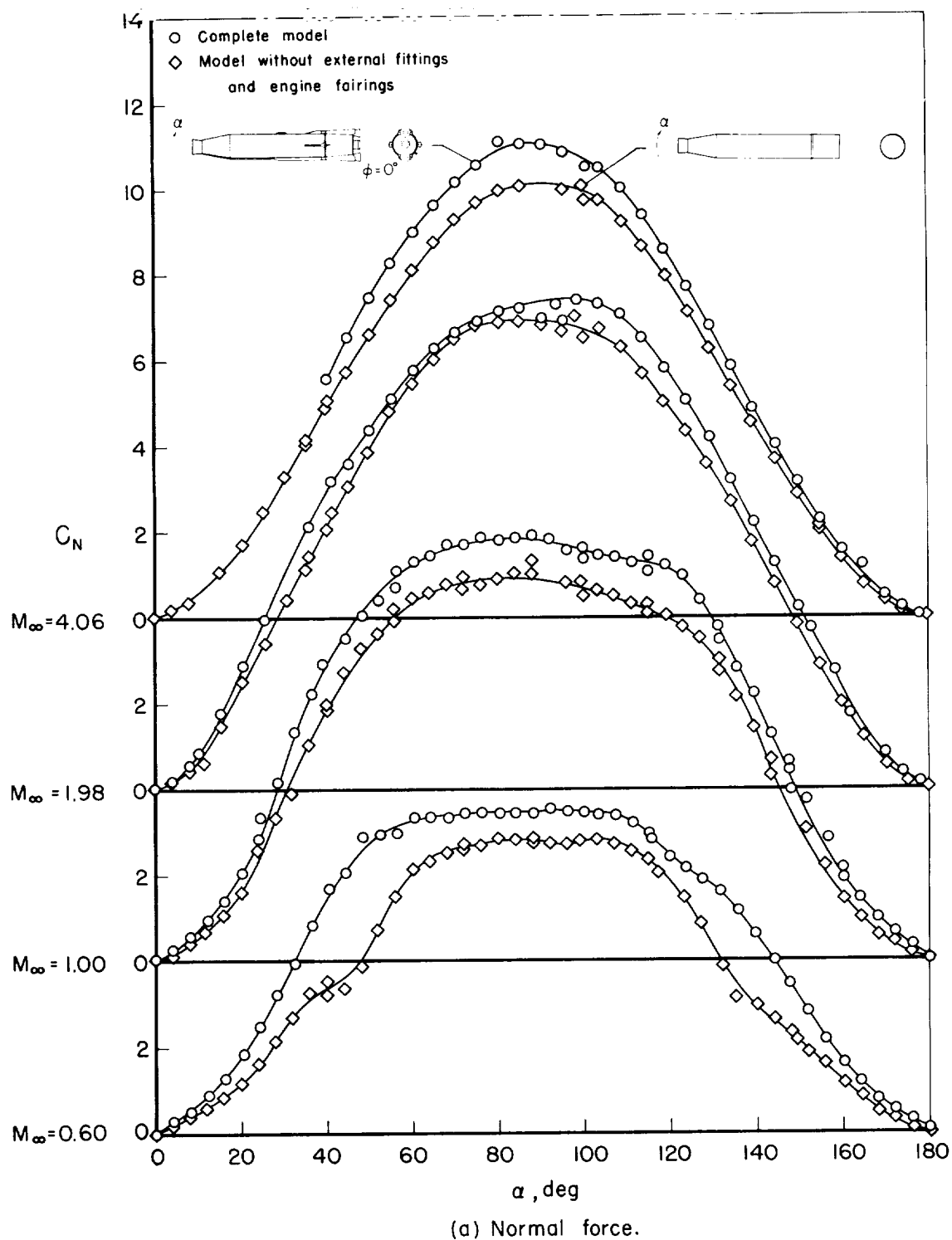
Figure 20.- Effects of external fittings and engine fairings on the aerodynamic characteristics for models at $\varphi = 0°$.
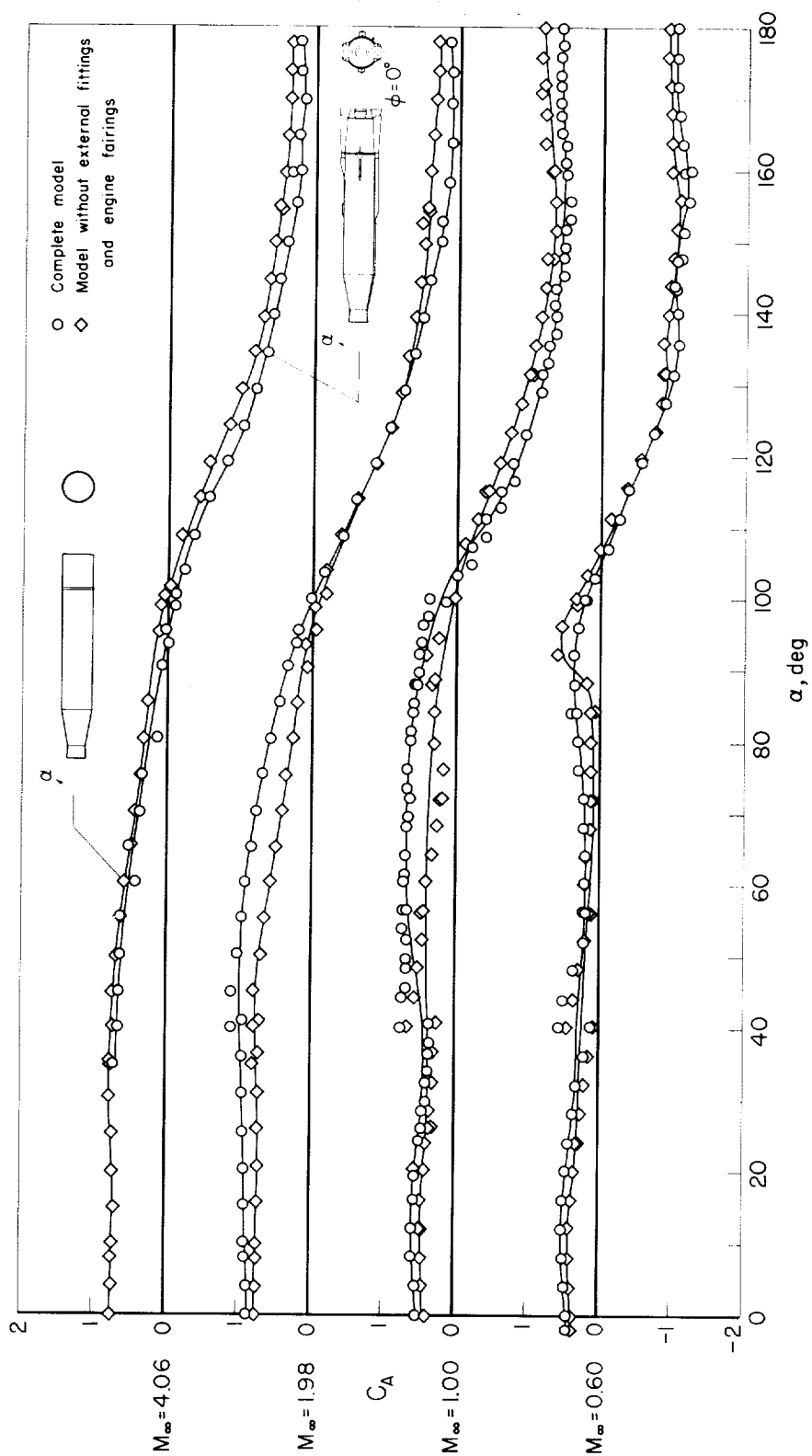
(b) Axial force

Figure 20.- Continued.
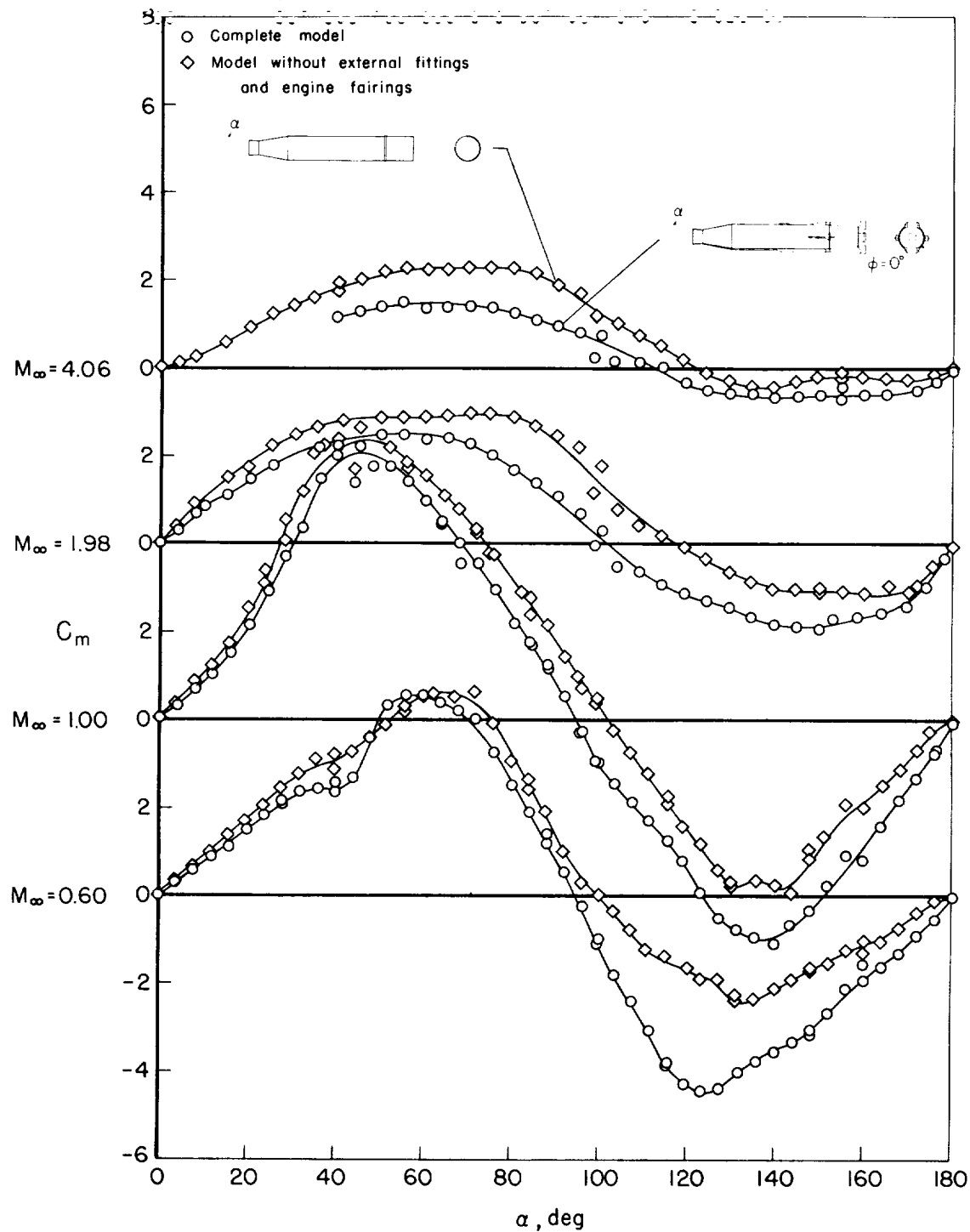
(c) Pitching moment.

Figure 20.- Continued.
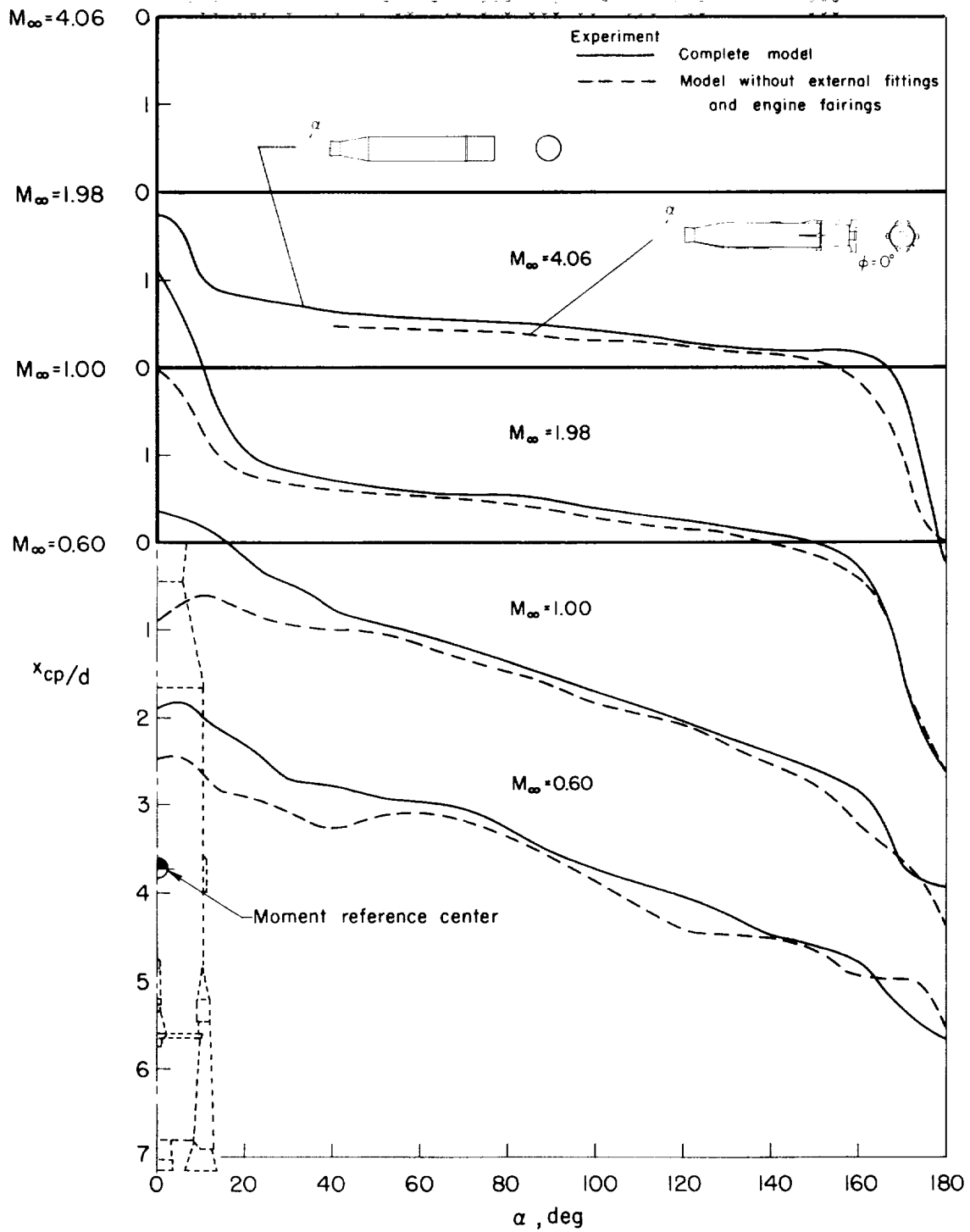
(d) Center of pressure.

Figure 20.- Concluded.

(a) Normal force.
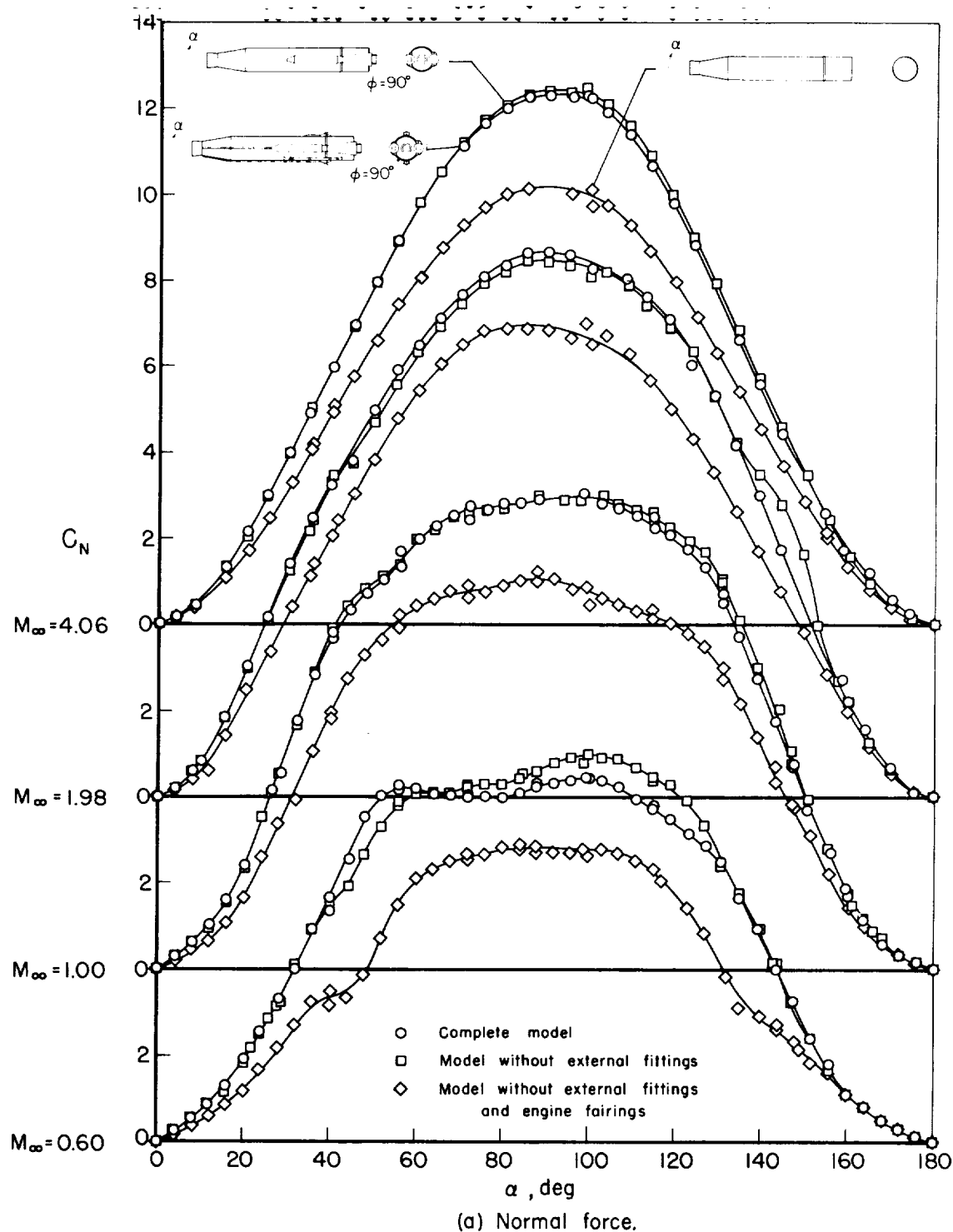
Figure 21.- Effects of external fittings and engine fairings on the aerodynamic characteristics for models at $\varphi = 90°$.
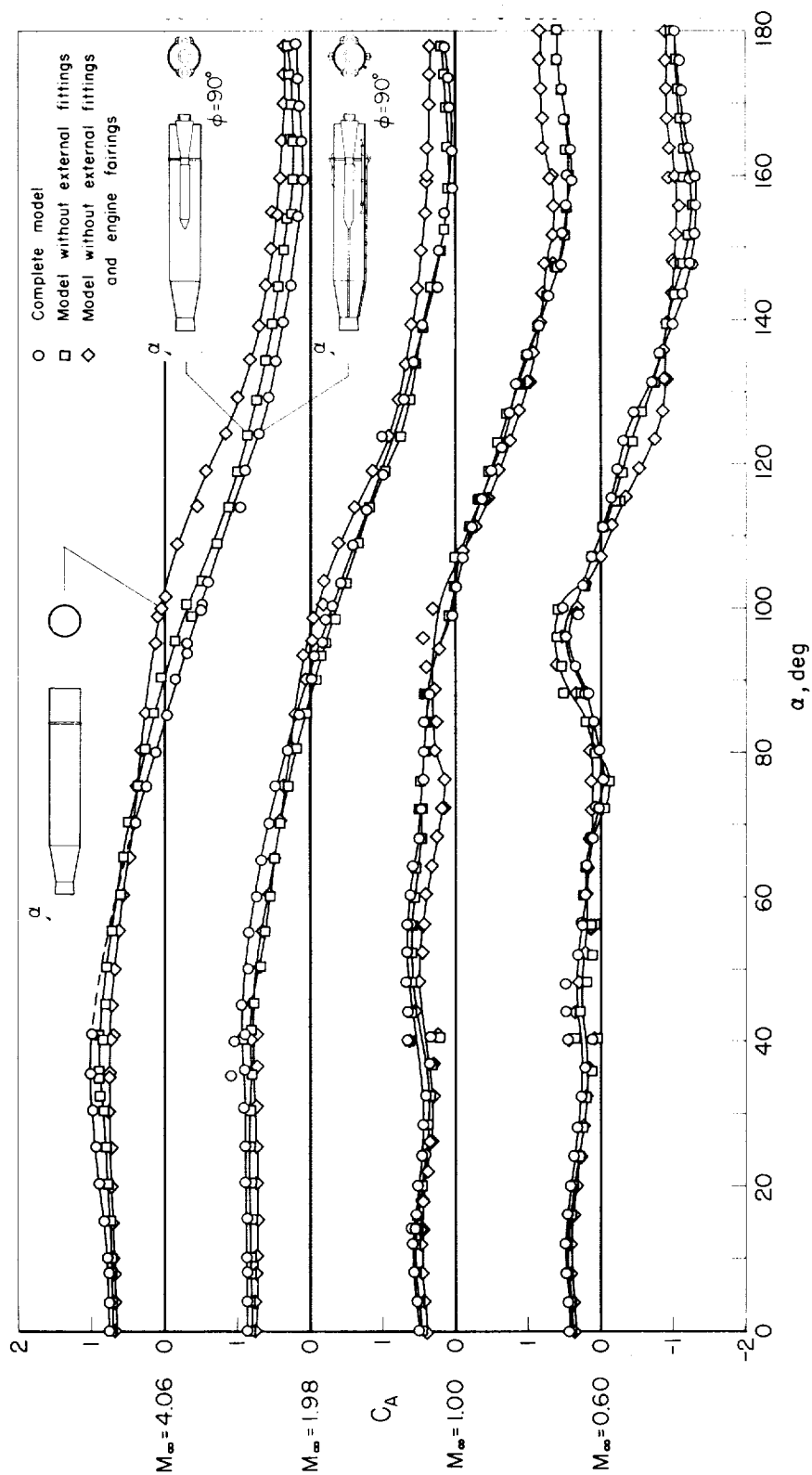
(b) Axial force.

Figure 21.- Continued.
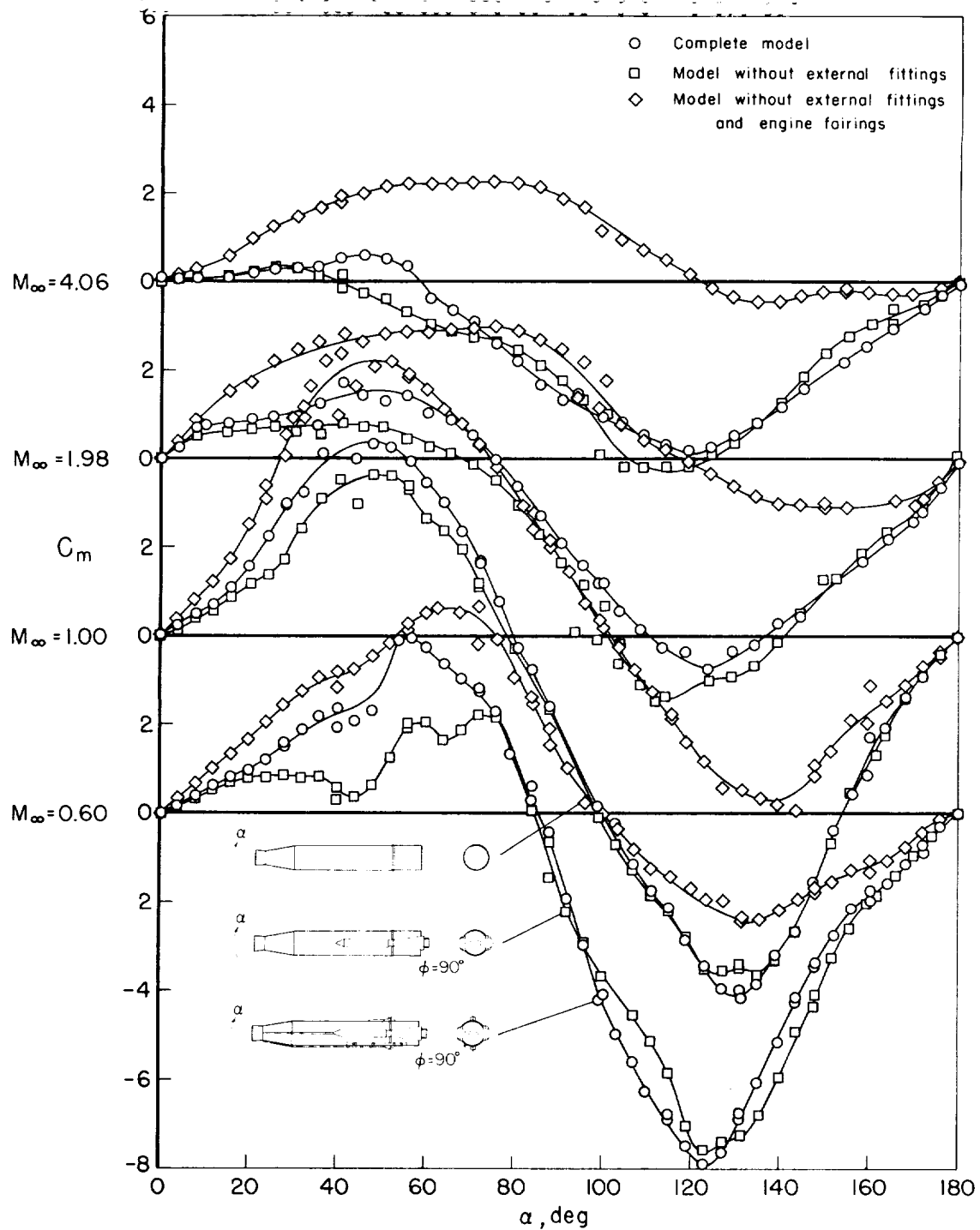
(c) Pitching moment.

Figure 21.- Continued.
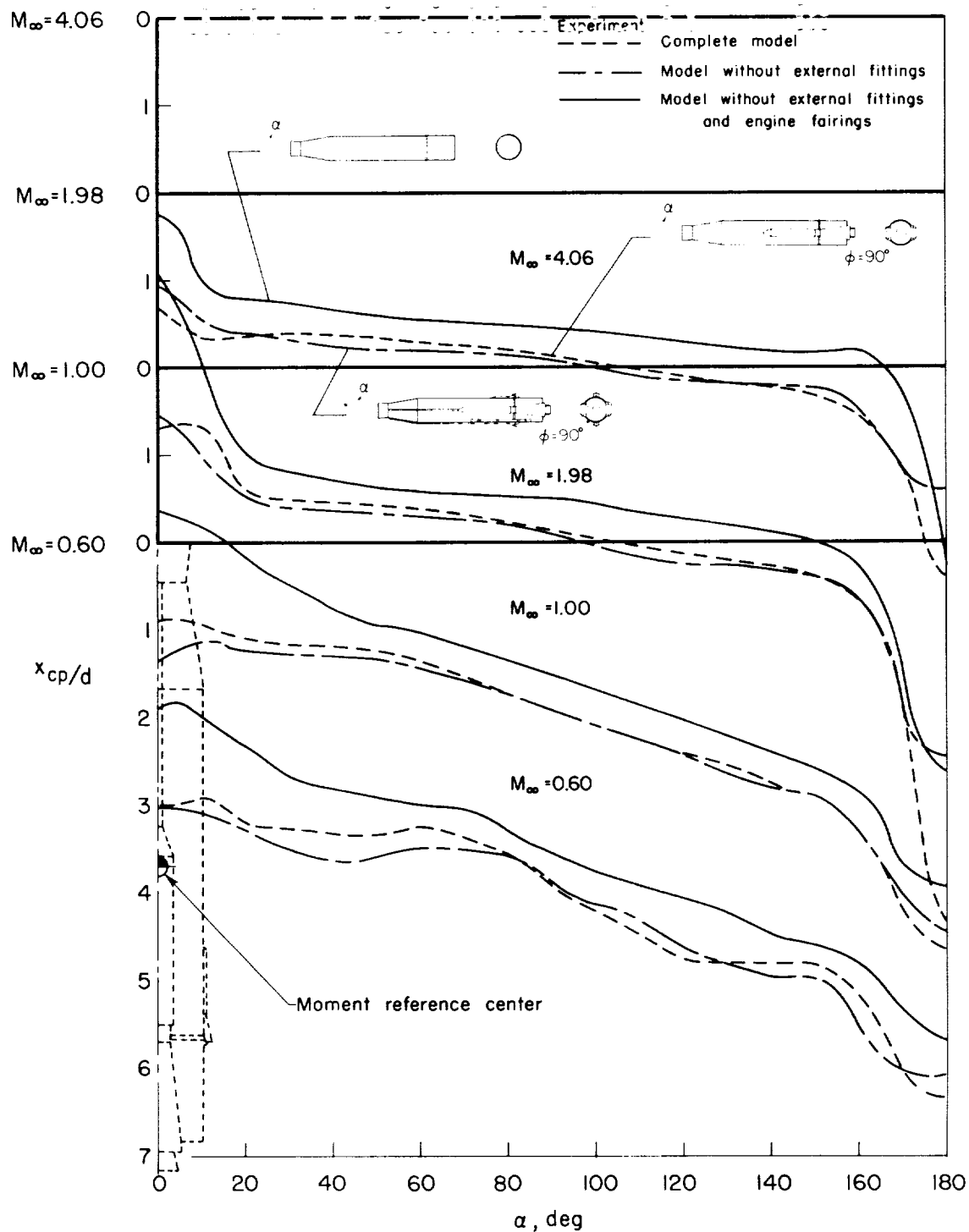
(d) Center of pressure.

Figure 21.- Concluded.
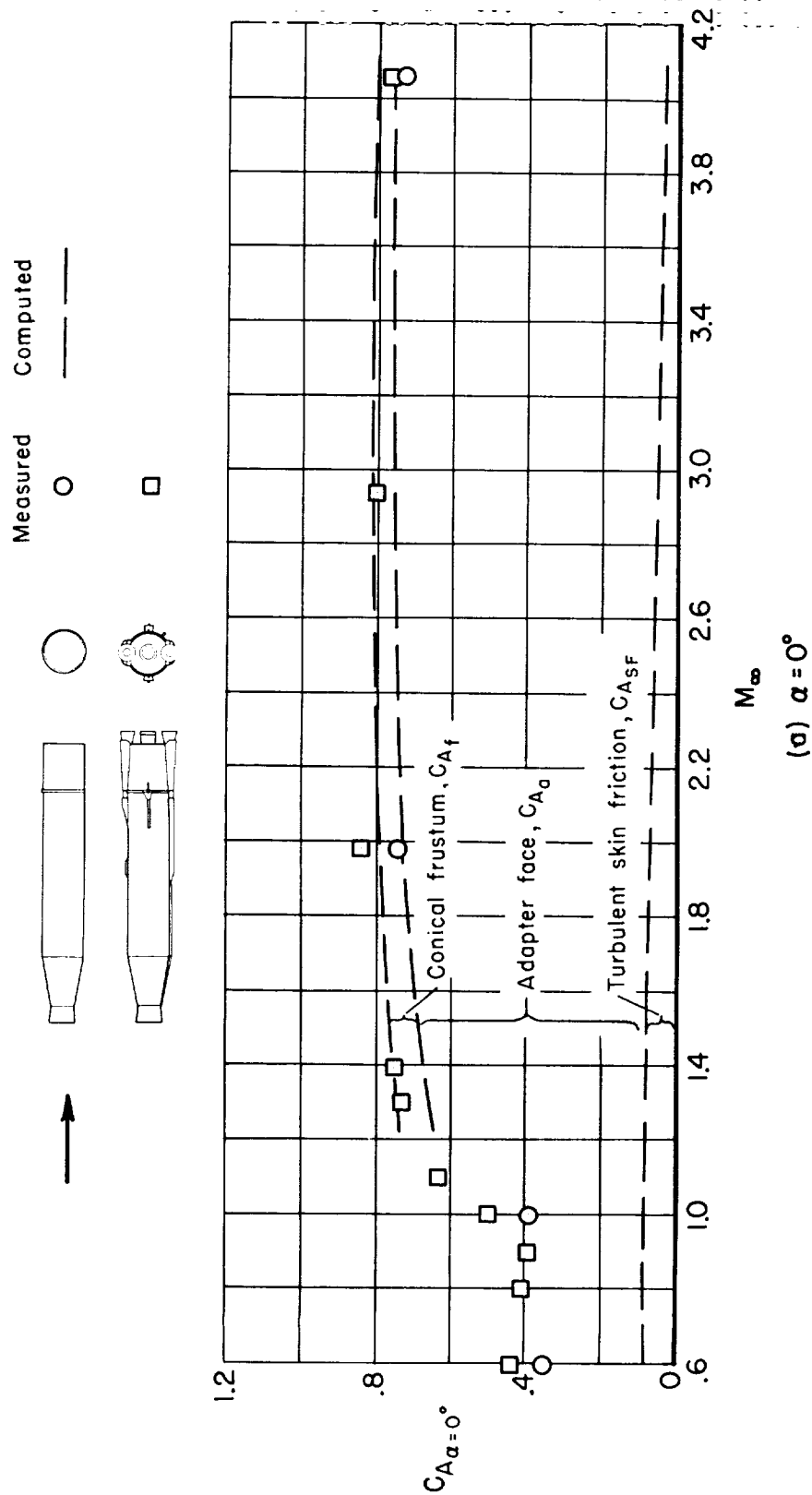
Figure 22.- Comparison of computed and measured variations of axial-force coefficient with Mach number for $\alpha = 0°$ and $180°$.
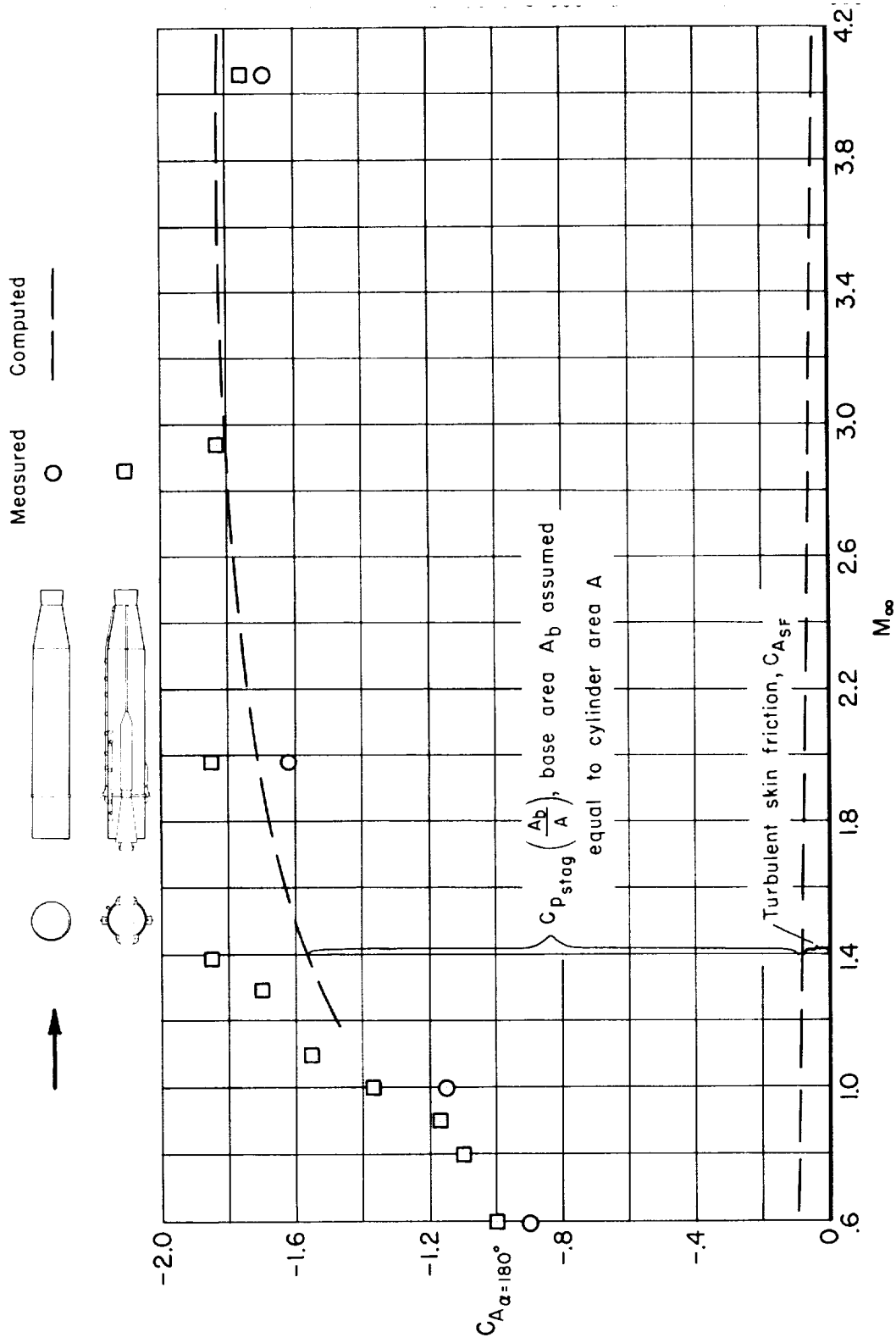
(b) α = 180°

Figure 22.- Concluded.

(a) Normal force
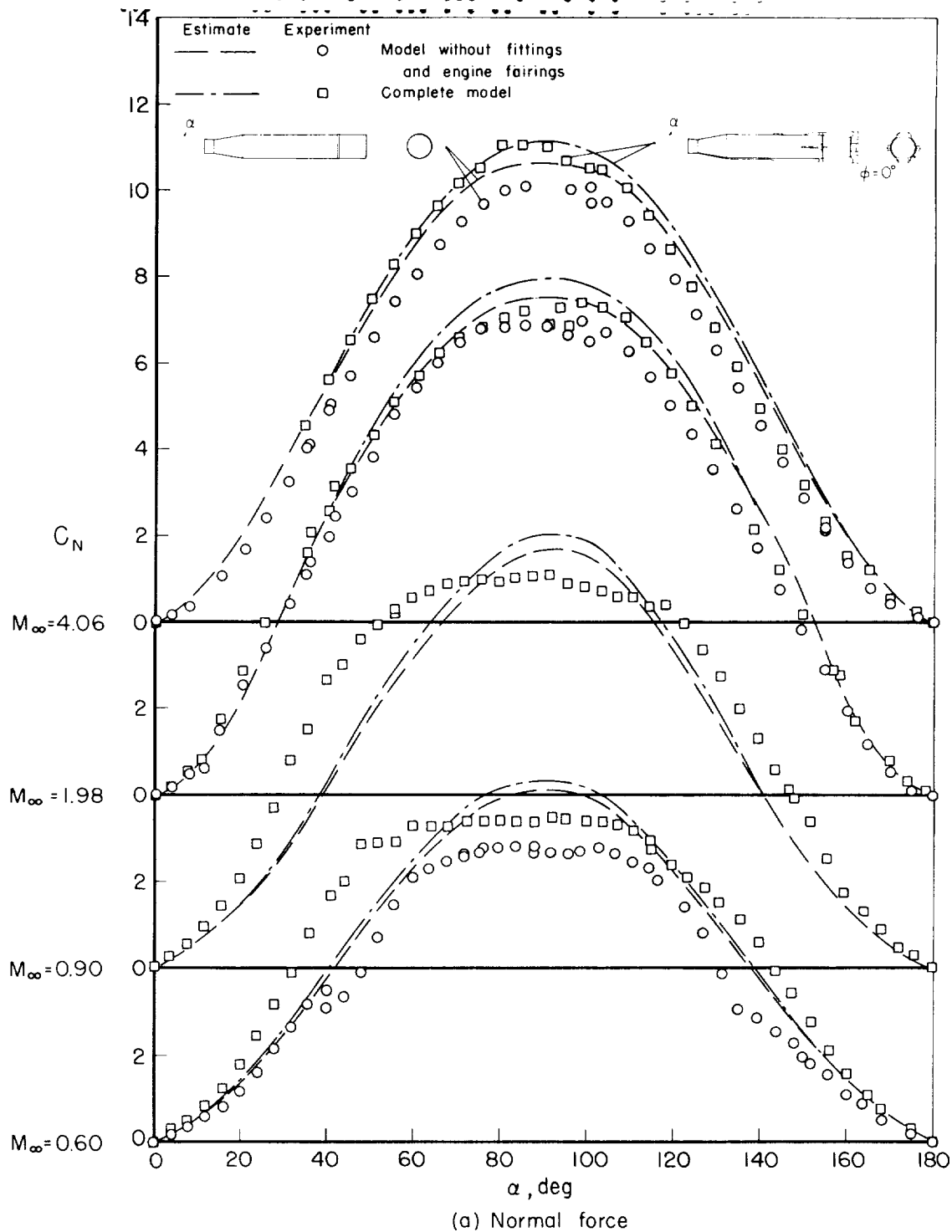
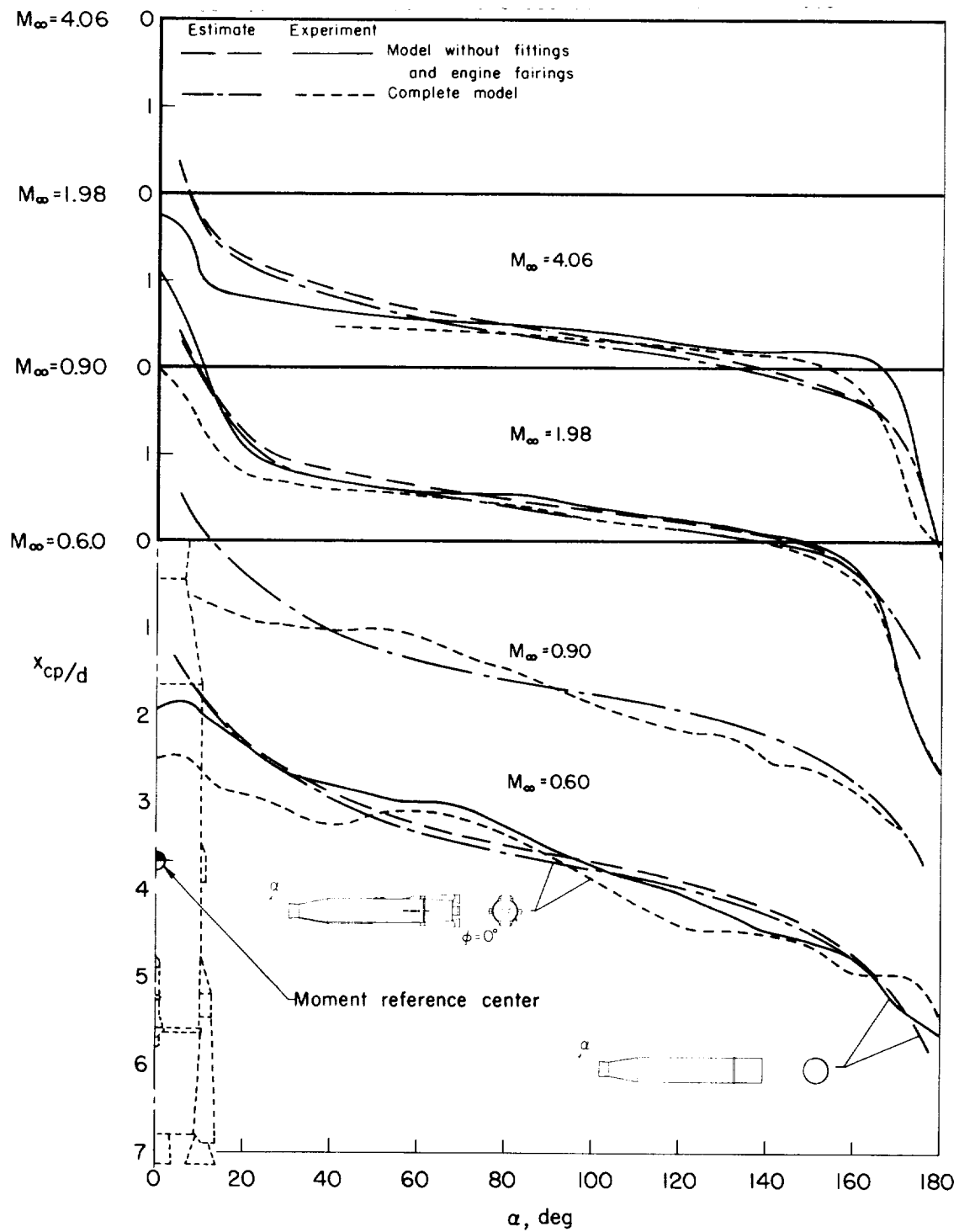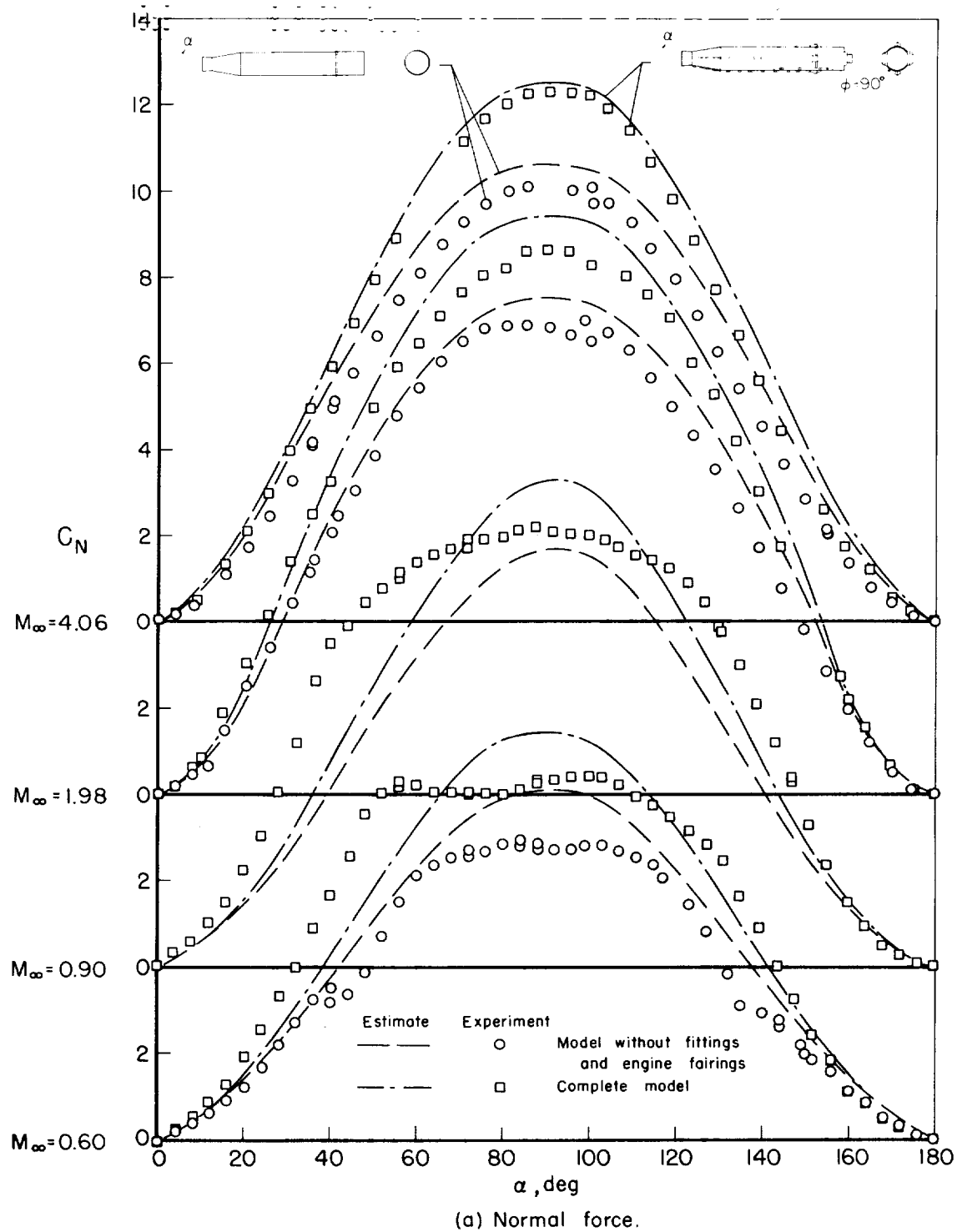Figure 23.- Comparison of estimated and experimental aerodynamic characteristics for models at $\varphi = 0°$.
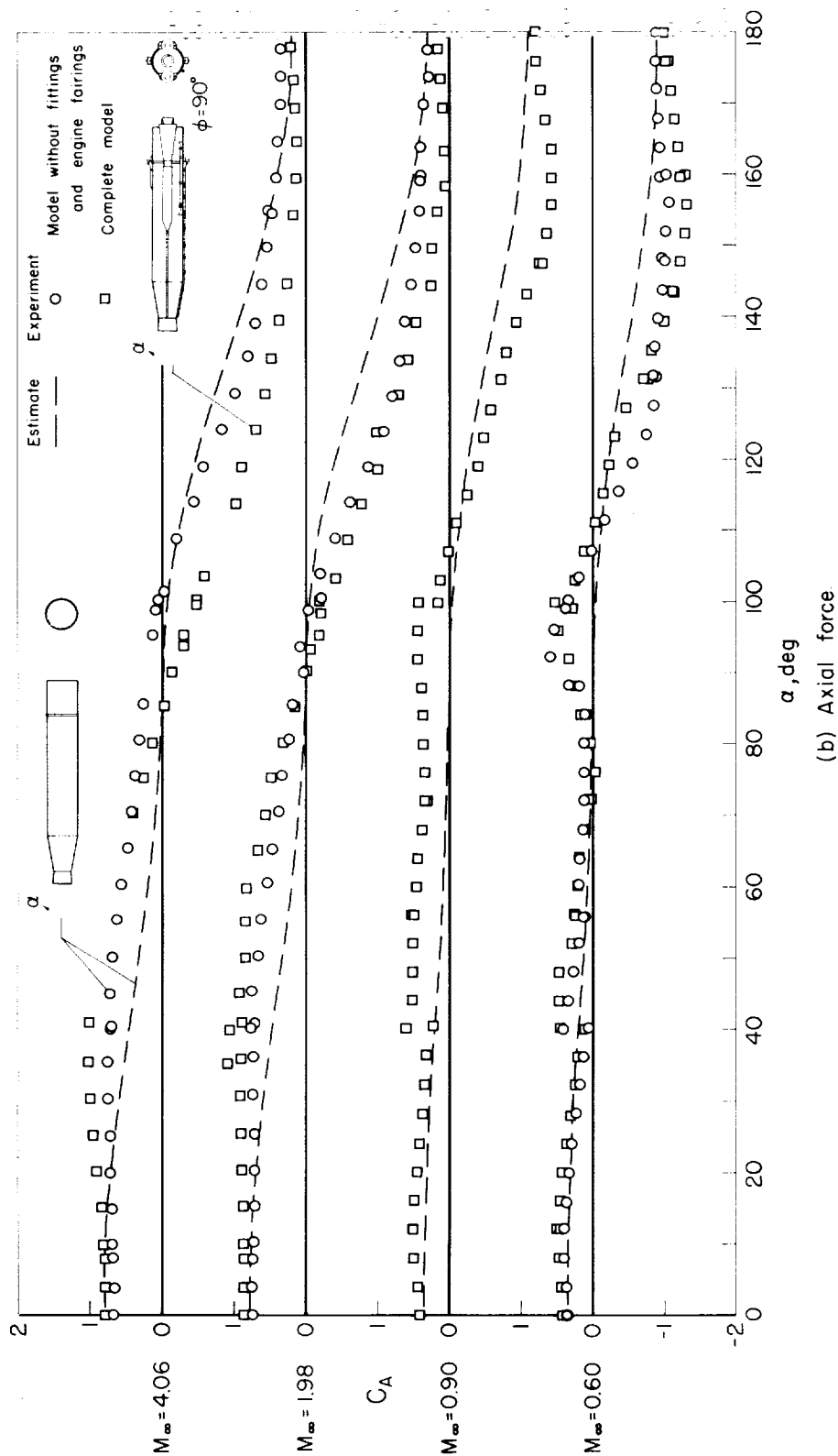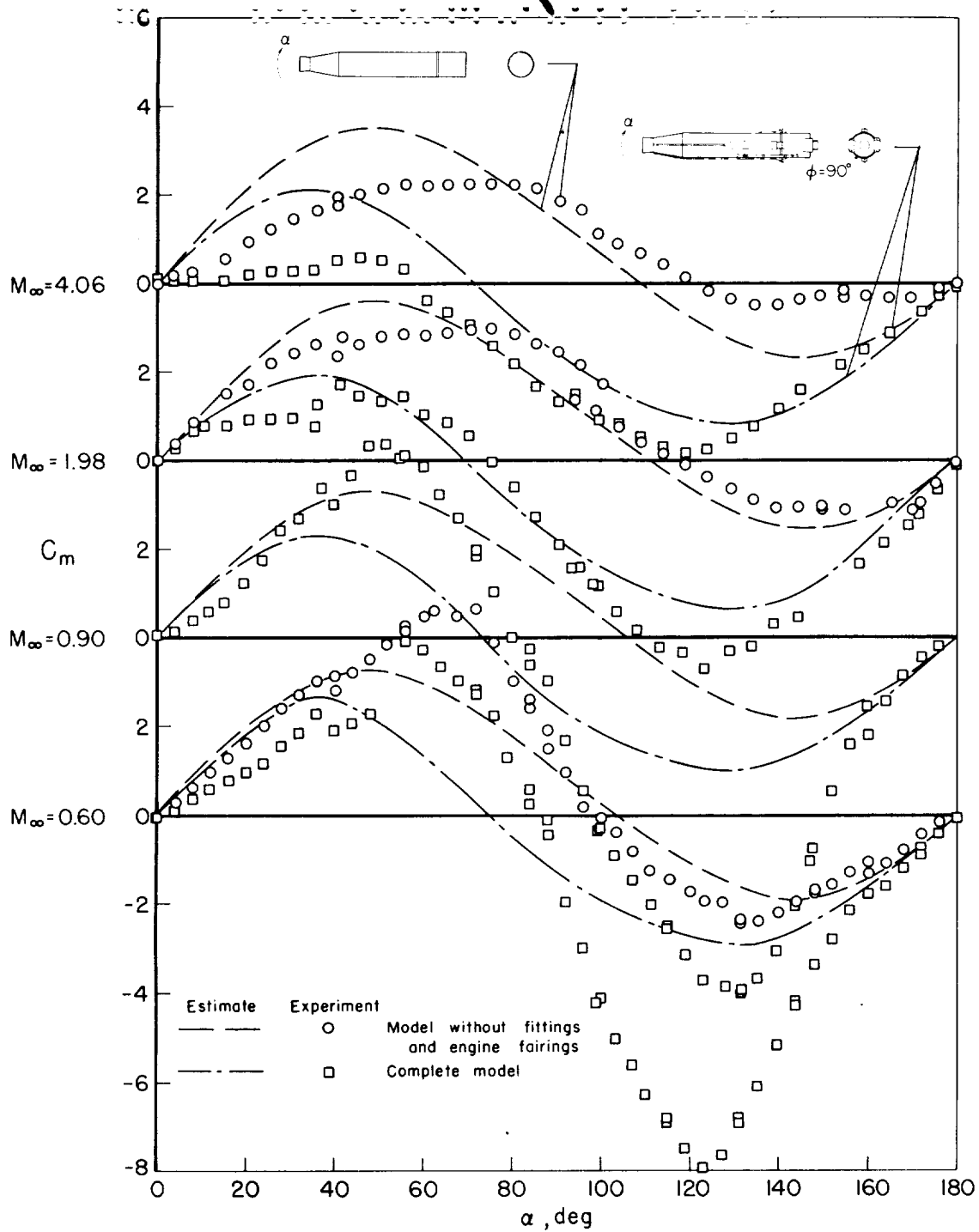
(b) Axial force.
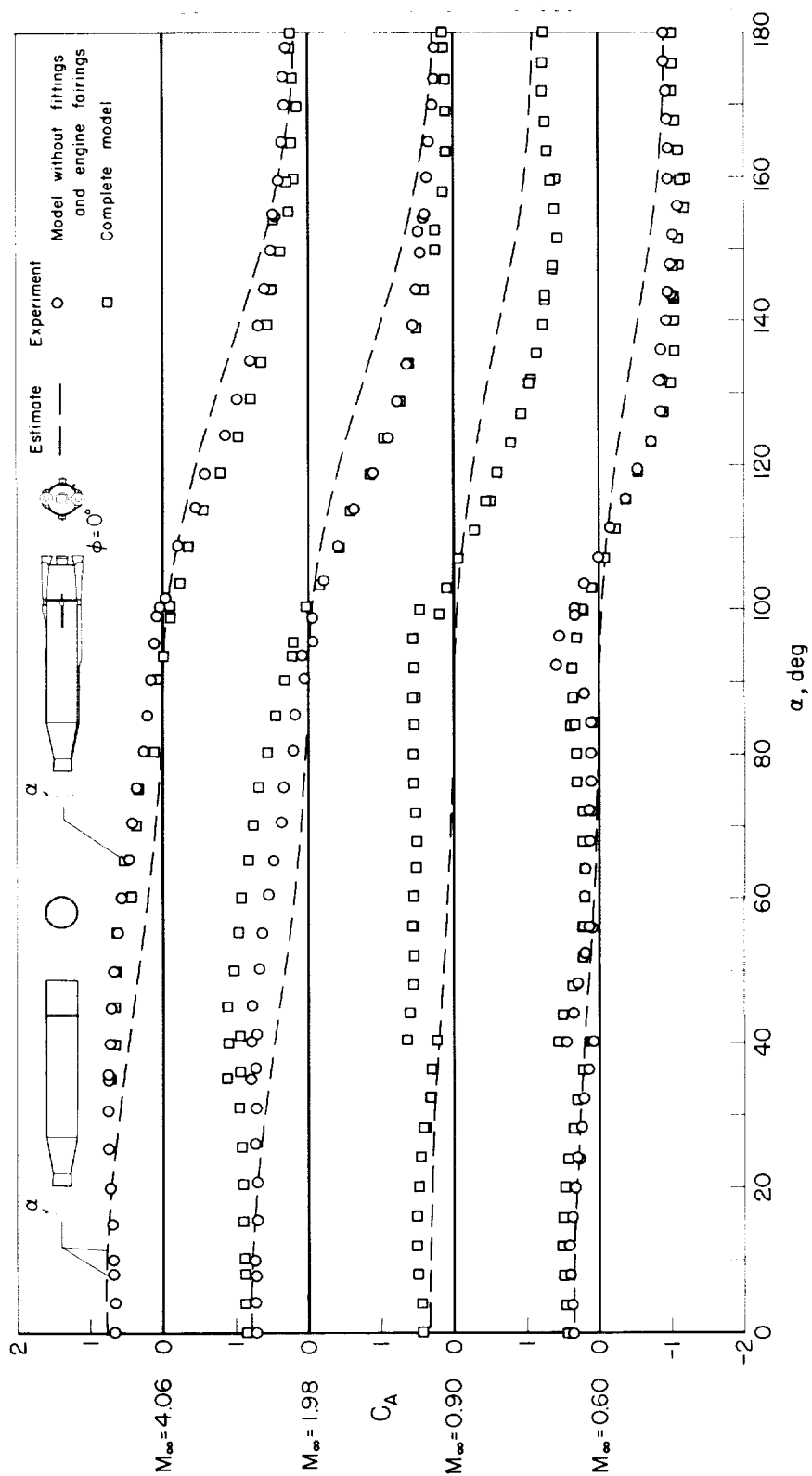
Figure 23.- Continued.
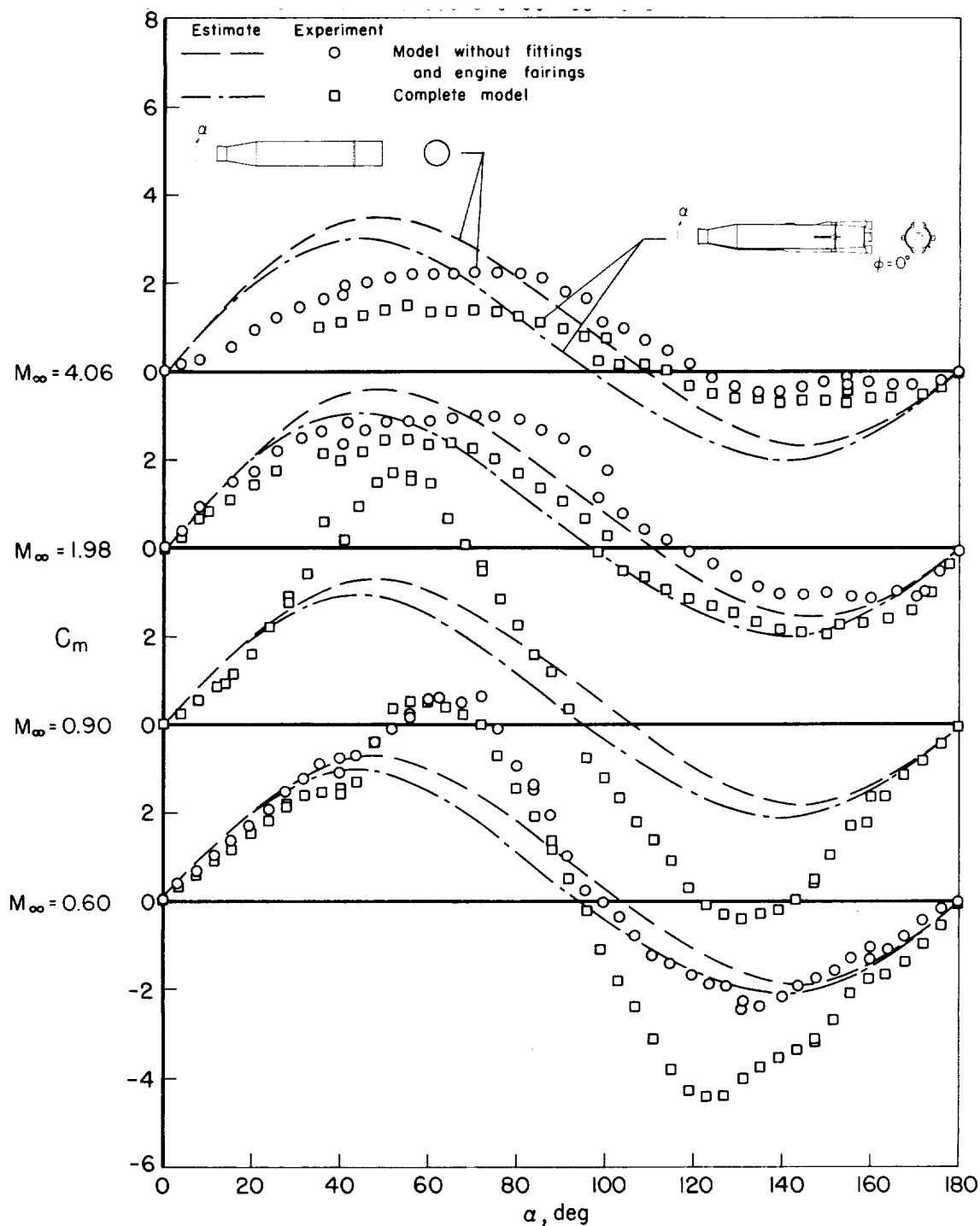
(c) Pitching moment.

Figure 23.- Continued.

(d) Center of pressure.

Figure 23.- Concluded.

(a) Normal force.

Figure 24.- Comparison of estimated and experimental aerodynamic characteristics for models at $\varphi = 90°$.
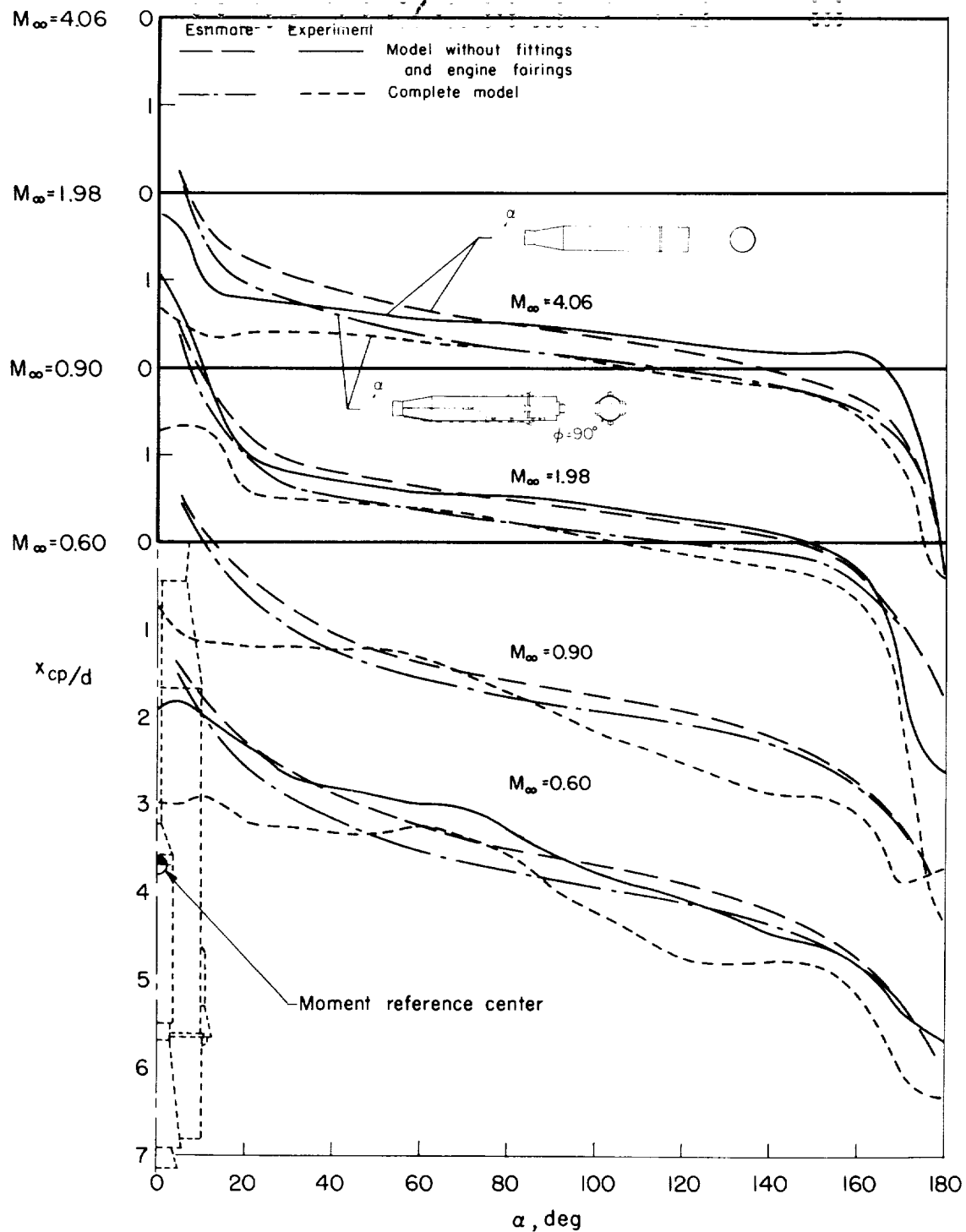
(b) Axial force

Figure 24.- Continued.

(c) Pitching moment.

Figure 24.- Continued.

(d) Center of pressure.

Figure 24.- Concluded.